The Regulation of Fatty Acid Metabolism by the NHR-14/HNF4α Transcription Factor in *Caenorhabditis elegans*

Rawan Hadi

A Dissertation Submitted to The Faculty of Graduate Studies in Partial Fulfillment of The Requirements for The Degree of Master of Science

Graduate Program in Biology

York University

Toronto, Ontario

March 2026

Author's Declaration

This thesis written under the supervision of Dr. Terrance J. Kubiseski, and it is solely authored by me**.** I acknowledge that this thesis may be made accessible to the public in electronic form.

Abstract

Energy production through metabolic reactions is essential for life in all organisms. Proper metabolic regulation strongly influences aging, as disruptions in these reactions can impair cellular homeostasis and stress response pathways. Lipid metabolism is a central metabolic process that contributes to energy balance and cellular function; however, disturbances in lipid regulatory pathways can increase susceptibility to oxidative damage and negatively affect organismal health and longevity. Accordingly, many organisms have evolved transcriptional regulators that coordinate metabolic activity with stress resistance. Our lab uses *Caenorhabditis elegans* to study the role of SKN-1/Nrf2 and its protective functions in conjunction with other, yet unknown, transcription factors. We have previously shown that transcription factors can influence stress resistance through detoxification gene regulation. I focused on the transcription factor NHR-14 and its role in oxidative stress responses. RNA-seq analysis of the *nhr-14(tm1473)* deletion showed downregulation of multiple fatty acid degradation genes, suggesting that NHR-14 functions as a positive regulator of metabolic pathways. I found that the mutation in the *nhr-14(tm1473)* gene resulted in decreased survival under oxidative stress, reduced brood size, and shortened lifespan. My investigation of NHR-14's function, along with characterization of its role as a positive regulator, provides new understanding into the mechanisms that maintain stress resistance and highlights important implications for longevity.

Acknowledgment

I would like to begin by thanking my supervisor, Dr. Terrance J. Kubiseski. your patience, guidance, and support have shaped me as a researcher, and the lessons I learned under your mentorship will remain with me throughout my career. I would also thank my advisor, Dr. John Charles McDermott, for your advice and feedback, which strengthened my research and inspired me to think critically and from new perspectives. Special thanks to Dr. Magdalena Jaklewicz for your excellent guidance in microscope, which allowed me to capture meaningful and important images for my project.

I am thankful to my lab partners, Aaron and Mahnoor, for making my research experience both enjoyable and inspiring. I would like also to give special acknowledgement to my lab partner, Fozia, for being an incredible mentor and a true friend, your support and kindness made my time in the lab unforgettable. I also wish to thank Sai from Dr. Kother's lab. Brittney and Conor from Dr. Bayfield's lab, for their help, and kindness.

To my best friend, Wardah, thank you for your constant friendship and support throughout my graduate school. To my family, Mom**,** Dad, thank you for always believing in me and supporting me every step of the way. Your love and sacrifices have been the foundation of my success.

Finally, I want to acknowledge my own dedication, and hard work throughout this challenging journey. I am proud of overcoming difficulties and reaching this important milestone in my academic.

Table of Contents

List of Figures

List of Tables

Table 1: List of Mammalian Homologs of *C. elegans* Genes and their Functions.
Information of the genes were taken from WormBase and/or cited within this project.

***C. elegans* gene**	**Mammalian Homolog**	**Function in *C. elegans***
acdh-8	**ACADM** (Acyl-CoA Dehydrogenase, Medium-Chain)	- Encodes a mitochondrial enzyme that initiates the oxidation of medium-chain fatty acids, supporting fatty acid catabolism and mitochondrial energy metabolism.
acdh-4	**ACADSB** (Acyl-CoA Dehydrogenase, Short/Branched Chain)	- Encodes a mitochondrial dehydrogenase that catalyzes the first step in the breakdown of short and branched-chain fatty acids, contributing to lipid utilization and metabolic homeostasis.
acs-18	**ACSL1** (Acyl-CoA Synthetase Long-chain family).	- Encodes a long-chain acyl-CoA synthetase that activates fatty acids for entry into β-oxidation and lipid biosynthetic pathways.
acs-2	**ACSL1, ACSL3, ACSL4** (Acyl-CoA Synthetase Long-chain family). (Acyl-CoA Synthetase Family Member 2)	- Encodes an acyl-CoA synthetase that converts fatty acids into acyl-CoA.
act-1 (ACTin)	**ACTB** (Actin Beta) **ACTG1** (Actin γ 1)	- Encodes an essential cytoskeletal protein involved in organizing the cortical actin network and facilitating mitotic cytokinesis.

gcs-1 (γ Glutamyl Cysteine Synthetase)	**GCLC** (Glutamate-cysteine ligase catalytic subunit)	- Encodes the catalytic subunit of glutamate–cysteine ligase, responsible for the ATP-dependent synthesis of γ-glutamylcysteine, a critical step in glutathione production.
gst-4 (Glutathione S-Transferase)	**GSTs** **(**Glutathione-S-Transferase)	- Encodes a glutathione S-transferase that facilitates conjugation of glutathione to toxic compounds, supporting phase II detoxification and cellular stress protection.
hsp-16.2 (Heat Shock Protein)	**HSPB9** (Heat Shock Protein Family B (Small) Member 9)	- Encodes a small heat shock protein that associates with unfolded or misfolded proteins under stress conditions to prevent protein aggregation and maintain proteostasis.
nhr-49	**HNF4α** (Hepatocyte nuclear factor 4α)	- Encodes a nuclear hormone receptor that controls lipid metabolic gene expression, including fatty acid desaturation, and plays a role in oxidative stress resistance.
tba-1 (TuBulin, α)	**TUBA4A** and **TUBA8** (Tubulin α 4a and 8)	- Enables GTPase binding and activation and is involved in mitotic spindle orientation, regulation of cytokinesis, and embryonic development.
hacd-1	**HACD1** (3-hydroxyacyl-CoA dehydratase 1)	- Encodes a 3-hydroxyacyl-CoA dehydrogenase involved in mitochondrial fatty acid β-oxidation, catalyzing the third step of the pathway essential for

		energy production and lipid metabolism.
mtl-1 (Metallothione)	**MT1** and **MT2** (Metallothionein)	- Encodes a metal-binding protein that maintains metal ion balance and limits cellular damage caused by metal-induced stress.
sdz-8 (SKN-1 Dependent Zygotic transcript)	**CBR3** (Carbonyl reductase 3)	- Regulated by *daf-2*, *daf-16*, and *skn-1*, and encodes a protein containing NAD(P)-binding domains.
skn-1 (SKiNhead)	**Nrf2** (Nuclear factor erythroid 2-related factor 2)	- Encodes a protein involved in phase II detoxification and antioxidant responses activated during oxidative and xenobiotic stress.
sod-1	**SOD** (Superoxide Dismutase)	- Encodes a cytosolic superoxide dismutase that converts superoxide radicals into less reactive species, reducing oxidative damage.
sod-2		- Encodes a mitochondrial superoxide dismutase that detoxifies reactive oxygen species generated during mitochondrial respiration.
sod-3		- Encodes a stress-responsive mitochondrial superoxide dismutase regulated by DAF-16, contributing to enhanced oxidative stress tolerance and longevity.

tba-1 (TuBulin, α)	**TUBA4A and TUBA8** (Tubulin α 4 and 8)	- Encodes an α-tubulin that is a core component of microtubules, required for proper cytokinesis and embryonic development.

Table 2: List of Abbreviations

3' UTR	3′ untranslated region of an mRNA transcript
AAK	AMP-activated kinase
AA	Amino Acids
ABC	ATP-binding cassette transporter
ACT	Actin
AGE	Ageing Alteration
AKT	Protein Kinase B (PKB)
AMPK	AMP-Activated Protein Kinase
AS	Arsenite
BRAP2	Brca-1 Associated Binding Protein 2
BRCA	Breast Cancer susceptibility gene
C. elegans	*Caenorhabditis elegans*
CAT	catalase
CDC	Cell Division Control Protein
cDNA	Complementary DNA
CEP	*C. elegans* p53-like protein
D.melanogaster	Drosophila melanogaster
DAF	Abnormal Dauer Formation
DNA	Deoxyribonucleic Acid
DTT	Dithiothreitol
E. coli	*Escherichia coli*
E3	Ubiquitin ligase
ER	Endoplasmic Reticulum
ERK	Extracellular Signal-Regulated Protein Kinase
ETC	Electron Transport Chain
Fe^{2+}	Reduced (ferrous) iron
FOXO	Forkhead box O transcription factor
GFP	Green Fluorescent Protein
GO	Gene Ontology
GSK	Glycogen Synthase Kinase
GST	Glutathione S-transferase
H_2O_2	Hydrogen peroxide
HSP	Heat Shock Protein
HSR	Heat Shock Response
IGF	Insulin-like growth factor
IIS	Insulin/Insulin-like growth factor Signaling
IRE	Serine/threonine protein kinase
KEGG	Kyoto Encyclopedia of Genes and Genomes
KSR	Kinase Suppressor of RAS
MAF	Musculoaponeurotic Fibrosarcoma
MAPK	Mitogen-Activated Protein Kinase
MAPKK	Mitogen-Activated Protein Kinase Kinase

MAPKKK	Mitogen-Activated Protein Kinase Kinase Kinase
MPK	Map Kinase
mRNA	messenger RNA
NAD(P)H	Nicotinamide adenine dinucleotide
NADPH	Nicotinamide adenine dinucleotid
NF-$_{k}$B	Nuclear factor kappa-light-chain-enhancer of activated B cells
HNF4α	Hepatocyte nuclear factor 4 alpha
NGM	Nematode Growth Medium
NHR	Nuclear Hormone Receptor
$O2^{-}$	Superoxide radical
OH^{-}	Hydrogen peroxide radical
$OH^{\cdot}$	Hydroxyl radical
Oxidative Stress	OS
p38	Protein 38 MAPK
PI and PII	Phase I and Phase I
PMK	P38 Map Kinase family
qRT-PCR	quantitative Real Time- PCR
Ras	Rat Sarcoma Oncogene
RNA	Ribonucleic Acid
RNA-Seq	RNA sequencing
RNAi	RNA interference
ROS	Reactive Oxygen Species
SKN-1	Skinhead
SOD	Superoxide dismutase
SW-PCR	Single Worm-Polymerase Chain Reaction
tBHP	*tert*-Butyl Hydroperoxide
TF	Transcription factor
WT	Wild type
YF	Wormbase strain designation for Kubiseski lab
ZFP	Zinc Finger Protein
ORO	Oil Red O staining

Chapter 1: Introduction and Literature Review

1.1 General Introduction

Stress is one of the significant factors that can lead to the development of age-related diseases by causing cellular damage (Lupien et al., 2009). All living organisms undergo the physiological process of aging, which can lead to disruptions in signaling pathways (Niccoli & Partridge, 2012; El Assar et al., 2013; Deng et al., 2022). There are many factors that can contribute to age-related diseases, however one of the main causes of age-related illnesses is oxidative stress.

One cause of aging is due to the oxidative stress is the buildup of random molecular damage (Harman, 2002). Our understanding of the process of oxidative stress is an important aspect in cellular and molecular biology. In this thesis, I will examine the function of the NHR-14 transcription factor in the oxidative stress response using the microscopic nematode *Caenorhabditis elegans*.

1.2 *Caenorhabditis elegans* (*C. elegans*) as a Model Organism

Caenorhabditis elegans (*C. elegans*) is a useful model organism to study age-related diseases because it is small in size and short life cycle. The nematode *C. elegans* was first used in the 1960s by Sydney Brenner. The ease of use and the availability of genetic techniques has made *C. elegans* crucial for studying molecular biology, genetics, and developmental research.

1.2.1 Aging and Longevity in *C. elegans*

Using *C. elegans* as a model organism to study longevity and aging has multiple benefits. Along with its small size and simple anatomy, *C. elegans* has a rapid life cycle and can self-fertilize (Son et al., 2019). *C. elegans* shows different age-related distinctions in the expression of stress response genes and microRNAs. As a result, *C. elegans* can be effectively examined using a range of molecular techniques. Indeed, because of their simplicity, *C. elegans* remains one of the best organisms for studying the signaling pathways involved in aging and longevity. *C. elegans* shares multiple signaling pathways and molecular mechanisms with more complex animals. For example, it has several human gene homologs, providing helpful prospects for studying human conditions (Qin et al., 2018). Table 1 lists the functions of a number of gene homologs of *C. elegans* present in humans.

1.2.2 *C. elegans* as a Genetic Model

C. elegans has a life cycle of three to four days at 20 °C, which enables researchers to quickly observe how mutations are passed through generations (Byerly et al., 1976). *C. elegans* is a useful model for analyzing the gene regulatory network underlying the expression of stress response genes (Raamsdonk & Hekimi, 2010; Hu et al., 2018).

Mapping of mutations has demonstrated that a single gene deletion can greatly influence an organism's lifespan. The first genetic screen in *C. elegans* showed that a mutation called *age-1* is able to increase the lifespan in *C. elegans* (Klass, 1983). This has strongly influenced the development of a huge amount of the research in *C. elegans*. This model

organism has been used in many different genetic experiments, such as producing transgenic lines, using fluorescent markers to track the location of proteins, studying the functions and effects of proteins using RNA interference (RNAi), and measuring gene expression at the mRNA level by qRT-PCR. Indeed, biological studies conducted on *C. elegans* might directly impact human diseases and development (O'Brien et al., 2004).

1.2.3 The Features of the *C. elegans*

C. elegans is a small nematode that generally measures approximately 1 mm in length. The fast life cycle of *C. elegans* allows scientists to obtain hundreds of progeny in a short period. Additionally, due to its small size, *C. elegans* is easy to handle in laboratory settings, which helps researchers to conduct experiments on entire organisms rather than just isolated cells.

This species has two sexes, males and hermaphrodites. Hermaphrodites can self-fertilize and produce up to 250–300 eggs (Gami et al., 2006). Males can be visually recognized under the microscope from their tails, which has a special hook-like form. *C. elegans* has a well-defined cellular structure that consists of 1,031 somatic cells in males and 959 in hermaphrodites (Corsi, 2006). Its transparency helps researchers use fluorescence confocal microscopy to image cells, tissues, and developmental processes in *vivo* (White et al., 1986). According to Yoshimura et al. (2019), *C. elegans* is a highly valuable laboratory organism, having been the first multicellular organism to have its whole genome sequenced in 1998 (*C. elegans* Sequencing Consortium, 1998). Indeed, *C.*

elegans has proven to be a great model organism in laboratory settings, providing critical insights into different human diseases such as diabetes, cancer, and Alzheimer's.

1.3 Oxidative Stress (OS)

Oxidative stress (OS) is a process that can occur when the body's capacity is unable to neutralize reactive oxygen species (ROS), which indicates an imbalance (increase) in the number of ROS compared to antioxidants, and this has been linked to several diseases and may generate damage to the cell (Pizzino et al., 2017). Lipid damage can happen via a process called lipid peroxidation which leads to the production of toxic byproducts that can damage cell membranes. DNA, specifically guanine, can be oxidized by ROS to become 8-oxo-guanine which may lead to DNA damage and mutations. As a result, these mutations can disrupt genetic function and can result in improper pairing of 8-oxo guanine and adenine during DNA replication (Andrés Juan et al., 2021). ROS can also directly change the function and structure of proteins by oxidizing amino acids like cysteine and methionine (Andrés Juan et al., 2021).

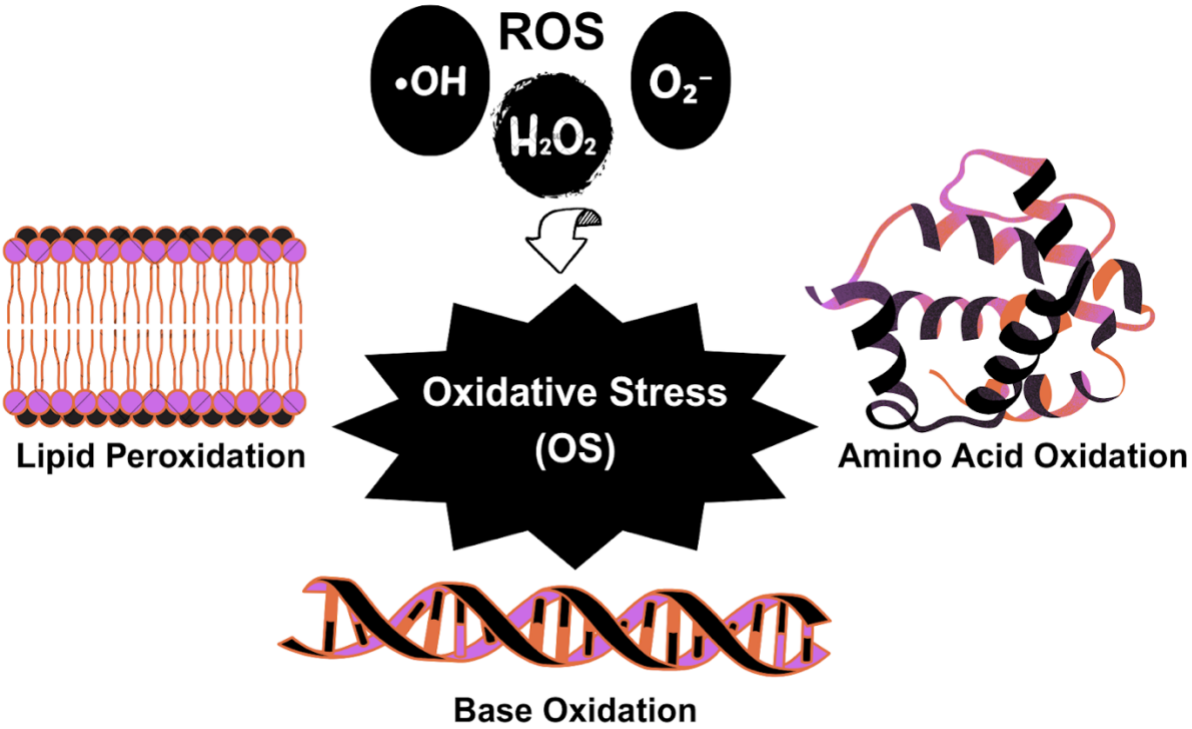

Figure 1.1: Reactive Oxygen Species (ROS) can Cause Cellular Damage. Reactive oxygen species, including hydrogen peroxide (H_2O_2), the hydroxyl radical (•OH), and the superoxide anion (O_2^-), contribute to oxidative stress when produced in excess, leading to damage of cellular components. Figure created using Canva.

1.3.1 ROS Generation and Detoxification

ROS can originate from both endogenous (internal) and exogenous (external) sources within the cell. ROS are primarily produced in the electron transport chain (ETC) of mitochondria and other compartments like the endoplasmic reticulum. Endogenous ROS generation can occur when the oxygen molecules interact with electrons that leak from the electron transport chain (ETC), while xenobiotic foreign compounds introduced into the body serve as a major exogenous source of ROS. When foreign molecules enter the cell, they go through a process called xenobiotic metabolism to help eliminate toxic compounds (Figure 1.2). The most common kinds of ROS that can be generated are superoxide ($\bullet O_2^-$), hydroxyl radicals (•OH), and hydrogen peroxide (H_2O_2) (Sato et al., 2013; Navarro-Yepes et al., 2014; Halliwell & Gutteridge, 2015).

In biology, ROS are important for survival and work as signalling molecules. They help macrophages remove bacteria from inside cells and regulate inflammation and healing (Martin & Barrett, 2002). However, if there is too much ROS, it can harm cells by damaging proteins, lipids, and DNA. As a result, a continued buildup of ROS can pose a serious risk to cellular health. Thus, it is essential to keep ROS levels in balance to maintain cellular homeostasis. Too much ROS can cause neurodegenerative diseases such as Parkinson's and Alzheimer's (Rodriguez et al., 2015). To maintain a balanced ROS level within the body, there are two important phases of detoxification enzymes that can balance ROS, referred to as Phase I and II. An example of a Phase I detoxification enzyme is superoxide dismutase (SOD), which the cell can use it to control ROS. An

example of Phase II detoxification enzymes is glutathione-S-transferase (GST), which the cell uses to neutralize glutathione.

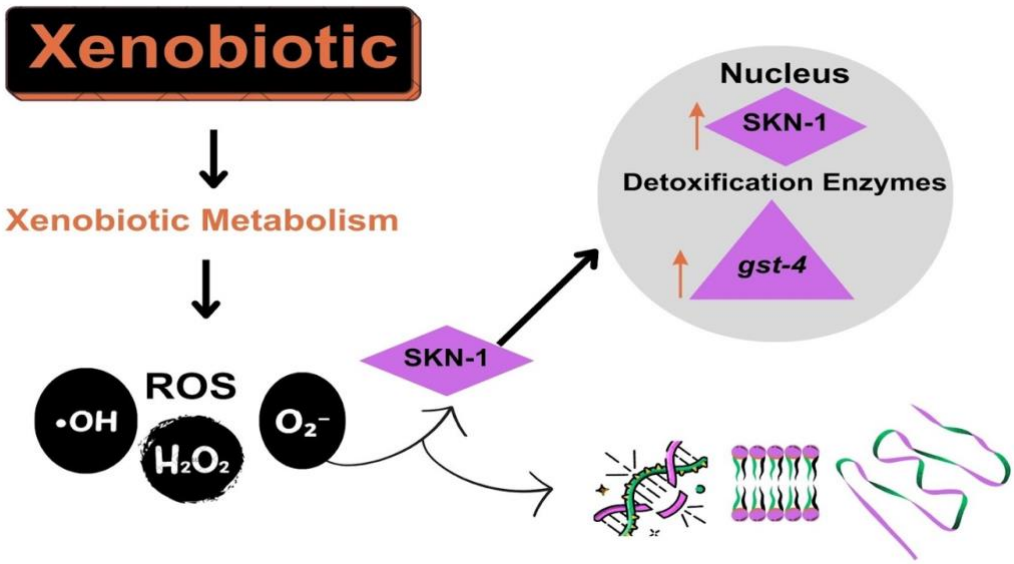

Figure 1.2: Exogenous Sources of Reactive Oxygen Species and Detoxification Pathways. Exogenous reactive oxygen species can be generated during mitochondrial oxidative phosphorylation as a consequence of xenobiotic metabolism, leading to the production of superoxide anions (O_2^-), hydrogen peroxide (H_2O_2), and hydroxyl radicals (•OH). Figure created using Canva.

1.3.2 Role of SKN-1 in Oxidative Stress Response

One important transcription factor involved in the defence against oxidative stress in *C. elegans* is the SKN-1 protein, which is an ortholog of the mammalian nuclear factor E2-related factor (Nrf) protein family (Kahn et al., 2008). Oxidative stress leads to phosphorylation and activation of SKN-1, causing it to translocate from the cytoplasm to the nucleus in *C. elegans* (Rafikova, 2020). SKN-1 binds to antioxidant response elements (AREs) found in the promoters of target genes (An & Blackwell, 2003). Numerous genes involved in detoxification, repair, and antioxidant defence are activated by this binding. For example, SKN-1 can control *gst-4* at its promoter once it enters the nucleus, which eventually raises the levels of *gst-4* expression (Hu et al., 2018). After that, GST-4 assists in balancing ROS levels and minimizing cell damage. Additionally, SKN-1 is crucial to the unfolded protein response (UPR) in *C. elegans*, a complex system of gene expression triggered by the formation of unfolded proteins in the Endoplasmic Reticulum (ER) (Glover-Cutter & Blackwell, 2013).

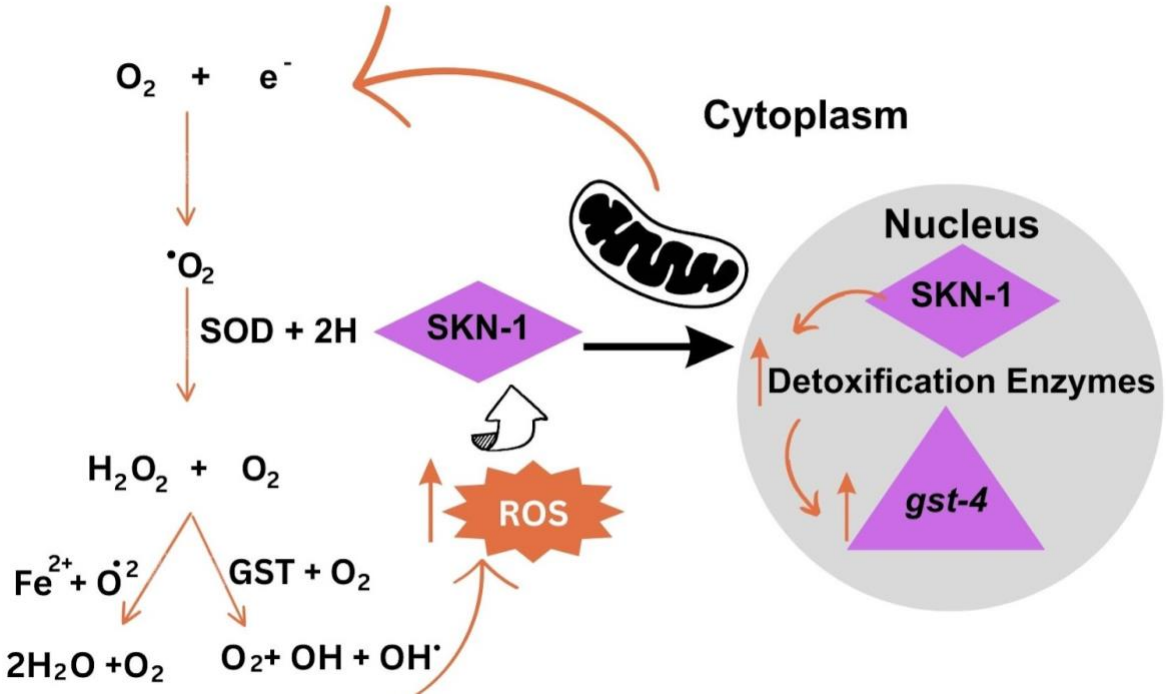

Figure 1.3: Role of SKN-1 in Oxidative Stress Response. The production of superoxide anion ($\bullet O_2^-$) is result from the extra electron in the mitochondrial electron transport chain during oxidative phosphorylation. ROS are converted by superoxide dismutase (SOD) into hydrogen peroxide (H_2O_2). The Hydrogen peroxide can make a highly reactive hydroxyl radical (OH•) in the presence of the transition metal, such as Fe2+. The high number of ROS can trigger the cytoplasmic SKN-1. This will decrease oxidative damage from it phosphorylates into the nucleus and upregulate genes that encode detoxification enzymes in this case is *gst-4* (created using Canva).

The phosphorylation of SKN-1 is controlled in the cell by a variety of signaling pathways. For example, glycogen synthase kinase-3 (GSK-3) phosphorylates SKN-1 to reduce its transcriptional activity (An et al., 2015). The p38 MAPK signaling pathway is essential for the activation of SKN-1 by promoting its nuclear translocation (Inoue et al., 2015). The phosphorylation status of SKN-1 is also regulated by insulin/IGF-1 signaling (Altintas, Park, & Lee, 2016) and AMP-activated protein kinase (AMPK). When AMPK is activated, SKN-1 is phosphorylated, which promotes its nuclear localization and the activation of stress-response genes (Blackwell et al., 2015). Under non-stressful conditions, SKN-1 activity is strongly regulated to maintain basal expression of stress response genes, whereas activation of SKN-1 under stress conditions stimulates the expression of genes that enhance stress resistance and longevity while repressing pathways associated with reduced lifespan. Many of these genes appear to be direct targets of SKN-1, as their promoters contain predicted SKN-1 binding sites (Oliveira et al., 2009). There are three functional isoforms of SKN-1: SKN-1A**,** SKN-1B, and SKN-1C (Blackwell et al., 2015). SKN-1A is the only isoform that contains a transmembrane domain and is attached to the endoplasmic reticulum (ER) membrane (Ruvkun & Lehrbach, 2023). In response to proteasome-related stress, SKN-1A translocates from the ER to the nucleus, where it activates genes that enhance proteasome function and restore cellular homeostasis (Lehrbach & Ruvkun, 2024). The digestive tract is the primary site of expression for SKN-1C, which is essential for protecting cells from environmental stimuli and oxidative damage (Tullet et al., 2008). SKN-1C also plays a crucial role in early embryonic development (Kormanik & Rothman, 2023). SKN-1B primarily functions as a nutritional sensor and regulates metabolic homeostasis (Oliveira et al., 2009).

1.3.3 Role of BRAP-2 in Oxidative Stress

BRCA1-associated protein-2 (BRAP-2) is a protein that was initially discovered as a BRCA1 interacting protein. Our laboratory characterized the *C. elegans* BRAP-2 ortholog and discovered that it is necessary to prevent larval arrest when exposed to high oxidative stress levels (Koon and Kubiseski, 2010). We showed that *brap-2(ok1492)* plays a crucial role in stress response. *C. elegans brap-2(ok1492)* mutants have enhanced production of Phase II detoxifying enzymes that are dependent on SKN-1 and PMK-1, a p38 MAPK ortholog of *C. elegans*. Since *brap-2* mutants have elevated levels of *gst-4* expression that is dependent on SKN-1, we used *brap-2(ok1492)* mutant worms for a transcription factor specific RNA-interference (RNAi) screen (Hu et al. 2017). Out of 912 tested clones, we identified 18 transcription factors that, when knocked down, resulted in decreased *gst-4* expression in *brap-2(ok1492)* mutant worms, which indicates that they may be required for *gst-4* expression. Among the candidates were two Nuclear Hormone Receptors, *nhr-49* and *nhr-14*. Both NHR-49 and NHR-14 share homology to the Hepatocyte nuclear factor 4α (HNF4α) found in humans.

1.4 Current Understanding of Nuclear Hormone Receptor Functions (NHR)

Hepatocyte nuclear factor 4α (HNF4α) is an orphan nuclear receptor that regulates numerous genes specific to hepatocytes (Walesky & Apte, 2015). HNF4α plays a critical role in lipid metabolism as well as in the development and function of the liver and pancreas (Doering et al., 2023).

A broad family of transcription factors known as nuclear hormone receptors (NHRs) is characterized by a highly conserved DNA-binding domain and structurally conserved ligand-binding domain (Sang et al., 2022). NHRs have similar molecular characteristics, such as a hinge region, a ligand-binding domain, an N-terminal activation domain, a DNA-binding domain, and an optional C-terminal F domain with an unidentified function (Doering et al., 2023; Sever & Glass, 2013; Weikum et al., 2018; Arao & Korach, 2021).

In addition to post-translational alterations in the ligand-binding domain, the ligand-binding domain binds ligands whose presence or absence can control NHR function (Doering et al., 2023; Berrabah et al., 2011). Transcriptional coregulators, such as coactivators and corepressors, which affect NHR transcriptional output, can also bind to the ligand-binding domain (Doering et al., 2023; Mouchiroud et al., 2014; Khan & Okafor, 2022; Scholtes & Giguère, 2022). The DNA-binding domain and ligand-binding domain are also involved in dimerization since NHRs can be homodimers, heterodimers, or monomers (Doering et al., 2023).

According to Antebi (2015) and Sang et al. (2022), *C. elegans* has 284 putative nuclear hormone receptor (NHR) genes. NHRs are known to regulate a wide range of biological processes, including physiology, metabolism, stress responses, aging, growth, development, and cellular proliferation (Doering et al., 2023). Multiple studies have demonstrated the critical roles of NHRs in key developmental pathways (Sang et al., 2022; Magner, 2013; Liang et al., 2010). Previous work from our laboratory identified NHR-49 as a pivotal regulator of the oxidative stress response in *C. elegans* (Hu et al.,

2018). NHR-49 modulates the expression of genes involved in both oxidative stress defense and fatty acid metabolism, playing an essential role in lipid homeostasis and protection against oxidative damage. Rajan et al. (2019) reported that NHR-14 influences iron absorption. Their findings showed that iron uptake increases upon *nhr-14* inactivation, suggesting that NHR-14 may regulate iron availability in *C. elegans*. However, despite its potential involvement in stress physiology, the role of NHR-14 in the oxidative stress response has not yet been characterized. This thesis examines the role of NHR-14 in oxidative stress regulation.

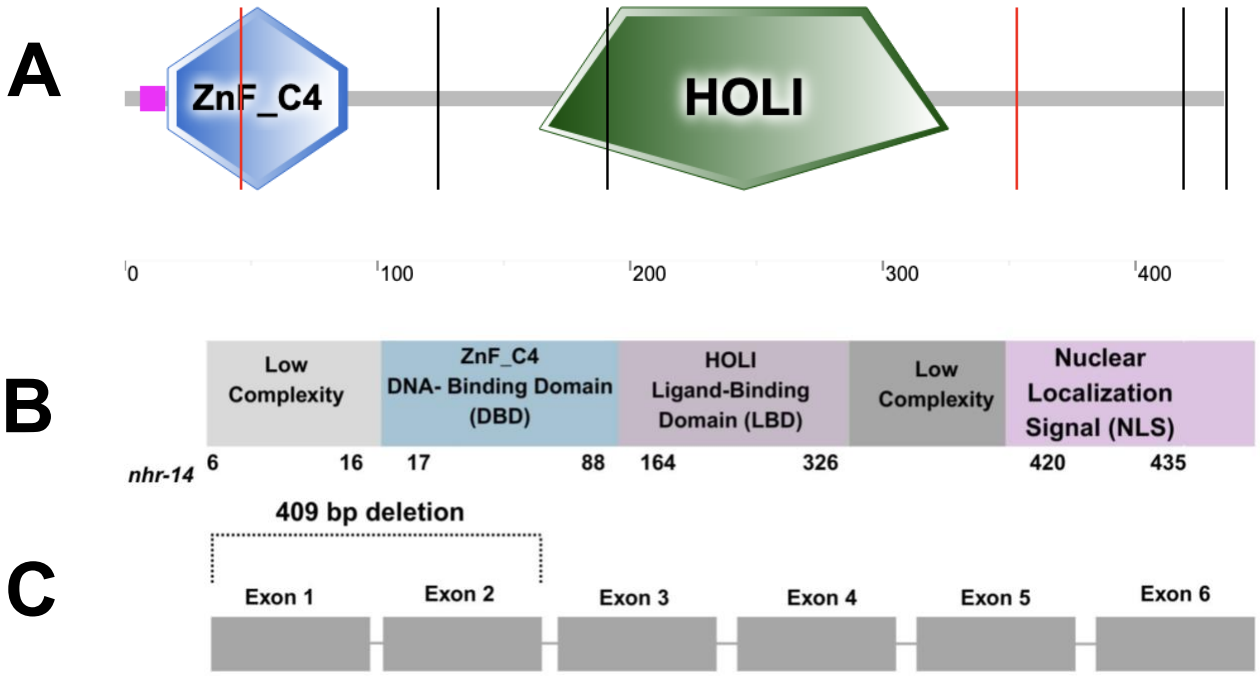

Figure 1.4: Structural and Genomic Features of NHR-14 *in C. elegans.* (A) The full-length NHR-14 protein comprises 435 amino acids (WormBase, 2022). Conserved domains include a C4 zinc-finger DNA-binding domain (ZnF_C4) spanning residues 17–88 and a hormone receptor ligand-binding domain (HOLI) located between residues 164–326. Domain architecture was visualized using the SMART database. **(B)** NHR-14 contains a DNA-binding domain (residues 17–88) composed of two C4-type zinc fingers that mediate sequence-specific binding to hormone response elements in DNA. The ligand-binding domain (residues 164–326) facilitates ligand recognition and receptor dimerization. A putative nuclear localization signal is present near the C-terminus (residues 420–435). Low-complexity regions are found at the N-terminus (residues 6–16) and within the central region (residues 312–330), which may contribute to protein–protein interactions. Transcript ID: T01B10.4a.1; Protein ID: NP_495342.1 (WormBase, 2022). **(C)** *The nhr-14* gene is located on Chromosome X and consists of six exons, with a coding sequence length of 1,308 bp (WormBase, 2022).

1.5 Cellular Signalling Pathways Involved in the *C. elegans* Oxidative Stress Response

Transcription factors (TFs) are crucial proteins that regulate gene expression by binding to specific DNA regions, such as promoters (Spitz & Furlong, 2012). Through this regulation, TFs play essential roles in key biological processes including metabolism, development, and immune responses, ensuring proper cellular signaling and function.

Disruptions in TF activity within cellular signaling pathways have been linked to a range of pathological conditions, including metabolic disorders, cancer, and neurological diseases (Vaquerizas et al., 2009). To preserve cellular homeostasis, TF activity is tightly regulated by complex signaling networks that dynamically modulate TF localization, stability, and transcriptional activity in response to both internal and external stimuli.

1.5.1 Insulin/Insulin-like Growth Factor (IGF)-1 Signaling (IIS) Pathway

The insulin-like signaling pathway plays a central role in regulating fat accumulation in *C. elegans* to maintain metabolic homeostasis (Murphy and Hu, 2018). Activation begins with the intrinsic tyrosine kinase activity of the insulin/IGF-1 receptor homolog DAF-2, which autophosphorylates and recruits the class I phosphatidylinositol (PI) 3-kinase complex (AGE-1 catalytic subunit and AAP-1 regulatory subunit) (Morris et al., 1996; Wolkow et al., 2002). PI3K catalyzes the conversion of membrane phosphatidylinositol bisphosphate (PIP2) into phosphatidylinositol trisphosphate (PIP3) (Narasimhan et al., 2009). PIP3 then recruits effector proteins containing pleckstrin homology (PH) domains to the plasma membrane, including 3-phosphoinositide-dependent protein kinase 1

(PDK-1), serum- and glucocorticoid-inducible kinase 1 (SGK-1), and the serine/threonine kinases AKT-1 and AKT-2 (Arcucci et al., 2021). Once activated, these kinases phosphorylate the FoxO transcription factor DAF-16, thereby excluding it from the nucleus and inhibiting its transcriptional activity. The lipid phosphatase DAF-18, a homolog of PTEN, serves as a negative regulator by dephosphorylating PIP3 back to PIP2.

Under conditions of reduced insulin-like signaling, unphosphorylated DAF-16 accumulates in the nucleus, where it activates transcriptional programs involved in lipid metabolism, including genes required for fatty acid synthesis and modification. Together, these mechanisms demonstrate the tight coupling between insulin-like signaling and the regulation of fat metabolism in *C. elegans* (Padmanabhan et al., 2009).

Polyunsaturated fatty acids (PUFAs), especially eicosapentaenoic acid (EPA), can function as signalling molecules that influence insulin signalling (An et al., 2023). *daf-2* signalling is downregulated in unfavourable environmental conditions, causing nematodes to enter a long-lived dauer diapause stage instead of continuing their development. During this phase, they store a significant amount of fat rather than using energy in their reproductive systems (Kimura, Riddle, and Ruvkun, 2011). In adult *C. elegans* with *daf-2* mutations, the fat content is significantly increased with stored triacylglycerols (TAGs) constituting the majority of this additional body fat (Ashrafi et al., 2003).

1.5.2 The RAS Signalling Pathway in *C. elegans*

The RAS/RAF/MEK/ERK signaling cascade, also known as the MAPK pathway, regulates fundamental cellular processes such as growth, survival, and differentiation, and plays a central role in both intracellular and intercellular communication (Degirmenci et al., 2020).

The Ras signaling pathway is not only essential for developmental processes like vulval induction but also plays a critical role in oxidative stress responses (Sundaram, 2013; Kishore et al., 2019). Elevated levels of reactive oxygen species (ROS), which are known to contribute to aging and cellular damage, can influence the activity of the Ras pathway and thereby impact stress response and lifespan regulation (Labuschagne & Brenkman, 2013; Kishore et al., 2019). Specifically, oxidative stress alters signaling through LET-60 (the *C. elegans* Ras homolog) and its downstream effector MPK-1 (a MAP kinase), which affects the organism's resistance to oxidative damage, as well as its overall cellular homeostasis and longevity (Kishore et al., 2019; Schieber & Chandel, 2014). A conserved regulatory relationship between growth signaling pathways and ROS management in *C. elegans* has been demonstrated through genetic manipulation of Ras pathway components, which has been shown to alter oxidative stress responses (Ewald et al., 2015; Labuschagne & Brenkman, 2013). For example, activation of MPK-1 signaling has been found to enhance resistance to oxidative stress, potentially by regulating the expression of antioxidant genes or stress-responsive transcription factors (Ewald et al., 2015). Furthermore, the nuclear localization and activity of transcription factors such as SKN-1, a key regulator of antioxidant responses in *C. elegans*, are influenced by changes in Ras pathway activity (Blackwell et al., 2015). Thus, the Ras-MAPK pathway acts as a

critical link between the control of cellular development and the oxidative stress response, ultimately affecting organismal survival under stressful environmental conditions (Kishore et al., 2019; Sundaram, 2013).

1.5.3 The SKN-1/Nrf2 Oxidative Stress Response Pathway

In *C. elegans*, the Nrf2/SKN-1 signaling pathway is a highly conserved mechanism critical for regulating detoxification, lifespan, cellular homeostasis, and adaptive responses to oxidative stress (Blackwell et al., 2015). Under non-stress conditions, the WD40 repeat protein WDR-23, a homolog of mammalian KEAP1, serves as a negative regulator of SKN-1 by sequestering it in the cytoplasm and targeting it for ubiquitin-mediated degradation, thereby limiting its transcriptional activity (Choe et al., 2009). However, upon exposure to reactive oxygen species (ROS), xenobiotics, or dietary restriction, SKN-1 is released from its inhibitory complexes, undergoes phosphorylation, and translocates into the nucleus (Inoue et al., 2005). Once inside the nucleus, SKN-1 binds to antioxidant response elements (AREs) in the promoter regions of its target genes, leading to the induction of a wide array of antioxidant and detoxification genes, including glutathione-S-transferase (*gst-4*), superoxide dismutases, catalases, and other Phase II detoxification enzymes (Oliveira et al., 2009; Park et al., 2009). In addition to detoxification, SKN-1 also promotes cellular defense by regulating genes involved in proteostasis, such as those encoding heat shock proteins and proteasomal components (Blackwell et al., 2015).

Additionally, metabolic and aging processes are closely related to the regulation of SKN-1. The activity of SKN-1 is negatively regulated by insulin/insulin-like growth factor-1 (IGF-

1) signaling through AKT kinases, which phosphorylate SKN-1, inhibiting its nuclear localization and transcriptional activity in nutrient-rich environments (Tullet et al., 2008). In contrast, the activation of SKN-1 is associated with increased longevity, and enhanced stress tolerance, making it a significant focus in aging research (Blackwell et al., 2015).

1.6 Rationale, Objectives and Hypothesis of Thesis

In *C. elegans*, oxidative stress responses are controlled by multiple transcription factors that control the expression of Phase I and Phase II detoxification genes to protect cells from damage caused by reactive oxygen species (ROS). The cellular defense system against oxidative stress primarily includes antioxidant enzymes such as superoxide dismutase (SOD), and glutathione S-transferase (GST), which work together to neutralize ROS and prevent cellular damage (Deponte, 2013). To investigate this protective mechanism, our laboratory previously demonstrated that *brap-2* mutant worms exhibit increased expression of *gst-4*, particularly under oxidative stress conditions. This observation led to the hypothesis that in the absence of BRAP-2, the transcription factor SKN-1 is then able to translocate to the nucleus, where it activates the expression of detoxification genes such as *gst-4* in response to oxidative stress.

This thesis is based on findings from a previous RNAi screen from our lab that screened 940 transcription factors in *C. elegans*. Using a *brap-2(ok1492)1;gst-4p::gfp* transgenic strain to monitor changes in stress-response gene expression, we were able to identify 20 novel candidates from the 940 TF RNAi library. One of them was NHR-14, which was

selected for further study due to its potential role in the oxidative stress response. This thesis, therefore, uses RNA-sequencing, gene expression, and survival assays to examine the role of NHR-14 in oxidative stress. My hypothesis is that NHR-14 is required for survival under oxidative stress conditions and functions as a transcriptional regulator that modulates specific genes and molecular pathways involved in the stress response.

The main objective of this thesis are to: (i) determine whether NHR-14 is required for survival under oxidative stress conditions, (ii) identify the genes regulated by NHR-14 using RNA-seq and qRT-PCR, and (iii) assess the biochemical consequences of *nhr-14(tm1473)* deletion on pathways predicted to be altered based on gene expression changes.

Chapter 2: Materials and Methods

2. Materials and Methods

This section presents a brief overview of the methods, materials and sources used in this thesis.

2.1 The Maintenance and Genetics of *C. elegans* Strains

All *C. elegans* strains used in this thesis were obtained from the National Bioresource Project (Tokyo, Japan) and the Caenorhabditis Genetics Center (CGC) at the University of Minnesota. Worms were cultured following the standard protocol established by Sydney Brenner (Brenner, 1974). A complete list of strains used in this thesis is provided in Table 9 in the Appendix. To maintain healthy populations, worms were transferred to freshly seeded Nematode Growth Medium (NGM) plates at least once a week. Transfers were performed either by selecting individual worms ("picking") or by transferring a small agar chunk containing a population of age-mixed worms ("chunking"). Both methods were conducted under clean conditions using flame-sterilized tools dipped in ethanol. All experiments were carried out at 20 °C using the N2 strain as the wild-type control.

2.2 Preparing *C. elegans* Nematode Growth Medium (NGM)

NGM was prepared weekly by dissolving 1.25 g peptone, 8.5 g agar, and 1.5 g NaCl in 500 mL of double-distilled water (ddH_2O). The mixture was autoclaved and then allowed to cool. Once sufficiently cooled, 0.5 mL of 1M $MgSO_4$, 0.5 mL of 1M $CaCl_2$, 0.5 mL of 5 mg/mL cholesterol (dissolved in ethanol), and 12.5 mL of 1M potassium phosphate buffer (pH 6.0) were added. The medium was poured into small and medium-sized sterile Petri dishes and allowed to dry overnight. Once dried, the plates were seeded with *E. coli*

OP50 under standard conditions, following the protocol established by Sydney Brenner (Brenner, 1974).

2.3 Preparing *Escherichia coli (E. coli)* OP50

The *E. coli* strain OP50 served as the food source for *C. elegans*. To prepare OP50, bacterial colonies were first streaked onto LB (lysogeny broth) agar plates. A single isolated colony was then picked using a sterile pipette tip and inoculated into a sterile flask containing 50 mL of LB broth. The culture was incubated at 37 °C for 16–18 hours in a shaking incubator. After incubation, the OP50 culture was stored at 4 °C and used over the following weeks to seed NGM plates for *C. elegans* maintenance.

2.4 Preparing M9 Buffer

M9 buffer was prepared by dissolving 6.0 g Na_2HPO_4, 3.0 g KH_2PO_4, 1.0 g NH_4Cl, and 0.5 g NaCl in distilled water to a final volume of 1 L, followed by autoclaving. The buffer was used for subsequent experiments as a control and for washing *C. elegans*.

2.5 Backcross and Genotyping

To eliminate unrelated background mutations in the *nhr-14(tm1473)* mutant strain, a backcrossing strategy was performed using the N2 strain. Male *him-5(e1490)* worms were first crossed with L2/L3 stage *nhr-14(tm1473)* hermaphrodites. Male progeny from this cross were then mated with L2/L3 stage N2 hermaphrodites. Individual progeny from this second cross were picked onto small NGM plates and considered P1 progeny. After being allowed to lay eggs, single F1 hermaphrodites were isolated and genotyped using single-worm PCR (SW-PCR) with primers specific to the *nhr-14(tm1473)* deletion (see

Appendix A, Figure S1 for a schematic of the cross). The primer sequences used for genotyping are listed in Table 10 in the Appendix. Worms confirmed to be homozygous for the *nhr-14(tm1473)* deletion were selected and used in subsequent experiments.

The *sod-3::gfp* strain was also backcrossed with the N2 strain using the same above approach (Appendix, Figure S3 for a schematic of the cross).

2.5 Generation of Transgenic Worms

To generate the *nhr-14(tm1473);gst-4::gfp* and *nhr-14(tm1473);sod-3::gfp*,, male *him-5(e1490)* worms were crossed with L2/L3 stage *gst-4::gfp* or *sod-3::gfp* hermaphrodites. *him-5::gfp* male progeny were identified under a fluorescence microscope and subsequently crossed with backcrossed L2/L3 stage *nhr-14(tm1473)* hermaphrodites. The resulting progeny from this cross were considered P1.

After allowing egg-laying on NGM plates, individual F1 hermaphrodites exhibiting GFP fluorescence were selected. These fluorescent F1 animals were allowed to self-fertilize, and the resulting F2 progeny were screened for GFP expression. Genotypes of individual GFP-positive worms were confirmed using single-worm PCR (SW-PCR) with primers specific to the *nhr-14(tm1473)* deletion. Primer sequences used for genotyping are listed in Table 10**.** Appendix A, Figure S2 illustrates a schematic of the *nhr-14(tm1473); gst-4::gfp* cross, and Figure S3 shows the *nhr-14(tm1473); sod-3::gfp* cross.

2.6 Single Worm – Polymerase Chain Reaction (SW-PCR)

To confirm the presence or absence of specific genetic mutations, SW-PCR was performed. Individual worms were transferred into 4 µL of Single Worm Lysis buffer in a 20 µL PCR tube. The lysis buffer was prepared by combining 10× ThermoPol buffer, proteinase K, and sterile-filtered water. Tubes were then stored at –80 °C overnight.

The following day, tubes were incubated in a thermocycler at 65 °C for 1 hour to digest the worm tissue, followed by a 15-minute incubation at 95 °C to inactivate proteinase K. After lysis, 20 µL of PCR master mix was added to each tube. The master mix for ten reactions consisted of 20 µL of 10× ThermoPol buffer, 20 µL of 2mM dNTPs, 1 µL of forward primer, 1 µL of reverse primer, 1 µL of Taq polymerase, and 157 µL of nuclease-free water. Genotyping was confirmed by gel electrophoresis, and PCR products were visualized under UV light to verify that the observed band sizes corresponded to the targeted mutations.

2.7 Worm Synchronization

To prevent variation, worms were synchronized to ensure age-matched populations for experiments. To achieve this, 5-7 young adult worms were placed on NGM plates to lay eggs. After allowing the worms to lay eggs for 6-7 hours, they were returned to their original plates. The eggs were then incubated for 62-65 hours under normal conditions. Over this period, the eggs hatched, and the worms reached the L4 stage and were ready for further experiments.

2.8 RNA Extraction and RNA Sequencing (RNA-seq) Analysis

For RNA extraction, worms were collected from 6 cm NGM plates by washing with 1 mL of M9 buffer. These plates had been chunked 62–65 hours earlier to allow the worms to reach the L4 stage. The worm suspension was transferred into microcentrifuge tubes and centrifuged for 1 minute. The pellet was washed three times with M9 buffer to remove bacteria. After the final wash, approximately 50 µL of the worm pellet was retained, and 250 µL of TRI Reagent (Zymo Research) was added immediately. The mixture was incubated overnight at -80 °C. On the day of extraction, following thawing, 250 µL of 100% ethanol was added, and the tube was vortexed thoroughly. The entire mixture was then transferred to a Zymo-Spin IC Column (Zymo R2060), and RNA extraction was performed according to the manufacturer's protocol. The concentration and purity of total RNA were measured using a Thermo Fisher NanoDrop 2000 spectrophotometer. The RNA samples were then sent to SickKids for sequencing.

2.9 Quantitative Reverse-Transcriptase PCR (qRT-PCR)

Complementary DNA (cDNA) synthesis was performed using the Thermo Scientific™ Maxima First Strand cDNA Synthesis Kit, according to the manufacturer's protocol. A cDNA synthesis reaction containing 5–8 worms (in 4 µL total volume) was prepared and placed in a thermal cycler step. The cDNA synthesis reaction mixture included oligo(dT) primers, random primers, 10mM dNTP mix, dsDNase, 5× RT buffer, 1 µL of Maxima Enzyme Mix, and nuclease-free water to bring the total volume to 20 µL per reaction. The samples were then stored at -80 °C for subsequent qRT-PCR analysis.

For the qRT-PCR, BlasTaq™ 2X qPCR MasterMix, distilled water, and specific primers (Table 8 in the Appendix) were mixed gently to measure the mRNA expression levels of different genes. Data from three separate trials were analysed using the ΔΔCT method. The N2 strain was used as a reference for standardizing the mRNA expression levels of the experimental strains, while the transcripts for *tba-1* and *act-1* were used as controls.

2.10 Confocal Microscopy and GFP Quantification

A total of 30-40 *gst-4p::gfp*, *nhr-14(tm1473);gst-4p::gfp, sod-3::gfp and nhr-14(tm1473);sod-3::gfp* worms were picked and placed on separate microscope slides for confocal microscopy analysis. To immobilize the worms and prevent movement, a bed of 2% agarose gel was placed onto the microscope slide, followed by addition of 2mM Levamisole. After mounting the worms on the slide, a coverslip was carefully placed on top. The Zeiss Observer Z1 Spinning Disk Confocal Microscope was then used to observe the fluorescent worms. Images were captured using the microscope's tiling, and ZEN 2.6 Software® was used for image analysis. The overall fluorescence of the worms was quantified using ImageJ software.

2.11 Oxidative Stress Assays

According to the method proposed by Ewald et al. (2017), oxidative stress assays were conducted using two different reagents: *tert*-butyl hydrogen peroxide (tBHP) and sodium arsenite (As). In both assays, synchronized L4-stage worms were used, and survival was assessed based on responsiveness to prodding. Three independent experiments were conducted, each in triplicate with 32 worms per trial per strain.

For the As assay, M9 buffer was used as the control group, while the experimental group was treated with 5mM As. L4 N2 and *nhr-14(tm1473)* mutant worms were picked and placed in a 24-well plate containing M9 buffer. The appropriate amount of As was added to the experimental group. Both groups of worms were observed hourly, and the number of living worms was recorded.

For the tBHP assay, 10mM tBHP plates were prepared one day prior to the experiment. To prepare the plates, 4 g of agar was dissolved in 100 mL of deionized water (ddH2O) and autoclaved. After cooling, 2.5 mL of phosphate buffer and 214 µL of tBHP liquid were mixed together and poured into 6 cm plates. These were left overnight at 20°C. On the day of the experiments, L4 *nhr-14(tm1473)* mutant and N2 worms were picked and transferred onto the unseeded tBHP plates (experimental group) and onto standard unseeded NGM plates (control group).

2.12 ER Stress Assay

An ER stress experiment was performed using dithiothreitol (DTT). All worms used were synchronized to the *L4* adult stage at 20 °C. One day prior to the experiment, 20mM DTT plates were prepared. To make the 20mM DTT solution, 0.308 g of DTT was dissolved in 99 mL of deionized water (ddH2O). For the agar medium, 4 g of agar powder, 0.17 g of NaCl, and 0.59 g of peptone were mixed. After autoclaving and cooling the agar, the 20mM DTT solution was added along with 2.4 mL of potassium phosphate buffer

(KH_2PO_4). The mixture was then poured into Petri dishes and stored at 20 °C for use the following day.

On the day of the experiment, L4 N2 and *nhr-14(tm1473)* mutant worms were transferred from regular plates to the DTT plates. The control were unseeded NGM plates without DTT. Worms were scored for survival every hour. A worm was considered dead if it did not respond to persistent prodding. Three independent experiments were conducted, each in triplicate with 32 worms per trial per strain. New plates were prepared before each experiment.

2.13 Thermotolerance Assay

After five hours of egg-laying, the L4 N2 and *nhr-14(tm1473)* mutant worms were returned to their original plates. The worms used were synchronized to the L4 adult stage at 20 °C. After reaching the L4 stage, both N2 and *nhr-14(tm1473)* mutant strains were placed on separate NGM plates for a heat test. These plates were then incubated at 37 °C. Every hour, the worms were observed, and those that did not respond to mild prodding with a worm pick were recorded as dead. Both strains were also grown on NGM plates at 20 °C as the control group. Three separate trials were conducted individually to gather data for analysis.

2.14 Longevity Assay

All worms were synchronized to the L4 adult stage at 20°C. Both N2 and *nhr-14(tm1473)* mutant worms were allowed to lay eggs and then removed (day 0). Hatched worms were monitored daily and transferred to fresh plates to avoid contamination, overcrowding, and

starvation until egg-laying stopped. Worms that crawled off the plates, dried out, burst, or disappeared were excluded from the sample. A worm was considered dead if it was unresponsive to constant prodding. Three independent experiments were conducted, each with three trials performed in triplicate.

2.15 Brood Size

To determine brood size, five pre-fertile young worms of each strain were placed on a single NGM plate. Worms were transferred to new NGM plates daily until offspring production stopped.

2.16 Oil Red O Staining for Lipid Quantification

According to the method described by Gerisch et al. (2020), Oil Red O staining was performed to assess lipid accumulation in *nhr-14(tm1473)* mutants and N2 worms. This method enabled both visualization and quantification of neutral lipid stores. Worms were stained following the standard protocol, and lipid levels were quantified using ImageJ software and normalized to N2 worm volume to allow comparison of relative lipid content between strains.

2.17 NHR-14 Fatty Acid Assay

Samples were synchronized and sent for analysis.

2.18 Generation of *nhr-14(tm1473);brap-2(ok1492)* Double Mutants

To produce *nhr-14(tm1473)*;*brap-2(ok1492)* worms, male *him-5(e1490)* mutants were crossed with L2/L3 stage *nhr-14(tm1473)* hermaphrodites. After three days, male *him-5*;*nhr-14(tm1473)* worms were selected under the microscope and crossed with L2/L3 *brap-2(ok1492)* hermaphrodites. Single progeny from this cross were picked onto small plates and designated as P1 progeny. The P1 worms were placed on NGM plates, where individual F1 hermaphrodites were allowed to lay eggs (Appendix, Figure S4 for a schematic of the cross). These F1 hermaphrodites were verified by single-worm PCR using primers specific to the deleted regions of *nhr-14(tm1473)* and *brap-2(ok1492)*. A list of primers used for genotyping used via SW-PCR is provided in Table 10. Worms identified as homozygous for the *nhr-14(tm1473)*;*brap-2(ok1492)* deletions were used for subsequent studies.

2.19 Primer Design

Primer3 and BLAST (NCBI) software were used to design primers for this thesis. Primer pairs were selected based on GC content, optimal melting temperature (T_m), and self-complementarity. Primers TK352 and TK353 were used to genotype the deletion mutants of *nhr-14(tm1473).*

2.20 Statistical Analysis

Figures and statistical analyses were generated using GraphPad Prism 8 software. Statistical tests were selected according to the data type and experimental design. For survival and longevity assays, significance was assessed using the log-rank (Mantel–

Cox) test. A p-value below 0.05 was considered statistically significant. Error bars indicate the standard error of the mean (± SEM). Survival data were further analyzed using the online survival analysis tool OASIS® (Yang et al., 2011).

2.21 Software and Tools Used

Throughout this thesis, various software and online tools were used for data analysis and figure generation. Statistical analyses and figure creation were performed using GraphPad Prism, while ImageJ (Fiji) was utilized to quantify Oil Red O staining and fluorescence microscopy images. RNA-seq data were processed using Galaxy, which facilitated quality control and differential gene expression analysis. Gene Ontology (GO) and KEGG pathway enrichment analyses were conducted with WormEnrichr, and protein domain prediction was performed using SMART. Schematic diagrams were created with Canva.

Chapter 3: Results

3. Results

3.1 *gst-4* Expression Levels Are Not Enhanced in Induced *nhr-14(tm1473)* Mutant Worms.

To test whether NHR-14 regulates *gst-4* expression under oxidative stress**,** we performed qRT-PCR on wild-type (N2) and *nhr-14(tm1473)* worms exposed to either 5mM sodium arsenite (As) for 2 h or M9 buffer (control). *gst-4* transcript levels were normalized to the reference gene *tba-1*. The condition was analyzed using three independent biological replicates, with technical triplicates for each sample. A significant increase in *gst-4* transcripts was observed after As treatment in N2 worms (***p*=0.0050). However, *nhr-14(tm1473)* after As treatment were not statistically significant relative to untreated controls (Figure 3.1A).

To further examine the effect of the *nhr-14(tm1473)* mutation on *gst-4* expression, we generated a transgenic strain expressing *gst-4p::gfp* in the *nhr-14(tm1473)* background, referred to as *nhr-14(tm1473);gst-4p::gfp*. Confocal microscopy was used to visualize GFP expression in both *nhr-14(tm1473);gst-4p::gfp* and *gst-4p::gfp* worms. Under basal conditions (M9 buffer treatment), GFP fluorescence did not differ significantly between the two strains. Following As treatment, *gst-4p::gfp* worms showed a significant induction of GFP (*****p* < 0.0001), whereas *nhr-14(tm1473);gst-4p::gfp* worms did not (Figures 3B–C).

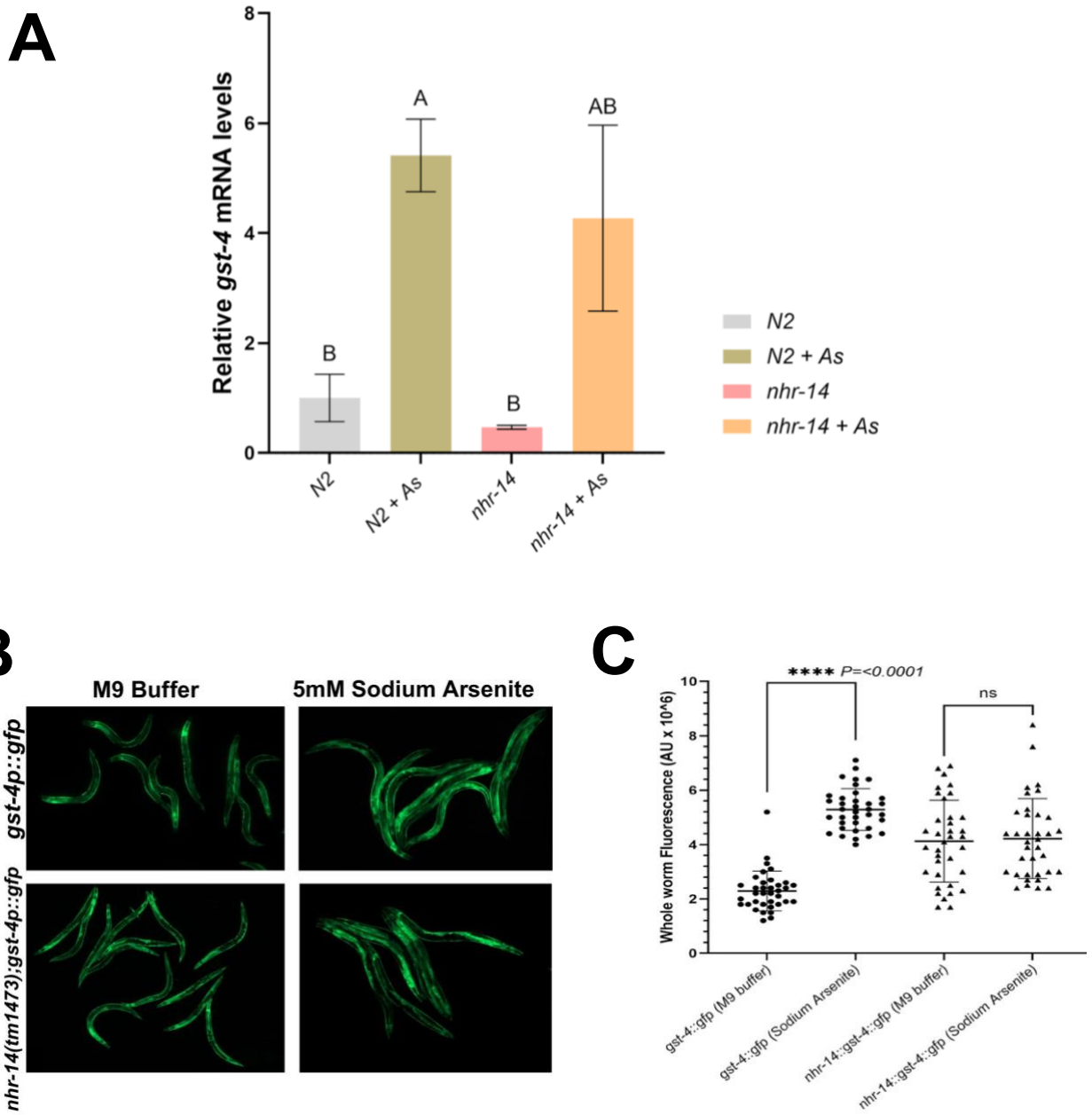

Figure 3.1*:***The Role of NHR-14 in *gst-4* Expression After Sodium Arsenite (As) Stress. (A)** mRNA expression levels of *gst-4* in presence of As, normalized to *tba-1.* The N2 was significant and ***p=0.0050*. Results were obtained from three independent trials. Different letters above bars indicate statistically significant differences between groups; bars sharing the same letter are not significantly different. The test used was Ordinary one-way ANOVA. **(B)** Fluorescence images of *gst-4::gfp* and *nhr-14(tm1473);gst-4p::gfp* transgenic worms exposed to 5 mM As or M9 buffer. **(C)** Quantification of whole-worm GFP fluorescence (arbitrary units ×10⁶) under control and As conditions. The compound As significantly increased GFP expression in N2 worms (****$p < 0.0001$), while there was no significant difference in *nhr-14(tm1473)* mutants (ns = not significant). A total of 32 worms were examined for each strain (n = 32). Error bars represent ± SEM.

3.2 The Loss of *nhr-14* Affects the Induced Expression of Detoxification Genes in the *sod* Family

After evaluating the role of NHR-14 in *gst-4* regulation, I next examined whether NHR-14 influences the expression of *sod* family genes. mRNA levels of *sod-1*, *sod-2*, and *sod-3* were quantified by qRT-PCR in N2 and *nhr-14*(*tm1473*). Worms were exposed to either M9 buffer (control) or As, with *tba-1* serving as the internal control. Under control conditions, no significant differences in *sod* gene expression were observed between N2 and *nhr-14*(*tm1473*) mutants, indicating that NHR-14 does not regulate these genes under basal conditions. Following As treatment, *sod-2* and *sod-3* mRNA levels were significantly reduced in *nhr-14*(*tm1473*) mutants compared to N2 worms, with an approximate 1.7-fold and 3-fold decrease in *sod-2* and *sod-3,* respectively *(**p* = 0.0011 for *sod-2*, ****p* = 0.0003 for *sod-3*) (n = 3 biological replicates). No significant effect was observed for *sod-1* (Figure 3.2A). These results suggest that NHR-14 positively regulates *sod-2* and *sod-3* expression during oxidative stress.

To discover this further, I wanted to visualize NHR-14 effect on *sod-3* expression, like how I analyzed *gst-4* expression. To do this, I generated a new transgenic worm line, *nhr-14(tm1473);sod-3p::gfp*, which carries the *nhr-14(tm1473)* deletion mutation along with the *sod-3::gfp* reporter. This allowed me to observe *sod-3* expression and compare it to *sod-3::gfp* expression in wild-type worms.

I first assessed basal *sod-3* expression levels by treating both strains with M9 buffer for two hours. In both the wild-type and *nhr-14(tm1473)* mutant, *sod-3* expression remained

low, with no significant difference. However, when I exposed the worms to arsenic (As) for 2 hours to induce stress, the *sod-3p::gfp* wild-type strain showed a significant increase compared to M9 control. Additionally, the *nhr-14(tm1473);sod-3p::gfp* strain showed a significant difference.

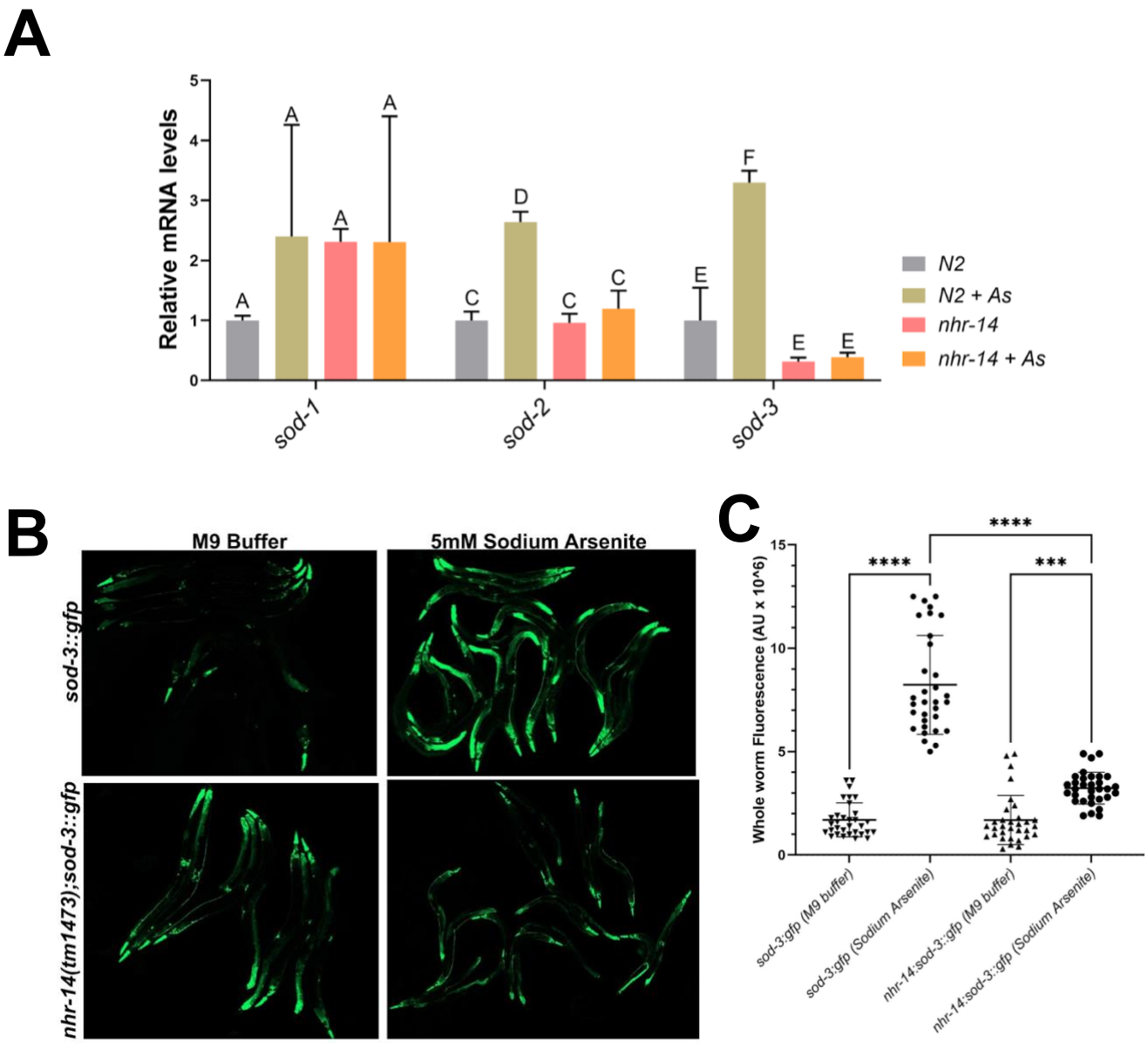

Figure 3.2: The Role of NHR-14 in *sod* Expression After Sodium Arsenite (As) Stress. (A) Relative mRNA levels of *sod-1, sod-2, and sod-3* in N2 and *nhr-14(tm1473)* mutant worms following exposure to 5 mM As or M9 buffer control for 2 hours. Expression was measured by qRT-PCR and normalized to *tba-1*. Data represent mean ± SEM of 3 biological replicates. Different letters above bars indicate statistically significant differences between groups (Ordinary one-way ANOVA*; **p* = 0.0011 *for sod-2, ***p* = 0.0003 *for sod-3*). **(B)** Fluorescence images of *sod-3::gfp* and *nhr-14(tm1473);sod-3::gfp* transgenic worms exposed to 5 mM sodium arsenite or M9 buffer. GFP fluorescence indicates expression from the *sod-3* reporter transgene. **(C)** Quantification of whole-worm GFP fluorescence (arbitrary units ×10⁶) under control and sodium arsenite conditions. Sodium arsenite significantly increased GFP expression in wild-type worms *(****p* < 0.0001*)*. A total of 32 worms were examined for each strain (n = 32).

3.3 NHR-14 Selectively Regulates Certain Detoxification Genes in Phase II and Non-Phase II Genes.

After confirming that NHR-14 positively regulates the induced expression of *sod-3* and *gst-4* levels, I next measured the mRNA expression levels of several Phase II and non-Phase II detoxification genes using qRT-PCR. The genes measured were *gcs-1*, *sdz-8*, *ugt-10*, *ugt-13* (Phase II), and *ctl-1*, *fmo-1*, *mtl-1* (non-Phase II), in both N2 and *nhr-14(tm1473)* mutant worms. Gene expression was measured with and without As treatment and normalized to the housekeeping gene *tba-1 for all genes*. Under control conditions (M9), there were no significant differences in *gcs-1*, *sdz-8*, *ugt-10*, *ugt-13* (Phase II) or *ctl-1*, *fmo-1*, *mtl-1* (non-Phase II) between N2 and *nhr-14(tm1473).* However, after As treatment, *nhr-14(tm1473)* mutants showed significantly reduced expression of *gcs-1* (Phase II) and *ctl-1* (non-Phase II) compared with N2 worms (*gcs-1*: ***p = 0.0009; *ctl-1*: **p = 0.0017; n = 3 biological replicates) (Figure 3.3A: non-Phase II genes and Figure 3.3B: Phase II genes). mRNA levels suggest NHR-14 contributes to induction of *gcs-1* and *ctl-1* upon As treatment.

An interesting finding among the Phase II genes was the expression of *ugt-13*. In *nhr-14(tm1473)* mutants, baseline (M9) levels were higher than after As treatment (*p = 0.0382), suggesting a complex regulation.

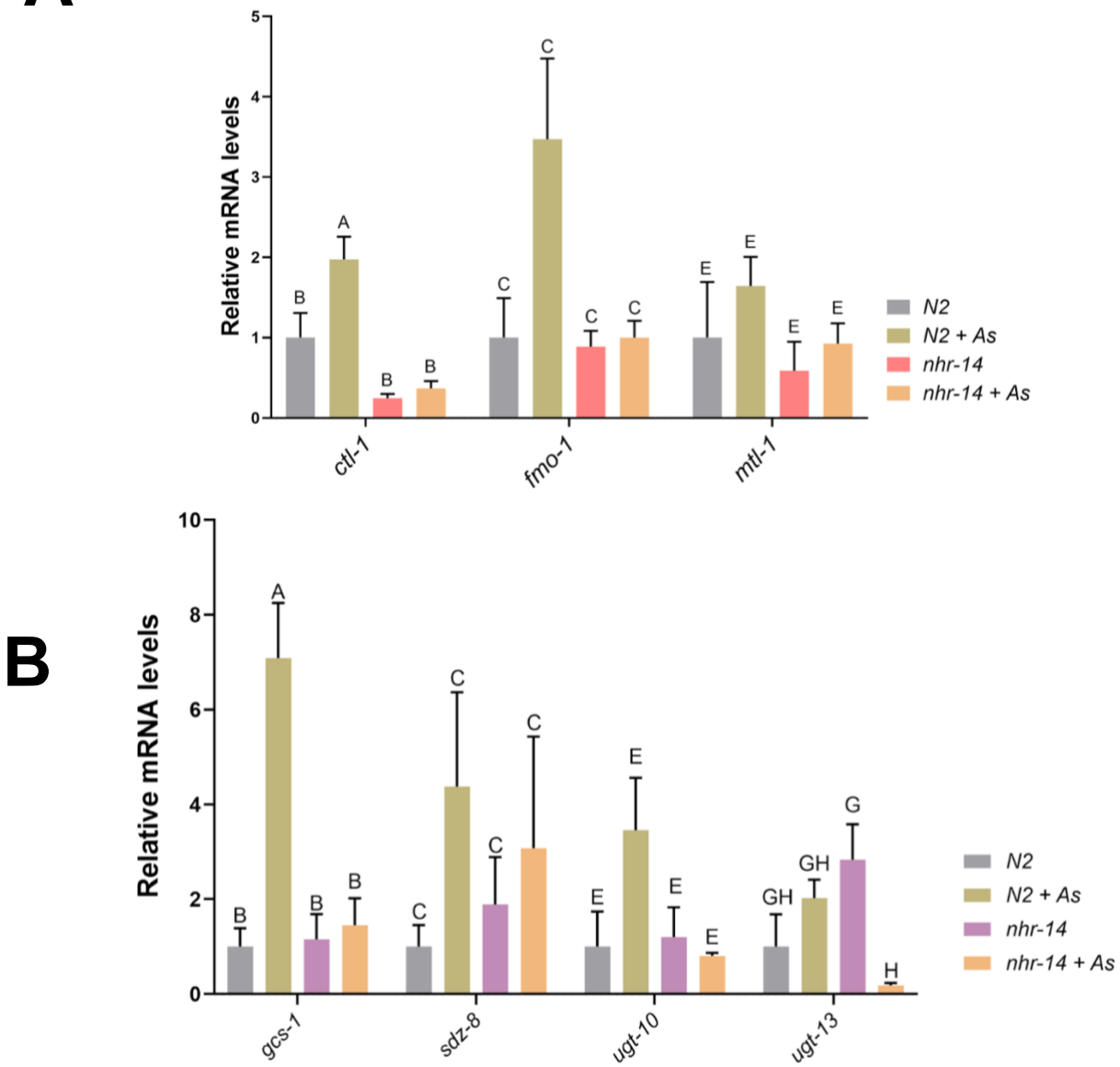

Figure 3.3: mRNA Expression Levels of Phase II and non-Phase II Detoxification Genes in Response to Sodium Arsenite (As) in N2 and nhr-14(tm1473) Mutants. **(A)** mRNA expression levels of non-Phase II genes (*ctl-1*, *fmo-1*, *mtl-1*). *ctl-1* was significantly decreased in the *nhr-14(tm1473)* compared to N2 after As (***p* = 0.0017). **(B)** mRNA expression levels of Phase II genes (*gcs-1*, *sdz-8*, *ugt-10*, *ugt-13*). *gcs-1* expression was significantly decreased in the nhr-14(tm1473) compared to N2 after As (****p* = 0.0009), whereas *ugt-13* expression significantly decreased following As exposure in *nhr-14(tm1473)* compared to M9 control (**p* = 0.0382). N2 and *nhr-14(tm1473)* mutant worms were treated with 5 mM As or M9 buffer control for 2 hours at the young adult stage. Gene expression was normalized to *tba-1* and represents the mean of three independent biological replicates. Statistical comparisons within

3.4 *nhr-14(tm1473)* Mutants are More Susceptible to Oxidative Stress, Endoplasmic Reticulum (ER) Stress, and Heat Stress

After examining how Phase I and Phase II detoxification genes are involved in the absence of *nhr-14(tm1473)*, I decided to determine if NHR-14 is necessary for the stress response in *C. elegans*. I performed two different oxidative stress assays, one ER stress assay, and a 37°C heat stress assay to test the biological function that NHR-14 might have in *C. elegans*.

The first oxidative stress assay was a tert-butyl hydroperoxide (tBHP) assay. Agar plates containing 10mM tBHP were prepared a day before the experiment, and on the day of the experiment, both N2 worms and *nhr-14(tm1473)* mutants were placed on these unseeded plates. Worms were recorded every hour, and those that did not respond to prodding were considered dead. Figure 3.4A represents one trial; the Kaplan–Meier survival plot shows that N2 worms (black line) survived longer than the *nhr-14(tm1473)* mutants (red line) (log-rank test, ***p = 0.0003; median survival: N2 = 5 h, *nhr-14(tm1473)* = 4 h; n = 36 biological replicates per trial).

The second oxidative stress assay that I performed was with sodium arsenic (As). On the day of the experiment, M9 buffer was added to a 24 well plate, and then a 5mM As solution was prepared and added to six wells containing the solution, three for *nhr-14(tm1473)* mutants and three for N2 worms. This assay was performed in three independent trials. One trial is presented in Figure 3.4B, which shows that N2 worms (black line) survived longer in the As solution compared to *nhr-14(tm1473)* mutants (red line). N2 worms

reached 50% mortality by hour 3, whereas mutants reached 50% mortality by hour 1 (log-rank test, ****p = 0.0001; n = 36 biological replicates). All worms in M9 buffer controls remained alive throughout the experiment.

Following these oxidative stress assays, I performed an endoplasmic reticulum (ER) stress assay using dithiothreitol (DTT). Agar plates containing 20mM DTT were prepared and worms were scored every hour. Figure 3.4C represents one trial. The Kaplan Meier survival plot shows that N2 worms (black line) again survived longer than the *nhr-14(tm1473)* mutants (red line). N2 worms reached 50% mortality by hour 3, whereas mutants reached 50% mortality by hour 1 (log-rank test, ****p= < 0.0001; n = 36 biological replicates). Worms on NGM control plates remained alive throughout the experiment. Worms exposed to DTT also showed distinct morphological changes, becoming shrunken, and exploding when touched with a worm pick.

Following the ER stress assay, I performed a heat assay to further assess the biological role that NHR-14 might play in *C. elegans*. I started with the heat assay using regular NGM seeded plates and placed both *nhr-14(tm1473)* mutants and N2 worms on these plates, then exposed them to 37°C. For the control, the plates were kept at room temperature. The number of living worms was counted, and all worms were observed and probed every hour to determine if they were alive. There was a significant difference between the N2 and *nhr-14(tm1473)* mutants. Figure 3.4D shows N2 worms (black line) again survived longer than the *nhr-14(tm1473)* mutants (red line). N2 worms reached 50% mortality by hour 5, whereas mutants reached 50% mortality by hour 4 (log-rank test,

***p* = 0.0016; n = 36 biological replicates). Worms on seeded NGM control plates remained alive throughout the experiment at room temperature.

For all above experiments, data from three separate experiments were used for analysis. Tables 3, 4, 5, and 6 in the Appendix contain statistical analyses for each of the three biological replicates used respectively. These results indicate that *nhr-14(tm1473)* mutants show a higher susceptibility than N2 WT.

Next, I decided to measure the mRNA level of *hsp-16.2* using qRT-PCR because of its role in responding to heat shock and stress, as well as its ability to bind to unfolded proteins. I measured mRNA levels in both N2 and *nhr-14(tm1473)* mutant worms treated with either M9 buffer or As and normalized the results to the housekeeping gene *tba-1*. Under control (M9) conditions, no significant differences were observed in *hsp-16.2* mRNA levels between N2 and *nhr-14(tm1473)* mutants, indicating that NHR-14 does not influence *hsp-16.2* expression under non-stressed conditions. However, following As treatment, *hsp-16.2* mRNA levels were significantly reduced in *nhr-14*(tm1473) mutants compared to N2 worms after As treatment (*****p* < 0.0001); (Figure 3.5). This helps us understand that NHR-14 functions as a positive regulator of *hsp-16.2* expression during oxidative stress. The failure of *nhr-14(tm1473)* mutants to induce *hsp-16.2*, along with their decreased heat survival, shows that functional NHR-14 plays a crucial role in the heat stress response through *hsp-16.2* expression and enhancing survival under stress.

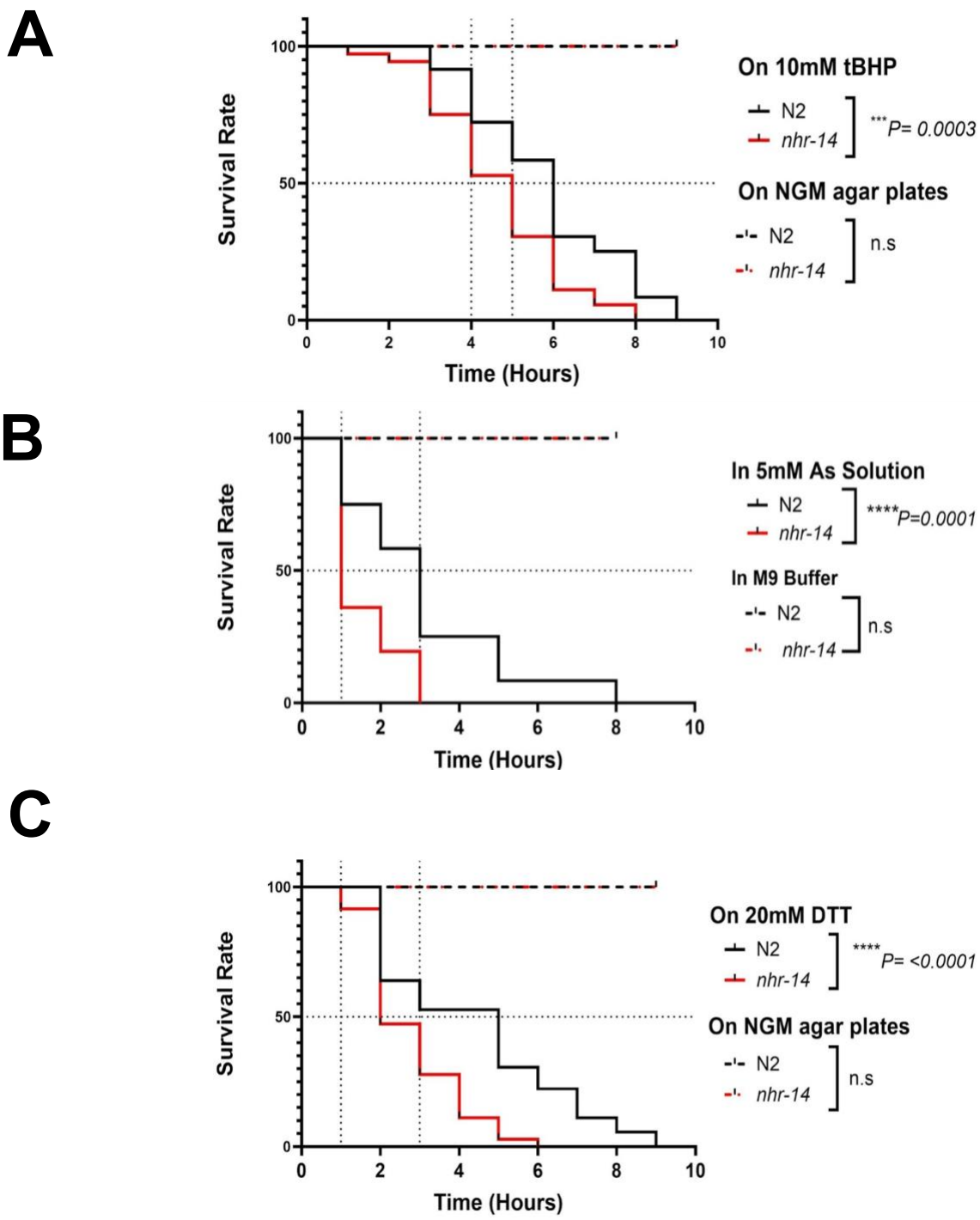

See figure caption on next page.

D

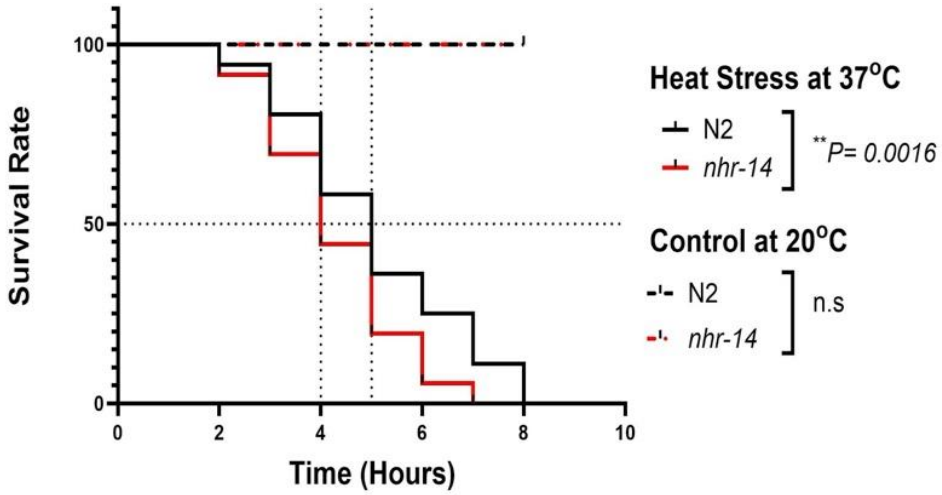

Figure 3.4: *nhr-14(tm1473)* Mutants Show Lower Survival Rate to Oxidative, ER, and Heat Stress Compared with N2. (***A)*** Survival plot of the tert-butyl hydroperoxide (tBHP) assay comparing *nhr-14(tm1473)* mutants (red line) to N2 (black line) on 10mM tBHP agar plates. Regular NGM plates were used as a control. Three independent trials were performed with a sample size of 36 worms for each strain (n = 36). N2 median survival was five hours and survived eight hours total. *nhr-14(tm1473)* mutant median survival was four hours and survived five hours total. ****p* = 0.0003 Statistical details presented in Table 3 in the appendix. **(B)** Survival plot of the sodium arsenic (As) assay comparing *nhr-14(tm1473)* mutants (red line) to N2 worms (black line) in 5mM As solution. M9 buffer served as a control. Three independent trials were performed with a sample size of 36 worms for each strain (n = 36). N2 median survival was three hours and survived 8 hours total. *nhr-14(tm1473)* mutant median survival was one hour and survived three hours total. *****p* = 0.0001 Statistical details presented in Table 4 in the appendix. **(C)** Survival plot of the dithiothreitol (DTT) assay comparing *nhr-14(tm1473)* mutants (red line) to N2 (black line) on 20mM DTT agar plates. Regular NGM plates were used as a control. Three independent trials were performed with a sample size of 36 worms for each strain (n = 36). N2 median survival was three hours and survived five hours total. *nhr-14(tm1473)* mutant median survival was one hour and survived two hours total. *****p*= < 0.0001**.** Statistical details presented in Table 5 in the appendix. **(D)** Survival plot of the heat stress assay comparing *nhr-14(tm1473)* mutants (red line) to N2 (black line) at 37°C. Both strains were placed on regular NGM seeded plates. Three independent trials were performed with a sample size of 36 worms for each strain (n = 36). N2 median survival was five hours, whereas *nhr-14(tm1473)* mutant median survival was four hours. ***p* = 0.0016**.** Statistical details presented in Table 6 in the appendix.

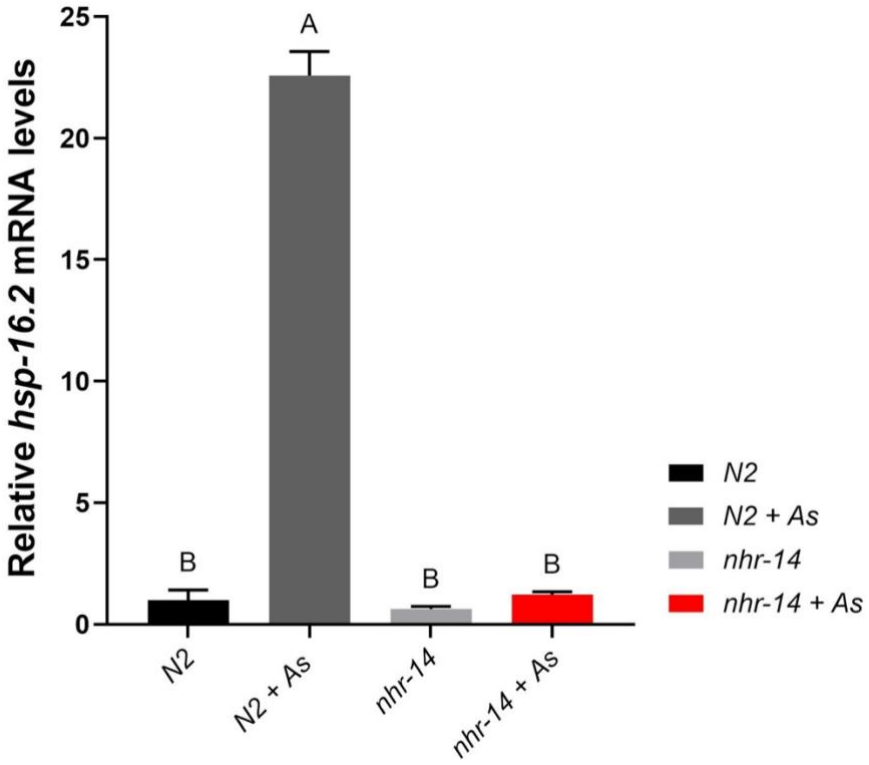

Figure 3.5: mRNA Expression Levels of Relative *hsp-16.2* in Response to Sodium Arsenite (As) in N2 and *nhr-14(tm1473)*. The expression was normalized to *tba-1* and was measured in N2 and *nhr-14(tm1473)* worms with and without 5 mM As. Three independent trials were performed. N2 worms exposed to As showed an increase in *hsp-16.2* expression *(****p < 0.0001)*, while *nhr-14(tm1473)* mutants failed to significantly induce expression. Data are presented as mean ± SEM. Statistical significance was determined using Ordinary one-way ANOVA. Bars labeled with different letters indicate statistically significant differences.

3.5 NHR-14 is Required for Brood Size and Longevity

To better understand the biological role of NHR-14 in *C. elegans*, I decided to measure how the *nhr-14(tm1473)* mutation affects reproduction and longevity by measuring brood size and life span.

For the brood size assay, five synchronized L1-stage worms from both N2 and *nhr-14(tm1473)* strains were individually placed on NGM plates. The total number of progenies produced by each worm from both strains was counted daily. *nhr-14(tm1473)* mutants produced an average of 190 progenies which significantly fewer progenies than N2 worms, which the average was 258 progenies indicating a reduced brood size (***p* = 0.0010); (Figure 3.6). These results suggest that NHR-14 is important for normal fertility function in *C. elegans.*

The next experiment I performed was a longevity assay to evaluate the effect of NHR-14 on lifespan. Worms were monitored daily, and those that failed to respond to prodding were considered as dead. Kaplan–Meier survival analysis shows a significant difference in lifespan between the two strains (****p= < 0.0001); (Figure 3.7). The median lifespan of N2 worms was 21 days, with 100% mortality by day 28. In contrast, *nhr-14(tm1473)* mutants had a median lifespan of 10 days and reached 100% mortality by day 15. A total of 36 worms were examined in this trial. Three independent biological replicates were performed, with combined statistical results summarized in Table 7 (Appendix). Together, these findings demonstrate that NHR-14 is required for normal lifespan in *C. elegans.*

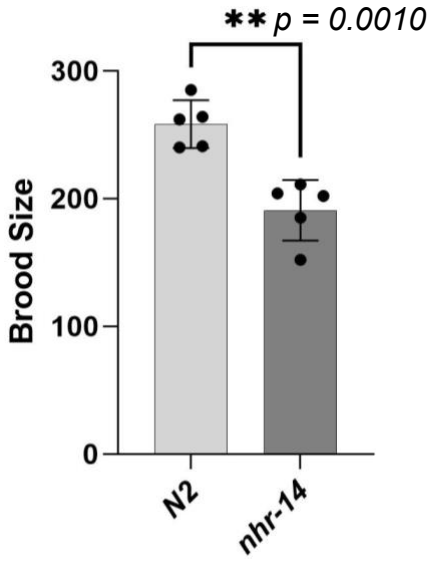

Figure 3.6: Brood Size Analysis of *nhr-14(tm1473)* Mutant Worms Compared to N2. The average brood size of individual *nhr-14(tm1473)* mutants is significantly lower than seen with N2 worms. Data represent mean ± SEM from five worms (n = 5 worms per groups). Statistical significance was determined by unpaired t-test *(**p* = 0.0010).

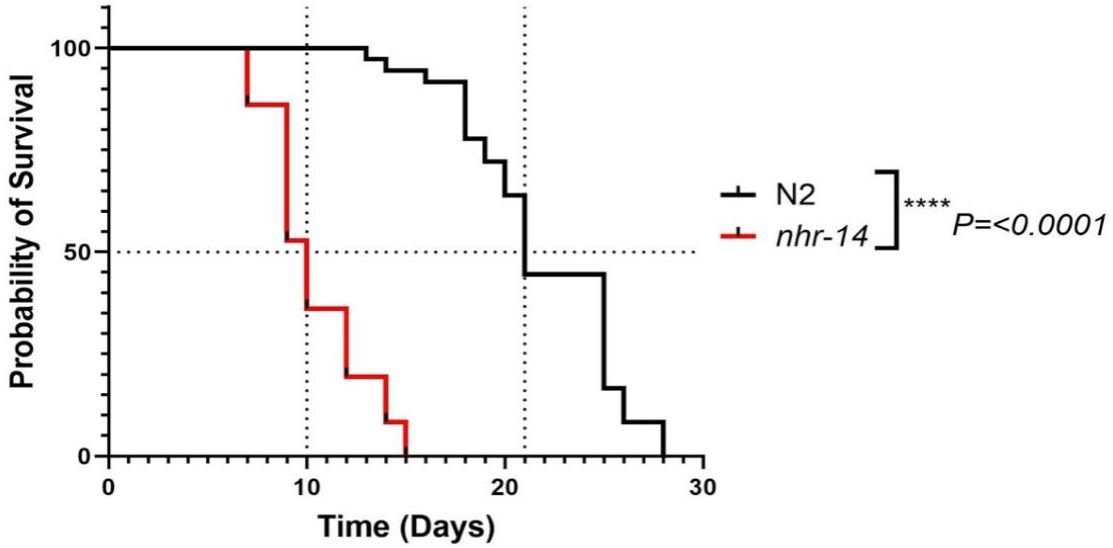

Figure 3.7: Reduced Lifespan in *nhr-14(tm1473)* Mutants Compared with N2. Survival curves representing the lifespan of *nhr-14(tm1473)* mutants (red line) and N2 worms (black line). Three independent trials were performed with a sample size of 36 worms for each strain (n = 36). The median lifespan of N2 worms was 21 days, with complete mortality by day 28. *nhr-14(tm1473)* mutants had a median lifespan of 10 days and reached 100% mortality by day 15. The longevity functions were estimated using the Kaplan–Meier method, and significance was assessed using the log-rank (Mantel-Cox) test. ****p = < 0.0001**.** Statistical details presented in Table 7 in the appendix.

3.6 NHR-14 Enhances Fatty Acid Metabolism Through Regulation of Lipid Degradation Genes

Since NHR-14 influences both Phase II and non-Phase II detoxification genes, and to better understand the baseline molecular function of NHR-14, I set out to determine what NHR-14 genes regulate more. To investigate this, I performed transcriptome (RNA-seq) analysis comparing *nhr-14(tm1473)* mutants to N2 worms.

After RNA extraction, The RNA-seq analysis showed that 233 genes were upregulated and 842 were downregulated in the *nhr-14(tm1473)* mutants compared to N2. Gene Ontology (GO) analysis of biological processes, cellular components, and molecular functions for both upregulated and downregulated genes was obtained using WormEnrichr (Figure 3.8A, B, C, D, E, and F). In addition, transcription factor enrichment analysis in *nhr-14(tm1473)* mutants (Figure 3.9A and B), shows a significant enrichment of NHR-49 and SKN-1 target genes among the differentially expressed genes in *nhr-14* mutants in the upregulated genes (Figure 3.9B).

KEGG pathway enrichment analysis (Figure 3.10A and B) demonstrated differential involvement of gene sets in various biological processes. Upregulated genes were enriched in pathways related to homologous recombination, non-homologous end-joining, and mRNA surveillance, indicating increased expression of genes involved in DNA repair and stress responses. In contrast, downregulated genes were enriched in pathways such as fatty acid degradation, branched-chain amino acid degradation, and fatty acid biosynthesis, suggesting suppression of genes involved in lipid metabolism and

amino acid catabolism. These results suggest a key role for NHR-14 in regulating metabolic processes.

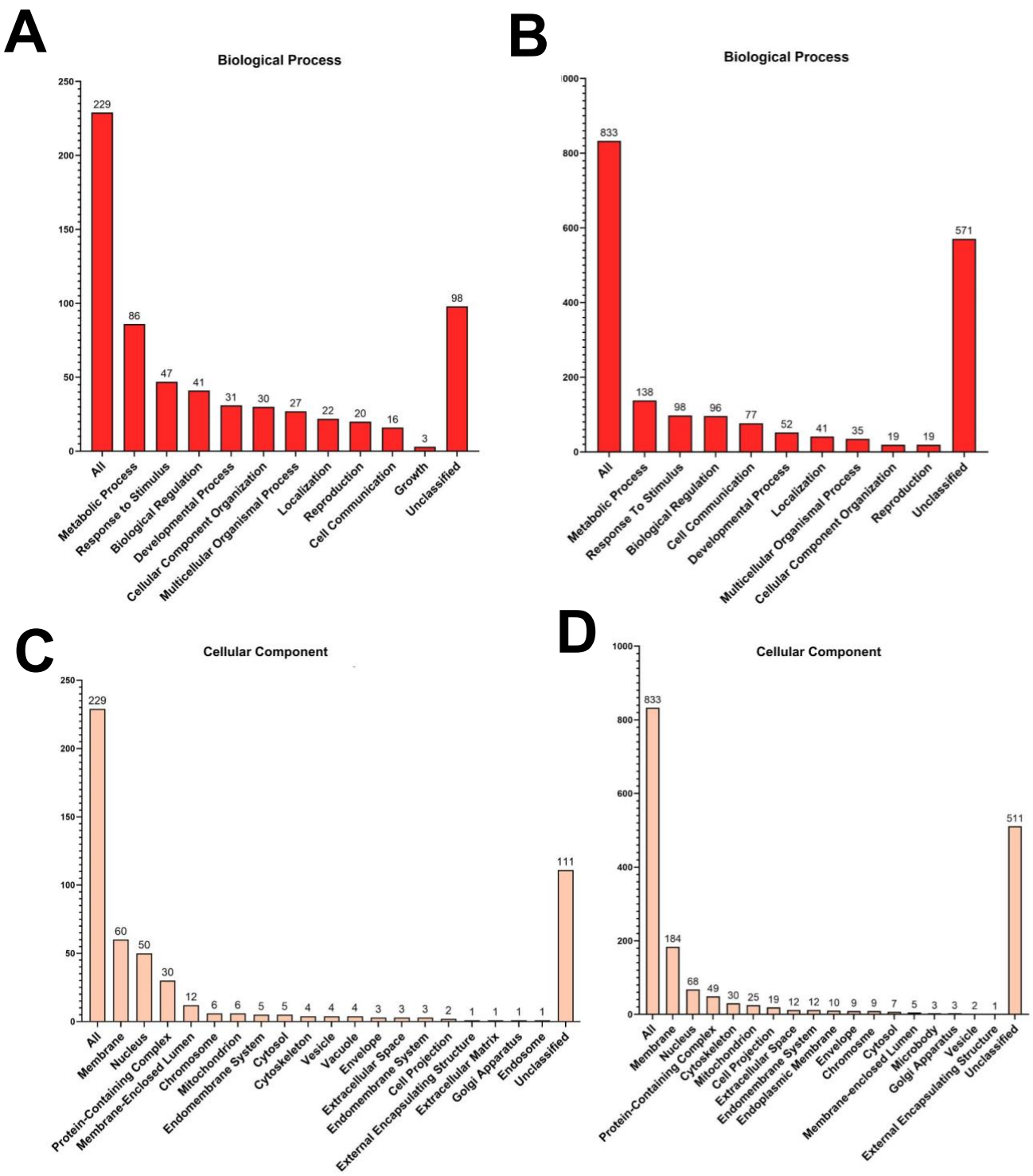

See figure caption on next page.

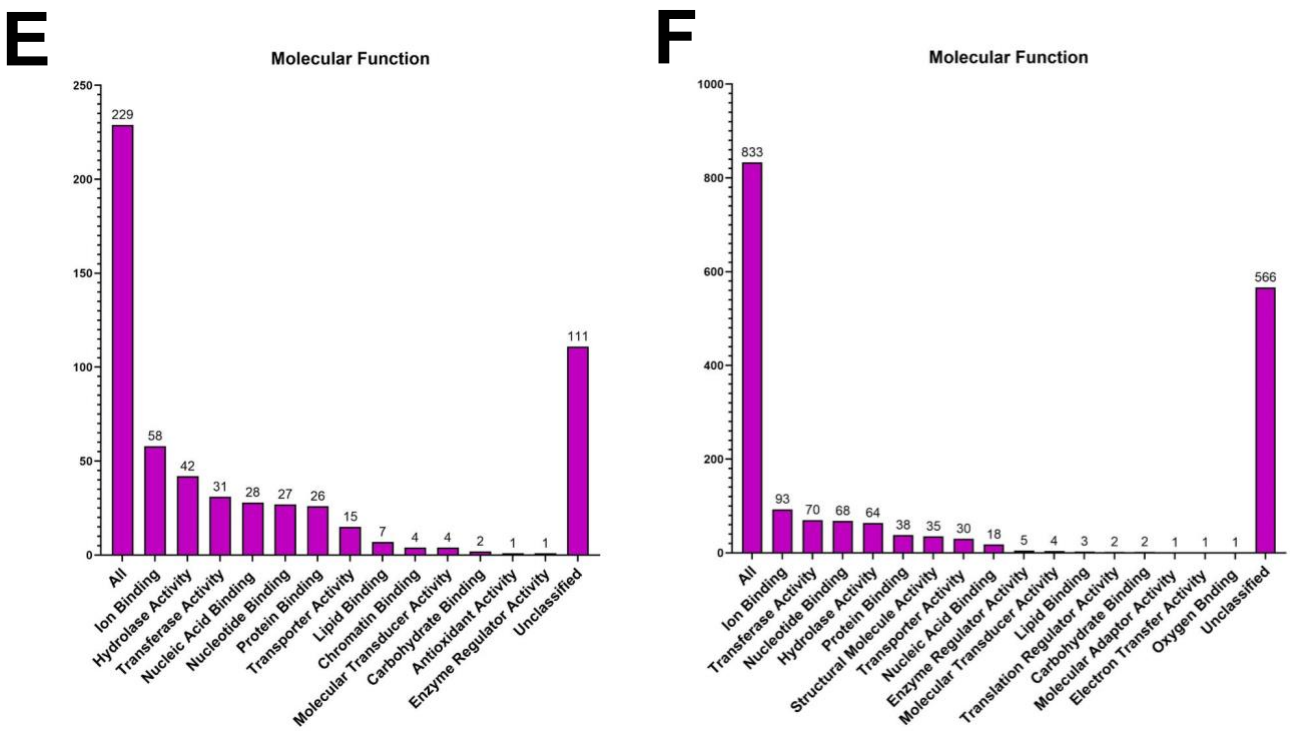

Figure 3.8: Gene Ontology (GO) Annotation Analysis of Upregulated and Downregulated Genes in *nhr-14(tm1473)* Mutants Compared to N2 Under Normal Conditions using WebGestalt. The analysis covers Biological Process **(A, B)**, Cellular Component **(C, D)**, and Molecular Function **(E, F)** categories for upregulated and downregulated genes, respectively. The y-axis represents the number of genes assigned to each GO category, while "Unclassified" refers to genes that could not be associated with any GO term. Genes that were upregulated or downregulated were strongly linked to metabolic processes and membrane-related functions. However, the greater number of downregulated genes indicates that *nhr-14* mostly functions as a transcriptional activator, enhancing the expression of numerous structural and metabolic genes. Genes essential for molecular binding activities and cellular metabolism are suppressed when *nhr-14(tm1473)* is absent.

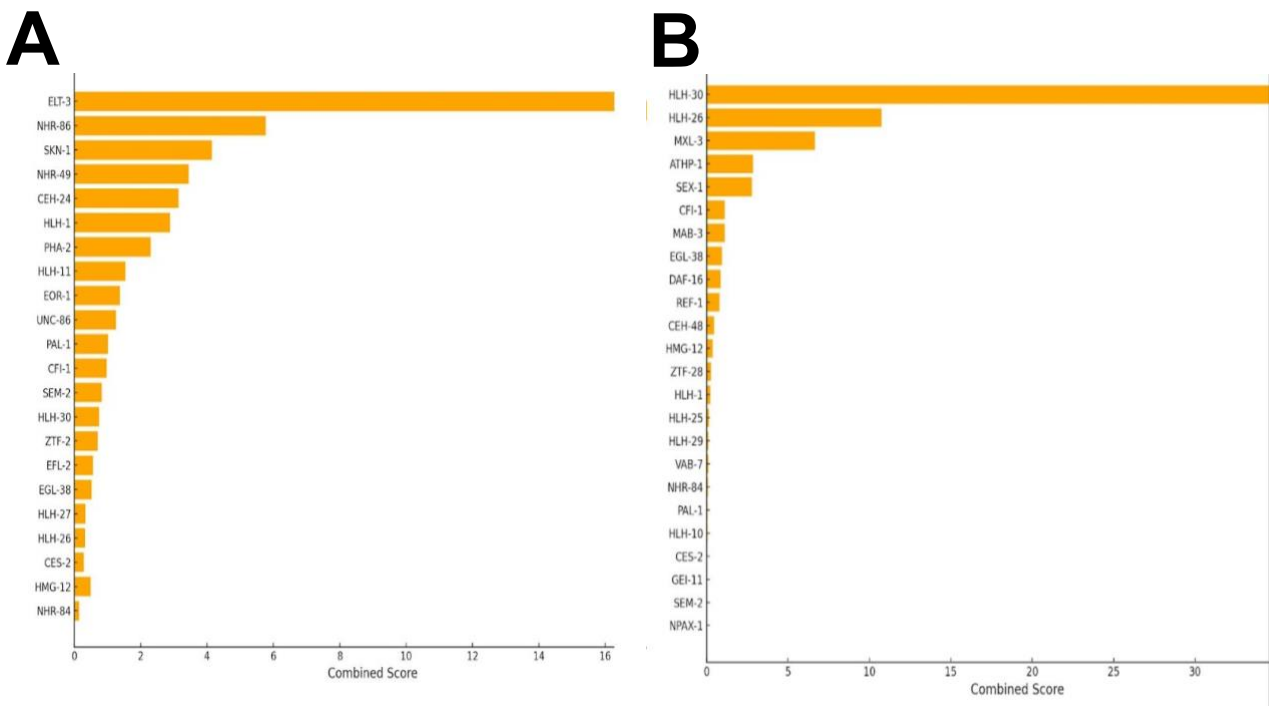

Figure 3.9: Transcription Factor Enrichment in *nhr-14(tm1473)* Mutants. **(A)** Top 24 transcription factors involved in regulating genes significantly upregulated in the *nhr-14(tm1473)* mutant under normal conditions. **(B)** Top 24 transcription factors likely involved in regulating genes significantly downregulated in the *nhr-14(tm1473)* mutant under normal conditions. Transcription factors were identified using TF2DNA (2018) and ranked based on a combined score that includes both p-value significance and z-score deviation (n=2). Results are presented in Tables 11 and 12 in the Appendix.

A

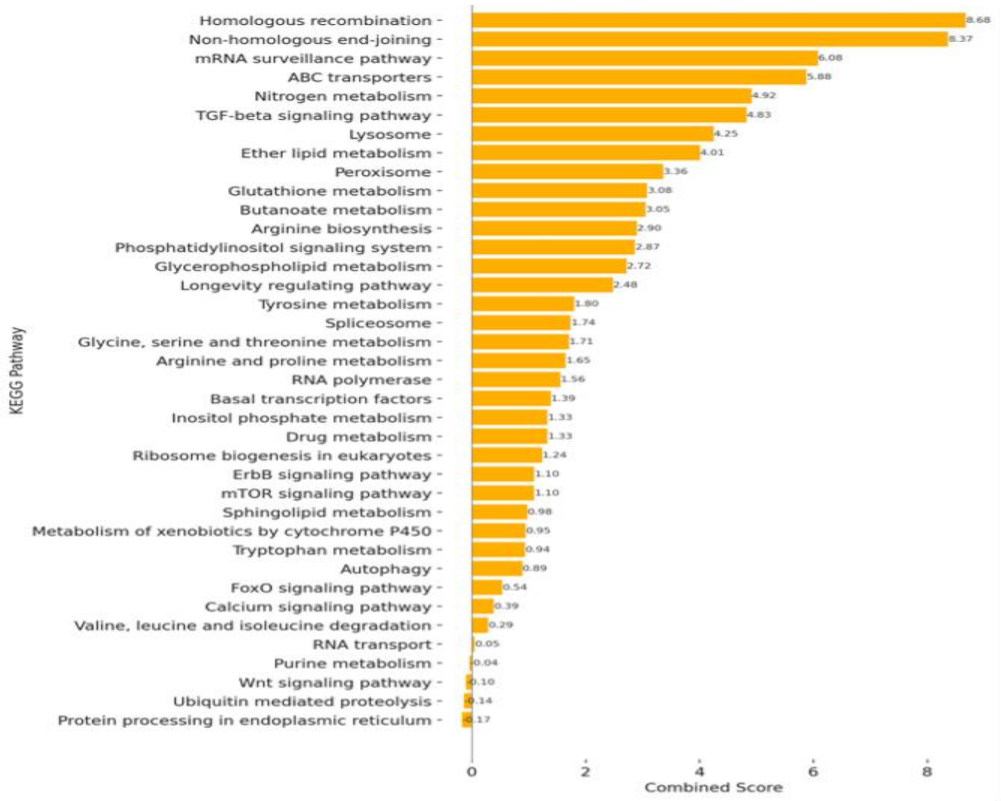

B

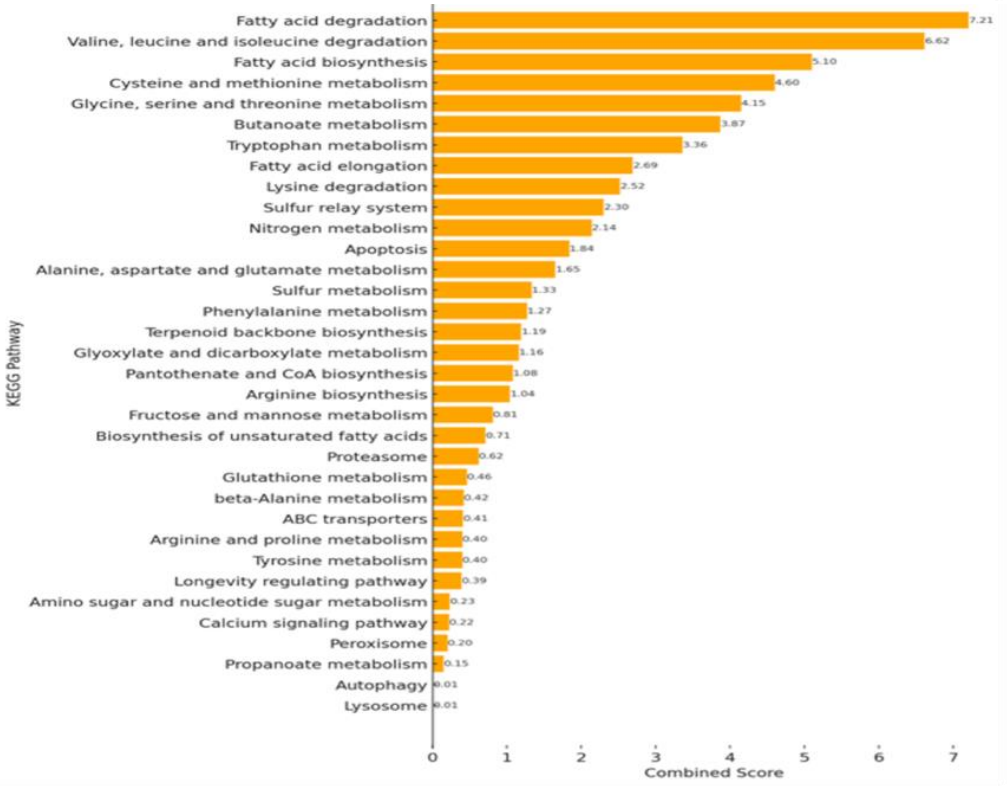

See figure caption on next page.

Figure 3.10: KEGG Pathway Enrichment Analysis of *nhr-14(tm1473)* Mutants. (A) KEGG pathway enrichment of significantly upregulated genes in *nhr-14(tm1473)* mutants under normal conditions. The analysis was performed using WormEnrichr on RNA-seq data from two independent trials. Pathways such as homologous recombination, non-homologous end-joining, and mRNA surveillance showed the highest combined scores, indicating increased expression of genes involved in DNA repair and stress responses. All pathways shown have adjusted p-values < 0.5 (Table 13). **(B)** KEGG pathway enrichment of significantly downregulated genes in *nhr-14(tm1473)* mutants under normal conditions. The analysis was conducted using WormEnrichr on RNA-seq data from two independent trials. Pathways such as fatty acid degradation; valine, leucine, and isoleucine degradation; and fatty acid biosynthesis demonstrated the highest combined scores, suggesting suppression of genes involved in lipid metabolism and amino acid degradation (Table 14).

To validate the RNAseq findings relating to NHR-14's potential regulation of lipids, I measured the mRNA levels of five downregulated genes involved in fatty acid degradation, biosynthesis, and elongation (*acs-2*, *hacd-1*, *acdh-4*, *acdh-8*, and *acs-18*) in both N2 and *nhr-14(tm1473)* mutants using qRT-PCR. Gene expression was normalized to *act-1* housekeeping genes. A significant reduction in the expression of all five genes was observed in *nhr-14* mutants compared to N2 (Figure 3.11). These findings confirm that NHR-14 enhances fatty acid metabolism through regulation of lipid degradation genes**,** supporting its role as a key regulator of metabolic gene expression.

After confirming my RNA-seq results by qRT-PCR and identifying several lipid metabolism genes, such as *acs-2*, *hacd-1*, *acdh-4*, *acdh-8*, and *acs-18*, that were significantly downregulated in *nhr-14(tm1473)* mutants, I decided to investigate whether the reduced expression of these genes was associated with changes in overall fat content. I therefore examined the lipid composition within the worms using Oil Red O staining for visualizing and quantifying neutral lipid stores.

To determine if NHR-14 could improve the total lipid accumulation under basal conditions, I first synchronized N2 and *nhr-14(tm1473)* mutant worms and performed Oil Red O staining. After staining both strains separately, images were taken using confocal microscope, and lipid content was quantified using ImageJ analysis. The *nhr-14(tm1473)* mutants showed stronger Oil Red O staining compared to N2, which means there is an increase in stored lipid levels. Overall, NHR-14 likely plays a role in regulating lipid

metabolism, and that its loss leads to the buildup of neutral lipids within the worm's body (Figure 3.12 A, B, and C).

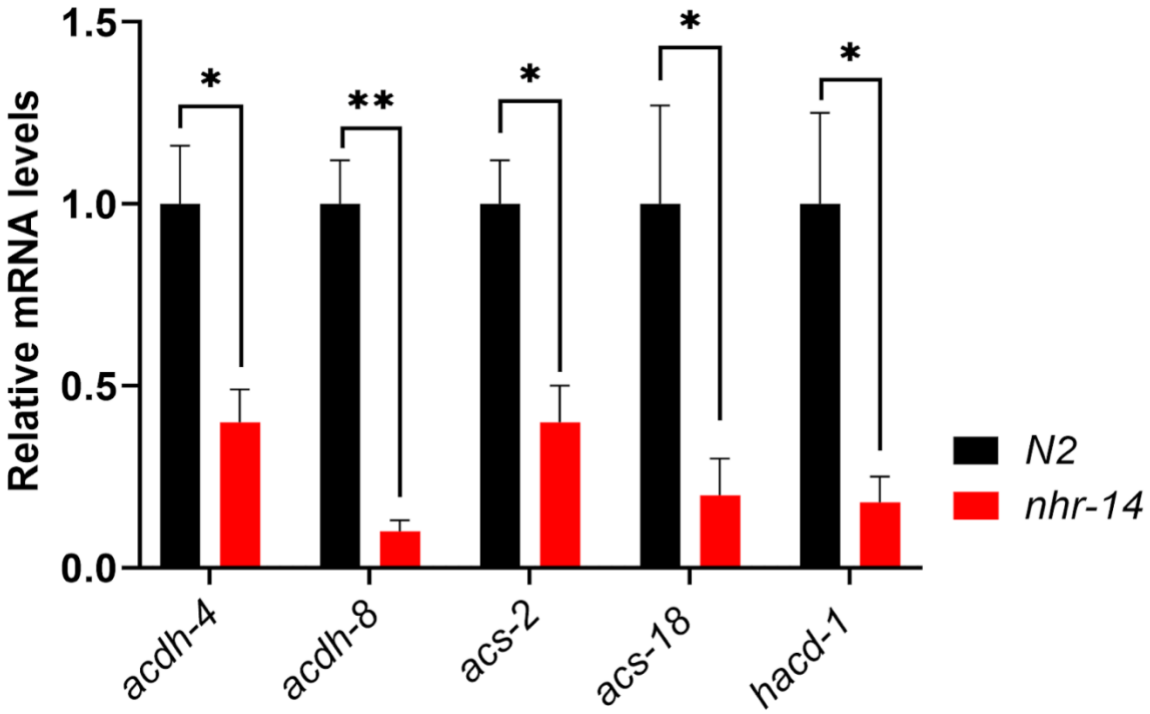

Figure 3.11: qRT-PCR Validation of Downregulated Fatty Acid Metabolism Genes Identified by RNA-seq in *nhr-14(tm1473)* Mutants. qPCR was done to measure the mRNA levels of *acdh-4, acdh-8, acs-2, acs-18, and hacd-1* in both N2 and *nhr-14(tm1473)* mutant worms. Gene expression was normalized to the *act-1* housekeeping gene. All five genes showed significantly decreased expression in *nhr-14* mutants compared to WT. Results were obtained from three independent trials. Statistical analysis was carried out using Unpaired t-test; **p* =0.0308 *for acdh-4,* ***p* = 0.0019 *for acdh-8,* **p* = 0.0184 *for acs-2,* **p*= 0.0499 *for acs-18, and* **p* = 0.0342 *for hacd-1*. Error bars represent ± SEM.

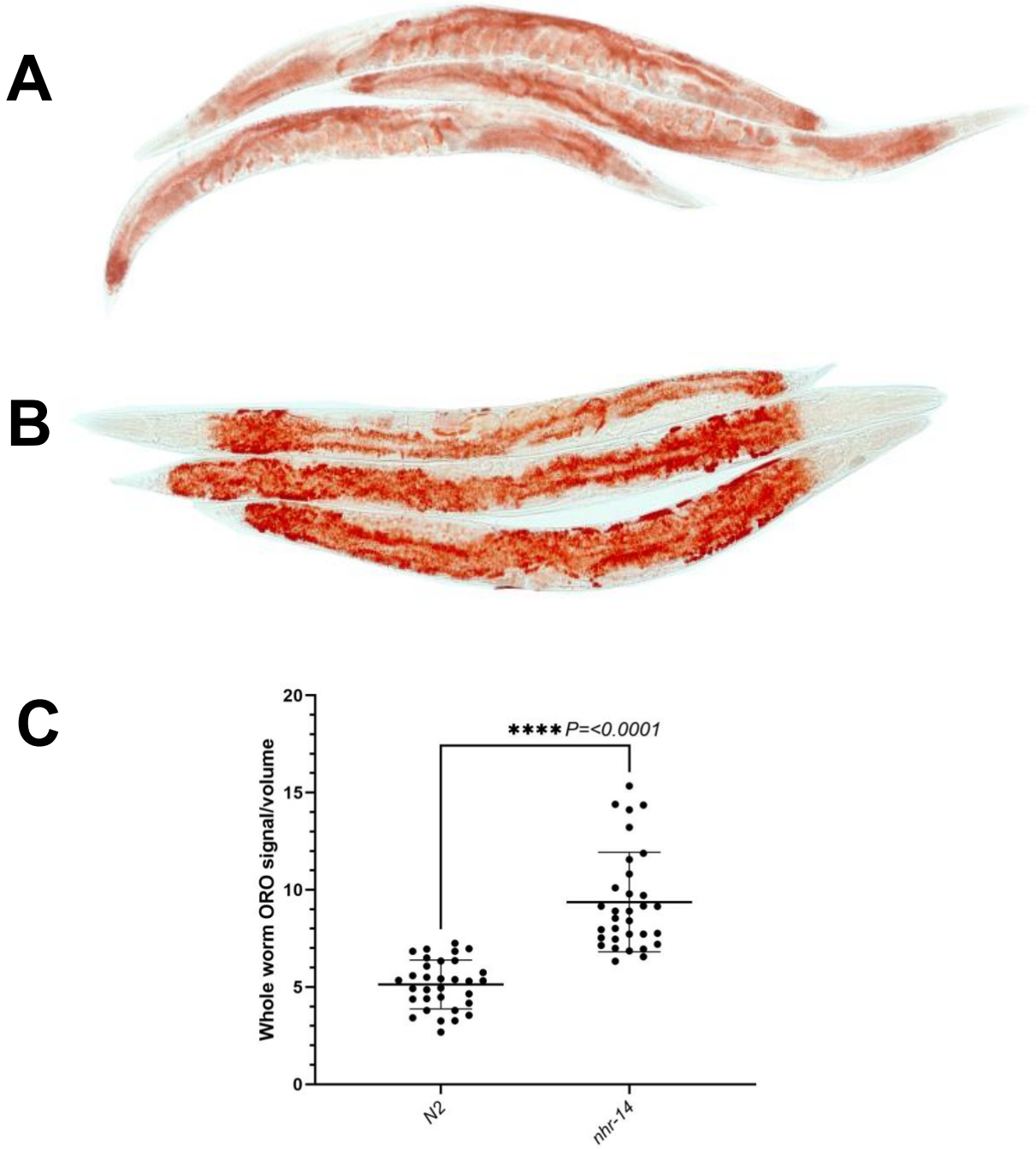

Figure 3.12: Increased Neutral Lipid Storage in *nhr-14(tm1473)* Mutants. (**A)** Oil Red O staining of N2 worms showing basal lipid content. **(B)** Oil Red O staining images of *nhr-14(tm1473)* mutants, showing stronger staining intensity meaning of increased neutral lipid accumulation. **(C)** Quantification of Oil Red O staining signal normalized to worm volume. *nhr-14(tm1473)* mutants showed significantly higher lipid levels compared to N2 controls (unpaired t-test; ****p= < 0.0001). Error bars represent mean ± SEM.

3.7 Lipidomics Analysis Shows Specific Polyunsaturated Fatty Acid Accumulation in *nhr-14(tm1473)* Mutants.

Having confirmed that *nhr-14(tm1473)* mutants exhibit increased neutral lipid storage and downregulation of fatty acid metabolism genes, I next wanted to determine which specific fatty acids accumulate in the absence of NHR-14. To address this question, we commissioned SUNY Biotech to perform gas chromatography–mass spectrometry (GC–MS) analysis to quantify the fatty acid composition in N2 and *nhr-14(tm1473)* mutants under normal growth conditions.

Synchronized young adult worms were collected, and total lipids were extracted and derivatized for GC–MS analysis. Fatty acid methyl esters (FAMEs) were identified and quantified, with each fatty acid expressed as a percentage of total fatty acids. Three independent biological replicates were analyzed for each strain. Statistical significance was assessed using multiple unpaired t-tests with false discovery rate (FDR) correction using the Benjamini–Krieger–Yekutieli method at Q = 5%.

The lipidomics analysis identified 30 distinct fatty acid species. Of these, five fatty acids showed statistically significant differences between N2 and *nhr-14(tm1473)* mutants after FDR correction ($Q < 0.05$) (Figure 3.13; Table 23 in Appendix). Most notably, C16:3, n-3c (hexadecatrienoic acid), an omega-3 polyunsaturated fatty acid (PUFA), was essentially undetectable in wild type worms but accumulated to substantial levels in *nhr-14(tm1473)* mutants (N2: 0.000 ± 0.014%; *nhr-14*: 0.275 ± 0.011%; Q = 0.000017). This represents a dramatic de novo appearance of this fatty acid in the mutant, representing the largest change observed in the fatty acid profile.

Additionally, C18:3, n-6c (γ-linolenic acid, GLA), an omega-6 PUFA, was significantly elevated in *nhr-14(tm1473)* mutants, increasing from 1.922 ± 0.124% to *nhr-14*: 2.236 ± 0.045% (Q = 0.011), representing a 1.16-fold (16%) increase. This finding is consistent with impaired catabolism of omega-6 fatty acids in the absence of NHR-14.

Interestingly, both C18:2, n-6c and C18:1, n-10t were also significantly decreased in *nhr-14(tm1473)* mutants (Figure 13.3). This unexpected finding suggests altered desaturase or isomerase activity in the mutant background. Another significant change was observed in C22:0 (behenic acid), a very-long-chain saturated fatty acid. This fatty acid in *nhr-14(tm1473)* mutants (N2: 0.000 ± 0.013%; *nhr-14*: 0.221 ± 0.020%; Q = 0.000069), suggesting dysregulation of fatty acid elongation pathways when NHR-14 is absent. Finally, 14-methyl C15:0, a branched-chain fatty acid, showed a modest but significant increase in the mutant (N2: 1.776 ± 0.057%; *nhr-14*: 1.890 ± 0.027%; Q = 0.004). The remaining 25 fatty acids analyzed, including major species such as C16:0 (palmitic acid), C18:0 (stearic acid), and C20:4, n-6c (arachidonic acid), did not show statistically significant differences after FDR correction (Q > 0.05), although some displayed trends toward changes (Table 23 in Appendix).

Taken together, these findings demonstrate that loss of NHR-14 leads to the specific accumulation of polyunsaturated fatty acids, particularly omega-3 and omega-6 PUFAs. This lipid profile is consistent with the downregulation of fatty acid β-oxidation genes (*acs-2*, *acdh-4*, *acdh-8*) observed in RNA-seq analysis, suggesting that NHR-14 is required for the efficient catabolism of these highly unsaturated lipid species. The increase in PUFAs, which are particularly susceptible to lipid peroxidation, may cause the increased oxidative

stress susceptibility and constitutive activation of stress response pathways seen in *nhr-14(tm1473)* mutants.

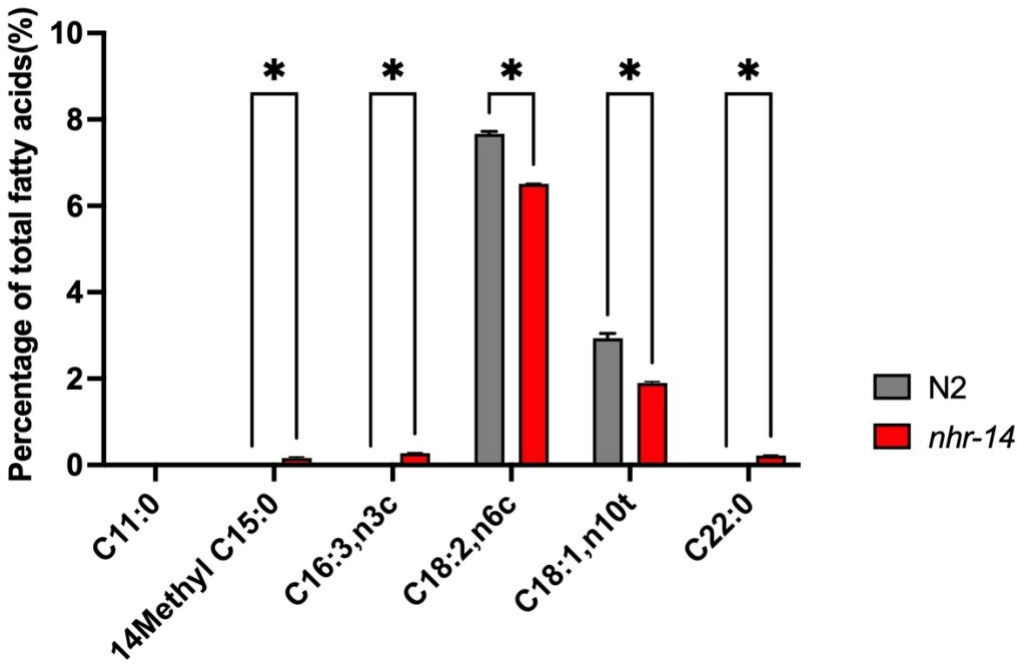

Figure 3.13: Fatty Acid Composition in N2 and *nhr-14(tm1473)*. Fatty acid composition (% of total fatty acids) in N2 and *nhr-14(tm1473)* measured by GC–MS. Data are presented as mean ± SEM from three biological replicates per group (n = 3)**.** Statistical significance between N2 and *nhr-14(tm1473)* was assessed using multiple unpaired two-tailed Student's ***t***-tests with false discovery rate correction (Benjamini–Krieger–Yekutieli)**.** Significant differences were observed for 14-methyl C15:0 (Q = 0.0183)*,* C16:3 n-3c (Q = 0.00044)*,* C18:2 n-6c (Q = 0.000484*),* C18:1 n-10t (Q = 0.00608*),* and C22:0 (Q = 0.000584*)***.*** All significant and non-significant fatty acid data are presented in Table 23 in the Appendix.

Chapter 4: Discussion

4.0 Discussion

4.1 General Overview

The primary objective of my thesis was to discover the primary role of NHR-14 in *C. elegans* oxidative stress response. To examine this objective, I used multiple experiments, such as GFP fluorescence imaging, qRT-PCR, RNA-seq, and several biological assays. As a result of these experiments, I was able to provide data showing an initial understanding of the important role of the NHR-14 transcription factor. I discovered that NHR-14 plays a significant role in lipid metabolism in response to oxidative stress in *C. elegans*. My RNA-seq analysis showed that deletion of *nhr-14(tm1473)* leads to downregulation of multiple genes involved in fatty acid degradation, including *acs-2*, *acs-18*, *hacd-1*, *acdh-4*, and *acdh-8*. These genes play key roles in fatty acid degradation pathways, suggesting that NHR-14 acts as a positive regulator of metabolic genes. I also examined the biological role of NHR-14 through survival assays, brood size, and longevity assays. The *nhr-14(tm1473)* deletion mutation was linked with decreased survivability against various stress and resulted in an overall decreased longevity. Thus, this chapter provides a detailed discussion of all the results obtained, aiming to uncover how NHR-14 regulates metabolism and contributes to stress resistance in *C. elegans*.

4.2 NHR-14 Selectively Regulates Detoxification Genes.

Our lab's goal is to study the cellular processes involved in the oxidative stress response. To better understand and identify the mechanisms involved in preventing oxidative stress, we use *C. elegans* as a model organism. The oxidative stress response is known to

involve and regulate several cellular signaling pathways, particularly components of these pathways that are transcription factors, which regularly interact with DNA to control biological processes. Thus, by examining their functions, we can identify new mechanisms that help us better understand how transcription factors relate to biological systems.

Detoxification proceeds in three phases: Phase I enzymes initiate xenobiotic breakdown, often generating ROS as byproducts; Phase II enzymes neutralize these ROS through conjugation reactions; and Phase III processes eliminate the conjugated products from the cell. Among Phase I enzymes, superoxide dismutases (SODs) are key for oxidative stress defense in *C. elegans*. SOD-3 is a mitochondrial matrix isoform of superoxide dismutase and is transcriptionally activated by DAF-16. GST-4 is a glutathione S-transferase involved in xenobiotic detoxification and is transcriptionally activated by SKN-1. Under oxidative stress, SKN-1 also translocates to the nucleus to upregulate Phase II detoxification genes, including *gst-4.*

The observation that NHR-14 does not regulate *gst-4* expression under oxidative stress was initially unexpected, given our hypothesis that NHR-14 might influence SKN-1-dependent detoxification pathways. qRT-PCR analysis demonstrated that As-induced *gst-4* upregulation occurs independently of NHR-14. Although fluorescence imaging of the *nhr-14(tm1473);gst-4::gfp* transgenic line showed no induction of *gst-4* in response to As, this apparent discrepancy may reflect elevated basal *gst-4* expression in the mutant background, suggesting that the stress response is already near its maximum capacity.

The lack of effect on *gst-4* is particularly notable because GST-4, which is mainly expressed in the intestine (An & Blackwell, 2003), represents a central component of the SKN-1-mediated oxidative stress response. This selective regulation pattern indicates that NHR-14 functions through mechanisms distinct from the classical SKN-1 pathway.

Also, NHR-14 does influence the expression of certain superoxide dismutase family members. The As induced upregulation of *sod-2* and *sod-3* was significantly reduced in *nhr-14(tm1473)* mutants, while *sod-1* remained unaffected. This selective regulation of *sod-2* and *sod-3*, but not *sod-1*, suggests that NHR-14 may specifically modulate mitochondrial and stress-responsive SOD isoforms rather than the constitutive cytoplasmic form. The fluorescence imaging of *nhr-14(tm1473);sod-3::gfp* confirmed this finding, showing reduced induction capacity in the mutant background. Given that SOD-3 is a DAF-16 target gene and functions in mitochondrial ROS defense (Zhao et al., 2016). NHR-14's influence on *sod-3* expression may reflect crosstalk between metabolic signaling and stress resistance pathways. This is consistent with the established role of nuclear hormone receptors in coordinating metabolic state with stress responses.

The examination of Phase I and Phase II detoxification genes showed that NHR-14 selectively regulates specific detoxification pathways rather than acting as a master regulator of the stress response. Among Phase I genes, only *ctl-1* showed NHR-14 dependent regulation, while *fmo-1* and *mtl-1* were unaffected. Similarly, among Phase II genes, *gcs-1* expression was reduced in *nhr-14* mutants under As stress, while other genes remained unchanged. This selective pattern suggests that NHR-14 does not

directly activate these detoxification genes but may influence their expression indirectly through its primary role in regulating metabolic processes. One reasonable mechanism is that NHR-14 mediated control of fatty acid metabolism affects cellular redox status, which in turn influences the expression of specific stress-responsive genes. The metabolic dysfunction resulting from impaired β-oxidation may create a chronic oxidative burden that alters the baseline stress state of the cell, thereby modulating the response to additional stressors like As.

Taken together, these findings show that NHR-14 is a selective regulator of stress response genes rather than a broad activator of detoxification pathways. Its main role appears to be in metabolic regulation, with indirect effects on stress responses that depend on the cell's metabolic state. This idea is consistent with the role of mammalian HNF4α, which also links metabolism to cellular stress responses.

4.3 Loss of NHR-14 Function Results in Increased Susceptibility to Multiple Stressors and Impaired Reproduction.

The selective downregulation of some detoxification genes in *nhr-14(tm1473)* mutants raised the question of whether these molecular changes translate into physiological phenotypes. Survival assays under multiple stress conditions revealed that NHR-14 is essential for stress resistance and reproductive fitness.

The heightened susceptibility of *nhr-14(tm1473)* mutants to both tert-butyl hydroperoxide (tBHP) and arsenite demonstrates that NHR-14 is critical for oxidative stress resistance.

tBHP directly targets lipids and proteins, generating lipid peroxides (Oliveira et al., 2009). The accumulated polyunsaturated fatty acids in *nhr-14* mutants, particularly C16:3 and C18:3 identified by lipidomics, are highly susceptible to peroxidation, making these worms especially vulnerable to tBHP-induced damage. The rapid mortality indicates that pre-existing lipid dysfunction along with oxidative challenge overwhelms cellular defense mechanisms.

The reduced survival after As treatment shows that these worms have a limited ability to cope with stress. They are likely already experiencing chronic oxidative stress due to the buildup of polyunsaturated fatty acids (PUFAs), which easily undergo peroxidation. This keeps them in a constant state of metabolic strain, leaving little capacity to respond to additional oxidative stress.

The susceptibility to ER stress induced by dithiothreitol (DTT) was unexpected. Because DTT disrupts disulfide bond formation in the endoplasmic reticulum (ER) and activates the unfolded protein response (Braakman et al., 1992), this finding suggests that NHR-14 may contribute to maintaining ER stability. The connection likely reflects the close relationship between lipid metabolism and ER function. In *nhr-14(tm1473)* mutants, characterized by PUFA accumulation and dysregulated elongation, may compromise ER membrane homeostasis, rendering it more vulnerable to proteotoxic stress.

The smaller brood size in *nhr-14(tm1473)* mutants is likely due to the extra strain caused by disrupted lipid metabolism. Because β-oxidation genes are downregulated, the worms

cannot efficiently break down stored fats to produce energy, which may leave less energy available for reproduction. At the same time, the buildup of PUFAs increases the risk of lipid peroxidation, generating harmful reactive molecules that can damage reproductive tissues (Esterbauer et al., 1991; Ayala et al., 2014). Together, the reduced fertility in *nhr-14(tm1473)* likely arises from disrupted metabolic homeostasis and dysregulated lipid, which interfere with the physiological processes necessary to support normal reproductive.

The shortened lifespan of *nhr-14(tm1473)* mutants shows the effect of chronic metabolic dysfunction and oxidative stress. *nhr-14(tm1473)* mutants experience disruption due to lipotoxicity. Chronic PUFA accumulation and peroxidation generates ongoing oxidative damage to proteins, DNA, and membranes. This positions NHR-14 as a longevity gene whose primary function, maintaining lipid homeostasis, has implications for organismal health span.

Together, these assays show that NHR-14 is not just a metabolic regulator but a key player in stress resistance, reproduction, and lifespan. The susceptibility to oxidative, ER, and heat stress all come from the primary defect in fatty acid metabolism, illustrating how disruption of a single transcriptional regulator can have cascading effects across multiple biological processes.

4.4 NHR-14 Positively Regulates Fatty Acid Metabolism by Activating Lipid Degradation Genes.

RNA-seq analysis of the *nhr-14(tm1473)* deletion mutant showed downregulation of multiple genes essential for fatty acid degradation, including *acs-2*, *acs-18*, *hacd-1*, *acdh-4*, and *acdh-8*. These genes encode enzymes critical to fatty acid catabolism, suggesting that NHR-14 serves as a positive transcriptional regulator of lipid metabolic processes.

The acyl-CoA synthetases *acs-2* and *acs-18* activate fatty acids by converting them to acyl-CoA derivatives, a necessary first step for β-oxidation. Van Gilst et al. (2005) demonstrated, that *acs-2* is essential for fat mobilization during fasting and infection responses in *C. elegans*. Lu and Qiu (2017) showed that high-glucose diets inhibit *acs-18*, reducing β-oxidation and stimulating fat accumulation. The acyl-CoA dehydrogenases *acdh-4* and *acdh-8* catalyze the first step of mitochondrial β-oxidation, generating acetyl-CoA for energy production. Additionally, *hacd-1* encodes a 3-hydroxyacyl-CoA dehydratase involved in elongation of very-long-chain fatty acids (Kniazeva et al., 2004). The downregulation of these genes in *nhr-14(tm1473)* mutants indicates severely impaired capacity for fatty acid catabolism.

Oil Red O staining confirmed that loss of NHR-14 leads to significant lipid accumulation (Figure 3.12), establishing NHR-14 as a critical regulator of lipid homeostasis. To determine which specific fatty acids accumulate, we performed lipidomics analysis using GC–MS, which showed a pattern of altered fatty acid composition with particular effects on polyunsaturated fatty acids (PUFAs). The most dramatic change was the appearance

of C16:3, n-3c (hexadecatrienoic acid), an omega-3 PUFA that was essentially undetectable in wild-type worms but accumulated to substantial levels in *nhr-14(tm1473)* mutants (Figure 3.13). This is particularly significant because PUFAs with multiple double bonds are highly susceptible to lipid peroxidation when exposed to ROS, generating toxic aldehydes such as 4-hydroxynonenal (4-HNE) and malondialdehyde (MDA) that damage cellular macromolecules. The accumulation of C16:3 in *nhr-14* mutants indicates that NHR-14 regulates lipid homeostasis, preventing their toxic buildup. Additionally, C18:3, n-6c (γ-linolenic acid), an omega-6 PUFA, showed a modest but significant 16% increase in *nhr-14(tm1473)* mutants. While this change is quantitatively smaller than the dramatic appearance of C16:3, it is biologically significant because it demonstrates that NHR-14 regulates catabolism of multiple PUFA species, preventing accumulation across both omega-3 and omega-6 pathways.

In *C. elegans*, PUFAs are synthesized through fatty acid desaturases (FAT-1, FAT-2, FAT-3, FAT-4) (Watts & Browse, 2002). The PUFA accumulation in *nhr-14* mutants suggests that while desaturases can still produce PUFAs, the capacity to catabolize them by β-oxidation is impaired, creating a toxic imbalance between synthesis and degradation.

Interestingly, C22:0 (behenic acid), a very-long-chain saturated fatty acid, appeared in *nhr-14* mutants. This suggests dysregulation of fatty acid elongation, possibly as a compensatory attempt to synthesize saturated fatty acids and dilute the highly oxidizable PUFAs. However, this mechanism appears insufficient to rescue the mutant phenotypes.

The lipidomics findings directly explain several phenotypes observed in *nhr-14(tm1473)* mutants. The constitutively elevated *gst-4p::gfp* expression under basal conditions (Figure 3.1D) results from chronic oxidative stress caused by PUFA peroxidation. Accumulated PUFAs undergo spontaneous oxidation, generating ROS that activate SKN-1 and upregulate *gst-4*. When exposed to additional arsenite stress, these worms cannot further induce *gst-4* because the system is already maximally activated, they are chronically stressed and have exhausted their adaptive capacity.

The reduced survival under oxidative stress (Figure 3.4A, B) is consistent with vulnerability conferred by accumulated PUFAs. Lipid peroxidation generates reactive aldehydes that damage proteins, DNA, and membranes, overwhelming antioxidant defenses. The reduced brood size (Figure 3.6) reflects both metabolic dysfunction, inability to mobilize lipids for energy, and oxidative damage to reproductive tissues. The shortened lifespan (Figure 3.7) results from combined metabolic dysfunction and chronic oxidative stress from continuous PUFA peroxidation.

These findings establish NHR-14 as a critical metabolic checkpoint coordinating fatty acid catabolism with oxidative stress defense. NHR-14 activates genes required for β-oxidation, ensuring that PUFAs are efficiently catabolized rather than accumulating to toxic levels. In the absence of NHR-14, PUFA accumulation leads to spontaneous lipid peroxidation, constitutive stress pathway activation, exhaustion of adaptive responses, and lipotoxicity affecting metabolism, reproduction, and longevity. This regulatory function

is consistent with broader roles of nuclear hormone receptors in coordinating metabolism with stress resistance (Doering et al., 2023) and parallels the function of the mammalian homolog HNF4α in regulating fatty acid metabolism.

4.5 Limitations and Future Direction and Future work

Although this thesis shows the absent of *nhr-14(tm1473)* leads to impaired fatty acid degradation, increase lipid accumulation and altered stress responses, there are limitations to consider when interpreting the results about the full function of NHR-14 in *C. elegans.*

One important limitation is that this study relies on a single mutant allele, nhr-14(tm1473). It is possible that some of the observed phenotypes are influenced by background mutations rather than the loss of NHR-14 alone. To address this, future studies could use additional independent nhr-14 mutant alleles or perform rescue experiments by reintroducing NHR-14 to confirm that the observed effects are specifically due to its loss.

Another limitation is the relatively small sample sizes used in some experiments. For example, the qRT-PCR experiments measuring Phase II and non-Phase II genes were performed with a limited number of replicates, and the RNA-seq analysis was based on only two trials. As a result, some results that appeared non-significant may actually represent real biological differences that were not detected due to low statistical power. Increasing the number of biological replicates would help clarify these trends and strengthen the conclusions.

Although this thesis demonstrates that deletion of *nhr-14* leads to impaired fatty acid degradation, increased lipid accumulation, and altered stress responses, the data presented are largely correlative. While the lipidomics and transcriptomic analyses establish a strong association between NHR-14, fatty acid metabolism, and the observed phenotypes (reduced stress resistance, decreased brood size, and shortened lifespan), they do not establish whether the accumulation of polyunsaturated fatty acids (PUFAs) is causally responsible for these phenotypes, or whether they arise from other, as yet uncharacterized, functions of NHR-14. Establishing this causal link should be a central priority of future work.

The most direct test of whether PUFA accumulation drives the *nhr-14* mutant phenotypes would be to genetically block PUFA synthesis in the *nhr-14* mutant background. FAT-3 is the Δ6-desaturase required for the synthesis of γ-linolenic acid (C18:3n6) and downstream PUFAs in *C. elegans* (Watts & Browse, 2002). Construction of an *nhr-14(tm1473); fat-3(wa22)* double mutant would prevent the synthesis of the PUFAs that accumulate in *nhr-14* single mutants, while leaving the β-oxidation defect intact. If PUFA accumulation is causally responsible for the observed phenotypes, the double mutant should show partial or complete rescue of lifespan, brood size, and stress sensitivity relative to the *nhr-14* single mutant. Conversely, if these phenotypes persist in the double mutant, this would indicate that NHR-14 affects fitness through mechanisms independent of PUFA toxicity. GC–MS lipidomics should be performed on the double mutant to confirm that PUFA levels are indeed reduced.

Overexpression experiments will help clarify whether increased levels of NHR-14 can activate metabolic function or stress-related observed in *nhr-14(tm1473)* mutants. For example, transgenic lines carrying multi-copy arrays or CRISPR/Cas9-mediated single-copy insertions of NHR-14 under endogenous. This would allow systematic testing of whether NHR-14 overexpression enhances β-oxidation gene expression, reduces lipid accumulation, or extends stress resistance and longevity.

In addition, experiments are needed to characterize the transcriptional network in which NHR-14 functions. RNA-seq analysis from this thesis identified key downregulated genes in fatty acid metabolism, but it remains unknown whether these are direct or indirect transcriptional targets. Chromatin immunoprecipitation (ChIP-seq) using FLAG-tagged NHR-14 would allow genome-wide identification of binding sites, thereby clarifying whether genes such as *acs-2, hacd-1*, and *acdh-8* are direct targets. This would help uncover pathways regulated by NHR-14.

Another important direction will be to identify interacting with other transcription factors that modulate NHR-14 activity. Similar to other nuclear hormone receptors, NHR-14 may require cofactors such as MDT-15 or NHR-49 to use full transcriptional control. These experiments would uncover whether NHR-14 interacts with stress response regulators such as SKN-1 providing mechanistic into its role in redox balance. Combining NHR-14 overexpression with additional genetic backgrounds, would determine whether NHR-14 interacts with other major stress-responsive transcription factors.

5. Conclusion

Oxidative stress caused by reactive oxygen species (ROS) is involved in numerous age-related diseases and represents a fundamental challenge to cellular homeostasis. This thesis used *C. elegans* to investigate the role of the nuclear hormone receptor NHR-14 in coordinating metabolic regulation with oxidative stress resistance, a connection with significant implications for understanding aging and longevity.

This work establishes NHR-14 as a transcriptional regulator that maintains lipid homeostasis by activating genes essential for fatty acid β-oxidation, including *acs-2*, *acs-18*, *acdh-4*, *acdh-8*, and *hacd-1*. Loss of NHR-14 function leads to accumulation of polyunsaturated fatty acids (PUFAs). Lipidomics analysis shown a noticeable 24-fold increase in C16:3 and significant elevation of C18:3 in *nhr-14* mutants. These highly oxidizable lipids undergo spontaneous peroxidation, generating chronic oxidative stress that impairs stress adaptation and compromises survival and longevity.

The physiological consequences are significant: *nhr-14(tm1473)* mutants exhibit increased susceptibility to oxidative, ER, and heat stress; reduced reproductive capacity; and dramatically shortened lifespan. These phenotypes occur from a common mechanism, the failure to properly catabolize fatty acids creates lipotoxicity that disrupts redox balance, impairs energy metabolism, and accelerates aging. Thus, NHR-14 functions as a checkpoint integrating lipid homeostasis with stress resistance and longevity.

The mammalian homolog of NHR-14, hepatocyte nuclear factor 4α (HNF4α), similarly regulates fatty acid metabolism and has been implicated in metabolic diseases including diabetes and liver dysfunction. The evolutionary conservation of this mechanism suggests that the connection between PUFA metabolism, oxidative stress, and aging may extend to human health, potentially informing therapeutic strategies for age-related metabolic diseases.

In summary, this thesis shows that NHR-14 helps as a molecular guardian against lipotoxicity, ensuring that polyunsaturated fatty acids are efficiently catabolized before they generate oxidative damage. By linking fatty acid metabolism to stress resistance and longevity, this work establishes NHR-14 as a key regulator at the intersection of metabolism and aging.

References

Altintas, O., Park, S., & Lee, S. J. V. (2016). The role of insulin/IGF-1 signaling in the longevity of model invertebrates, *C. elegans* and *D. melanogaster*. *BMB reports*, *49*(2), 81.

An, J. H., & Blackwell, T. K. (2003). SKN-1 links *C. elegans* mesendodermal specification to a conserved oxidative stress response. *Genes & development*, *17*(15), 1882-1893.

An, J. H., Vranas, K., Lucke, M., Inoue, H., Hisamoto, N., Matsumoto, K., & Blackwell, T. K. (2005). Regulation of the *Caenorhabditis elegans* oxidative stress defense protein SKN-1 by glycogen synthase kinase-3. *Proceedings of the National Academy of Sciences*, *102*(45), 16275-16280.

An, L., Fu, X., Chen, J., & Ma, J. (2023). Application of *Caenorhabditis elegans* in lipid metabolism research. *International journal of molecular sciences*, *24*(2), 1173.

Anderson, C. P., Shen, M., Eisenstein, R. S., & Leibold, E. A. (2012). Mammalian iron metabolism and its control by iron regulatory proteins. *Biochimica et Biophysica Acta (BBA)-Molecular Cell Research*, *1823*(9), 1468-1483.

Andrés Juan, C., Pérez de Lastra, J. M., Plou Gasca, F. J., & Pérez-Lebeña, E. (2021). The chemistry of reactive oxygen species (ROS) revisited: outlining their role in biological macromolecules (DNA, lipids and proteins) and induced pathologies.

Antebi, A. (2015). Nuclear receptor signal transduction in C. elegans. *WormBook*, *1*(10.1895).

Apfeld, J., & Alper, S. (2018). What can we learn about human disease from the nematode C. elegans?. *Disease Gene Identification: Methods and Protocols*, 53-75.

Arcucci, S., Ramos-Delgado, F., Cayron, C., Therville, N., Gratacap, M. P., Basset, C., ... & Guillermet-Guibert, J. (2021). Organismal roles for the PI3Kα and β isoforms: Their specificity, redundancy or cooperation is context-dependent. *Biochemical Journal*, *478*(6), 1199-1225.

Ashrafi, K., Chang, F. Y., Watts, J. L., Fraser, A. G., Kamath, R. S., Ahringer, J., & Ruvkun, G. (2003). Genome-wide RNAi analysis of *Caenorhabditis elegans* fat regulatory genes. *Nature*, *421*(6920), 268-272.

Ayala, A., Muñoz, M. F., & Argüelles, S. (2014). Lipid peroxidation: production, metabolism, and signaling mechanisms of malondialdehyde and 4-hydroxy-2-nonenal. *Oxidative medicine and cellular longevity*, *2014*(1), 360438.

Bienert, G. P., Schjoerring, J. K., & Jahn, T. P. (2006). Membrane transport of hydrogen peroxide. *Biochimica et Biophysica Acta (BBA)-Biomembranes*, *1758*(8), 994-1003.

Blackwell, T. K., Steinbaugh, M. J., Hourihan, J. M., Ewald, C. Y., & Isik, M. (2015). SKN-1/Nrf, stress responses, and aging in Caenorhabditis elegans. *Free Radical Biology and Medicine*, *88*, 290-301.

Bokov, A., Chaudhuri, A., & Richardson, A. (2004). The role of oxidative damage and stress in aging. *Mechanisms of ageing and development*, *125*(10-11), 811-826.

Brenner, S. (1974). The genetics of Caenorhabditis elegans. *Genetics*, *77*(1), 71-94.

Buonocore, G., Perrone, S., & Tataranno, M. L. (2010, August). Oxygen toxicity: chemistry and biology of reactive oxygen species. In *Seminars in Fetal and Neonatal Medicine* (Vol. 15, No. 4, pp. 186-190). WB Saunders.

Byerly, L., Cassada, R. C., & Russell, R. L. (1976). The life cycle of the nematode Caenorhabditis elegans: I. Wild-type growth and reproduction. *Developmental biology*, *51*(1), 23-33.

Canva. (2025). Canva. Canva. https://www.canva.com/

Cho, H. Y., Marzec, J., & Kleeberger, S. R. (2015). Functional polymorphisms in Nrf2: implications for human disease. *Free Radical Biology and Medicine*, *88*, 362-372.

Choe, K. P., Przybysz, A. J., & Strange, K. (2009). The WD40 repeat protein WDR-23 functions with the CUL4/DDB1 ubiquitin ligase to regulate nuclear abundance and activity of SKN-1 in Caenorhabditis elegans. *Molecular and cellular biology*, *29*(10), 2704-2715.

Collin, F. (2019). Chemical basis of reactive oxygen species reactivity and involvement in neurodegenerative diseases. *International journal of molecular sciences*, *20*(10), 2407.

D'Amora, D. R., Hu, Q., Pizzardi, M., & Kubiseski, T. J. (2018). BRAP-2 promotes DNA damage induced germline apoptosis in *C. elegans* through the regulation of SKN-1 and AKT-1. *Cell Death & Differentiation*, *25*(7), 1276-1288.

Degirmenci, U., Wang, M., & Hu, J. (2020). Targeting aberrant RAS/RAF/MEK/ERK signaling for cancer therapy. *Cells*, *9*(1), 198.

Deng, Y., Liu, H., Huang, Q., Tu, L., Hu, L., Zheng, B., ... & Zhou, L. (2022). Mechanism of longevity extension of *caenorhabditis elegans* induced by schizophyllum commune fermented supernatant with added radix puerariae. *Frontiers in Nutrition*, *9*, 847064.

Deponte, M. (2013). Glutathione catalysis and the reaction mechanisms of glutathione-dependent enzymes. *Biochimica et Biophysica Acta (BBA)-General Subjects*, *1830*(5), 3217-3266.

Dhanasekaran, D. N., & Johnson, G. L. (2007). MAPKs: function, regulation, role in cancer and therapeutic targeting. *Oncogene*, *26*(22), 3097-3097.

Ding, J., Wang, X., Li, D. F., Hu, Y., Zhang, Y., & Wang, D. C. (2010). Crystal structure of human programmed cell death 10 complexed with inositol-(1, 3, 4, 5)-tetrakisphosphate: a novel adaptor protein involved in human cerebral cavernous malformation. *Biochemical and biophysical research communications*, *399*(4), 587-592.

Doering, K. R., Ermakova, G., & Taubert, S. (2023). Nuclear hormone receptor NHR-49 is an essential regulator of stress resilience and healthy aging in Caenorhabditis elegans. *Frontiers in Physiology*, *14*, 1241591.

Dues, D. J., Andrews, E. K., Schaar, C. E., Bergsma, A. L., Senchuk, M. M., & Van Raamsdonk, J. M. (2016). Aging causes decreased resistance to multiple stresses and a failure to activate specific stress response pathways. *Aging (Albany NY)*, *8*(4), 777.

El Assar, M., Angulo, J., & Rodríguez-Mañas, L. (2013). Oxidative stress and vascular inflammation in aging. *Free Radical Biology and Medicine*, *65*, 380-401.

Evans, R. M., & Mangelsdorf, D. J. (2014). Nuclear receptors, RXR, and the big bang. *Cell*, *157*(1), 255-266.

Ewald, C. Y., Hourihan, J. M., & Blackwell, T. K. (2017). Oxidative Stress Assays (arsenite and tBHP) in Caenorhabditis elegans. *Bio-protocol*, *7*(13), e2365-e2365.

Ewald, C. Y., Hourihan, J. M., Bland, M. S., Obieglo, C., Katic, I., Moronetti Mazzeo, L. E., & Hynes, N. E. (2017). NADPH oxidase-mediated redox signaling promotes oxidative stress resistance and longevity through memo-1 in C. elegans. *Elife*, *6*, e19493.

Esterbauer, H., Schaur, R. J., & Zollner, H. (1991). Chemistry and biochemistry of 4-hydroxynonenal, malonaldehyde and related aldehydes. *Free radical Biology and medicine*, *11*(1), 81-128.

Finkel, T. (2011). Signal transduction by reactive oxygen species. *Journal of Cell Biology*, *194*(1), 7-15.

Fisher, A. B. (2009). Redox signaling across cell membranes. *Antioxidants & redox signaling*, *11*(6), 1349-1356.

Fridovich, I. (1978). The Biology of Oxygen Radicals: The superoxide radical is an agent of oxygen toxicity; superoxide dismutases provide an important defense. *Science*, *201*(4359), 875-880.

Furtmüller, P. G., Burner, U., Jantschko, W., Regelsberger, G., & Obinger, C. (2000). Two-electron reduction and one-electron oxidation of organic hydroperoxides by human myeloperoxidase. *FEBS letters*, *484*(2), 139-143.

Gami, M. S., Iser, W. B., Hanselman, K. B., & Wolkow, C. A. (2006). Activated AKT/PKB signaling in *C. elegans* uncouples temporally distinct outputs of DAF-2/insulin-like signaling. *BMC developmental biology*, *6*, 1-14.

Gerisch, B., Tharyan, R. G., Mak, J., Denzel, S. I., Popkes-van Oepen, T., Henn, N., & Antebi, A. (2020). HLH-30/TFEB is a master regulator of reproductive quiescence. *Developmental Cell*, *53*(3), 316-329.

Gilst, M. R. V., Hadjivassiliou, H., Jolly, A., & Yamamoto, K. R. (2005). Nuclear hormone receptor NHR-49 controls fat consumption and fatty acid composition in C. elegans. *PLoS biology*, *3*(2), e53.

Glover-Cutter, K. M., Lin, S., & Blackwell, T. K. (2013). Integration of the unfolded protein and oxidative stress responses through SKN-1/Nrf. *PLoS genetics*, *9*(9), e1003701.

Halliwell, B., & Gutteridge, J. M. (2015). *Free radicals in biology and medicine*. Oxford university press.

Harman, D. (2002). Aging: a theory based on free radical and radiation chemistry. *Science of Aging Knowledge Environment*, *2002*(37), cp14-cp14.

He, F., Ru, X., & Wen, T. (2020). NRF2, a transcription factor for stress response and beyond. *International journal of molecular sciences*, *21*(13), 4777.

Hertweck, M., Göbel, C., & Baumeister, R. (2004). *C. elegans* SGK-1 is the critical component in the Akt/PKB kinase complex to control stress response and life span. *Developmental cell*, *6*(4), 577-588.

Hu, Q., D'Amora, D. R., MacNeil, L. T., Walhout, A. J., & Kubiseski, T. J. (2017). The oxidative stress response in *Caenorhabditis elegans* requires the GATA transcription factor ELT-3 and SKN-1/Nrf2. *Genetics*, *206*(4), 1909-1922.

Hu, Q., D'Amora, D. R., MacNeil, L. T., Walhout, A. J., & Kubiseski, T. J. (2018). The *Caenorhabditis elegans* oxidative stress response requires the NHR-49 transcription factor. *G3: Genes, Genomes, Genetics*, *8*(12), 3857-3863.

Inoue, H., Hisamoto, N., An, J. H., Oliveira, R. P., Nishida, E., Blackwell, T. K., & Matsumoto, K. (2005). The *C. elegans* p38 MAPK pathway regulates nuclear

localization of the transcription factor SKN-1 in oxidative stress response. *Genes & development*, *19*(19), 2278-2283.

Ishii, N. (2000). Oxidative stress and aging in Caenorhabditis elegans. *Free radical research*, *33*(6), 857-864.

Kahn, N. W., Rea, S. L., Moyle, S., Kell, A., & Johnson, T. E. (2008). Proteasomal dysfunction activates the transcription factor SKN-1 and produces a selective oxidative-stress response in Caenorhabditis elegans. *Biochemical Journal*, *409*(1), 205-213.

Kenyon, C. (2010). A pathway that links reproductive status to lifespan in Caenorhabditis elegans. *Annals of the New York Academy of Sciences*, *1204*(1), 156-162.

Kenyon, C. J. (2010). The genetics of ageing. *Nature*, *464*(7288), 504-512.

Kenyon, C., Chang, J., Gensch, E., Rudner, A., & Tabtiang, R. (1993). A *C. elegans* mutant that lives twice as long as wild type. *Nature*, *366*(6454), 461-464.

Kimura, K. D., Riddle, D. L., & Ruvkun, G. (2011, January). The *C. elegans* DAF-2 insulin-like receptor is abundantly expressed in the nervous system and regulated by nutritional status. In *Cold Spring Harbor symposia on quantitative biology* (Vol. 76, pp. 113-120). Cold Spring Harbor Laboratory Press.

Kimura, K. D., Tissenbaum, H. A., Liu, Y., & Ruvkun, G. (1997). daf-2, an insulin receptor-like gene that regulates longevity and diapause in Caenorhabditis elegans. *Science*, *277*(5328), 942-946.

Kniazeva, M., Crawford, Q. T., Seiber, M., Wang, C. Y., & Han, M. (2004). Monomethyl branched-chain fatty acids play an essential role in *Caenorhabditis elegans* development. *PLoS biology*, *2*(9), e257.

Koon, J. C., & Kubiseski, T. J. (2010). Developmental arrest of *Caenorhabditis elegans* BRAP-2 mutant exposed to oxidative stress is dependent on BRC-1. *Journal of Biological Chemistry*, *285*(18), 13437-13443.

Labuschagne, C. F., & Brenkman, A. B. (2013). Current methods in quantifying ROS and oxidative damage in *Caenorhabditis elegans* and other model organism of aging. *Ageing research reviews*, *12*(4), 918-930.

Lackner, M. R., & Kim, S. K. (1998). Genetic analysis of the *Caenorhabditis elegans* MAP kinase gene mpk-1. *Genetics*, *150*(1), 103-117.

Lambert, S. A., Jolma, A., Campitelli, L. F., Das, P. K., Yin, Y., Albu, M., ... & Weirauch, M. T. (2018). The human transcription factors. *Cell*, *172*(4), 650-665.

Li, W., Kennedy, S. G., & Ruvkun, G. (2003). daf-28 encodes a *C. elegans* insulin superfamily member that is regulated by environmental cues and acts in the DAF-2 signaling pathway. *Genes & development*, *17*(7), 844-858.

Liang, B., Ferguson, K., Kadyk, L., & Watts, J. L. (2010). The role of nuclear receptor NHR-64 in fat storage regulation in Caenorhabditis elegans. *PloS one*, *5*(3), e9869.

Lin, K., Dorman, J. B., Rodan, A., & Kenyon, C. (1997). daf-16: An HNF-3/forkhead family member that can function to double the life-span of Caenorhabditis elegans. *Science*, *278*(5341), 1319-1322.

Lu, Z., & Qiu, Z. (2017). High glucose concentration restricts fat consumption in Caenorhabditis elegans. *Int J Clin Exp Med*, *10*(7), 10554-10559.

Lupien, S. J., McEwen, B. S., Gunnar, M. R., & Heim, C. (2009). Effects of stress throughout the lifespan on the brain, behaviour and cognition. *Nature reviews neuroscience*, *10*(6), 434-445.

Ma, Q. (2013). Role of nrf2 in oxidative stress and toxicity. *Annual review of pharmacology and toxicology*, *53*(1), 401-426.

Martin, K. R., & Barrett, J. C. (2002). Reactive oxygen species as double-edged swords in cellular processes: low-dose cell signaling versus high-dose toxicity. *Human & experimental toxicology*, *21*(2), 71-75.

Matheny, S. A., Chen, C., Kortum, R. L., Razidlo, G. L., Lewis, R. E., & White, M. A. (2004). Ras regulates assembly of mitogenic signalling complexes through the effector protein IMP. *Nature*, *427*(6971), 256-260.

McCord, J. M., & Fridovich, I. (1969). The utility of superoxide dismutase in studying free radical reactions: I. Radicals generated by the interaction of sulfite, dimethyl sulfoxide, and oxygen. *Journal of Biological Chemistry*, *244*(22), 6056-6063.

Monaghan, P., Metcalfe, N. B., & Torres, R. (2009). Oxidative stress as a mediator of life history trade-offs: mechanisms, measurements and interpretation. *Ecology letters*, *12*(1), 75-92.

Morris, J. Z., Tissenbaum, H. A., & Ruvkun, G. (1996). A phosphatidylinositol-3-OH kinase family member regulating longevity and diapause in Caenorhabditis elegans. *Nature*, *382*(6591), 536-539.

Murphy, C. T., & Hu, P. J. (2018). Insulin/insulin-like growth factor signaling in C. elegans. *WormBook: The online review of C. elegans biology [Internet]*.

Murphy, C. T., McCarroll, S. A., Bargmann, C. I., Fraser, A., Kamath, R. S., Ahringer, J., ... & Kenyon, C. (2003). Genes that act downstream of DAF-16 to influence the lifespan of Caenorhabditis elegans. *Nature*, *424*(6946), 277-283.

Murphy, M. P. (2009). How mitochondria produce reactive oxygen species. *Biochemical journal*, *417*(1), 1-13.

Narasimhan, S. D., Mukhopadhyay, A., & Tissenbaum, H. A. (2009). InAKTivation of insulin/IGF-1 signaling by dephosphorylation. *Cell Cycle*, *8*(23), 3878-3884.

Navarro-Yepes, J., Zavala-Flores, L., Anandhan, A., Wang, F., Skotak, M., Chandra, N., ... & Franco, R. (2014). Antioxidant gene therapy against neuronal cell death. *Pharmacology & therapeutics*, *142*(2), 206-230.

nhr-14 (gene) - WormBase : Nematode Information Resource. (2022). Wormbase.org. https://wormbase.org/species/c_elegans/gene/WBGene00003613#0-9fg-10-9

Niccoli, T., & Partridge, L. (2012). Ageing as a risk factor for disease. *Current biology*, *22*(17), R741-R752.

Nigon, V. M., & Félix, M. A. (2018). History of research on *C. elegans* and other free-living nematodes as model organisms. *WormBook: The Online Review of C. elegans Biology.*

O'Brien, D., Jones, L. M., Good, S., Miles, J., Vijayabaskar, M. S., Aston, R., ... & van Oosten-Hawle, P. (2018). A PQM-1-mediated response triggers transcellular chaperone signaling and regulates organismal proteostasis. *Cell Reports*, *23*(13), 3905-3919.

O'Brien, K. P., Westerlund, I., & Sonnhammer, E. L. (2004). OrthoDisease: a database of human disease orthologs. *Human mutation*, *24*(2), 112-119.

Ogg, S., & Ruvkun, G. (1998). The *C. elegans* PTEN homolog, DAF-18, acts in the insulin receptor-like metabolic signaling pathway. *Molecular cell*, *2*(6), 887-893.

Ohmachi, M., Rocheleau, C. E., Church, D., Lambie, E., Schedl, T., & Sundaram, M. V. (2002). *C. elegans* ksr-1 and ksr-2 have both unique and redundant functions and are required for MPK-1 ERK phosphorylation. *Current Biology*, *12*(5), 427-433.

Oliveira, R. P., Abate, J. P., Dilks, K., Landis, J., Ashraf, J., Murphy, C. T., & Blackwell, T. K. (2009). Condition-adapted stress and longevity gene regulation by *Caenorhabditis elegans* SKN-1/Nrf. *Aging cell*, *8*(5), 524-541.

Orkin, S. H. (1995). Hematopoiesis: how does it happen?. *Current opinion in cell biology*, *7*(6), 870-877.

Padmanabhan, S., Mukhopadhyay, A., Narasimhan, S. D., Tesz, G., Czech, M. P., & Tissenbaum, H. A. (2009). A PP2A regulatory subunit regulates *C. elegans* insulin/IGF-1 signaling by modulating AKT-1 phosphorylation. *Cell*, *136*(5), 939-951.

Paradis, S., & Ruvkun, G. (1998). *Caenorhabditis elegans* Akt/PKB transduces insulin receptor-like signals from AGE-1 PI3 kinase to the DAF-16 transcription factor. *Genes & development*, *12*(16), 2488-2498.

Park, S. K., Tedesco, P. M., & Johnson, T. E. (2009). Oxidative stress and longevity in *Caenorhabditis elegans* as mediated by SKN-1. *Aging cell*, *8*(3), 258-269.

Pizzino, G., Irrera, N., Cucinotta, M., Pallio, G., Mannino, F., Arcoraci, V., ... & Bitto, A. (2017). Oxidative stress: harms and benefits for human health. *Oxidative medicine and cellular longevity*, *2017*(1), 8416763.

Rafikova, A., Hu, Q., & Kubiseski, T. J. (2020). The SEM-4 transcription factor is required for regulation of the oxidative stress response in Caenorhabditis elegans. *G3: Genes, Genomes, Genetics*, *10*(9), 3379-3385.

Rajan, M., Anderson, C. P., Rindler, P. M., Romney, S. J., Ferreira dos Santos, M. C., Gertz, J., & Leibold, E. A. (2019). NHR-14 loss of function couples intestinal iron uptake with innate immunity in *C. elegans* through PQM-1 signaling. *Elife*, *8*, e44674.

Rodriguez, M., Rodriguez-Sabate, C., Morales, I., Sanchez, A., & Sabate, M. (2015). Parkinson's disease as a result of aging. *Aging cell*, *14*(3), 293-308.

Ruvkun, G., & Lehrbach, N. (2023). Regulation and functions of the ER-associated Nrf1 transcription factor. *Cold Spring Harbor Perspectives in Biology*, *15*(1), a041266.

Sacks, D. B. (2006). The role of scaffold proteins in MEK/ERK signalling.

Sagasti, A., Hisamoto, N., Hyodo, J., Tanaka-Hino, M., Matsumoto, K., & Bargmann, C. I. (2001). The CaMKII UNC-43 activates the MAPKKK NSY-1 to execute a lateral signaling decision required for asymmetric olfactory neuron fates. *Cell*, *105*(2), 221-232.

Sakaguchi, A., Matsumoto, K., & Hisamoto, N. (2004). Roles of MAP kinase cascades in Caenorhabditis elegans. *Journal of biochemistry*, *136*(1), 7-11.

Sang, L., Dong, R., Liu, R., Hao, Q., Bai, W., & Sun, J. (2022). *Caenorhabditis elegans* NHR-14/HNF4α regulates DNA damage-induced apoptosis through cooperating with cep-1/p53. *Cell Communication and Signaling*, *20*(1), 135.

Sato, H., Shibata, M., Shimizu, T., Shibata, S., Toriumi, H., Ebine, T., ... & Suzuki, N. (2013). Differential cellular localization of antioxidant enzymes in the trigeminal ganglion. *Neuroscience*, *248*, 345-358.

Savova, M. S., Todorova, M. N., Apostolov, A. G., Yahubyan, G. T., & Georgiev, M. I. (2022). Betulinic acid counteracts the lipid accumulation in *Caenorhabditis elegans*

by modulation of nhr-49 expression. *Biomedicine & Pharmacotherapy*, *156*, 113862.

Schieber, M., & Chandel, N. S. (2014). ROS function in redox signaling and oxidative stress. *Current biology*, *24*(10), R453-R462.

Schumacher, B., Hofmann, K., Boulton, S., & Gartner, A. (2001). The *C. elegans* homolog of the p53 tumor suppressor is required for DNA damage-induced apoptosis. *Current biology*, *11*(21), 1722-1727.

Spitz, F., & Furlong, E. E. (2012). Transcription factors: from enhancer binding to developmental control. *Nature reviews genetics*, *13*(9), 613-626.

Sternberg, P. W., & Han, M. (1998). Genetics of RAS signaling in C. elegans. *Trends in Genetics*, *14*(11), 466-472.

Sulston, J. E., & Horvitz, H. R. (1977). Post-embryonic cell lineages of the nematode, Caenorhabditis elegans. *Developmental biology*, *56*(1), 110-156.

Sundaram, M. V. (2013). Canonical RTK-Ras-ERK signaling and related alternative pathways. *WormBook*, 1.

Suzuki, T., & Yamamoto, M. (2015). Molecular basis of the Keap1–Nrf2 system. *Free Radical Biology and Medicine*, *88*, 93-100.

Sykiotis, G. P., & Bohmann, D. (2010). Stress-activated cap'n'collar transcription factors in aging and human disease. *Science signaling*, *3*(112), re3-re3.

Taubert, S., Ward, J. D., & Yamamoto, K. R. (2011). Nuclear hormone receptors in nematodes: evolution and function. *Molecular and cellular endocrinology*, *334*(1-2), 49-55.

Tidyman, W. E., & Rauen, K. A. (2009). The RASopathies: developmental syndromes of Ras/MAPK pathway dysregulation. *Current opinion in genetics & development*, *19*(3), 230-236.

Troemel, E. R., Chu, S. W., Reinke, V., Lee, S. S., Ausubel, F. M., & Kim, D. H. (2006). p38 MAPK regulates expression of immune response genes and contributes to longevity in C. elegans. *PLoS genetics*, *2*(11), e183.

Tullet, J. M. (2015). DAF-16 target identification in C. elegans: past, present and future. *Biogerontology*, *16*(2), 221-234.

Tullet, J. M., Hertweck, M., An, J. H., Baker, J., Hwang, J. Y., Liu, S., ... & Blackwell, T. K. (2008). Direct inhibition of the longevity-promoting factor SKN-1 by insulin-like signaling in C. elegans. *Cell*, *132*(6), 1025-1038.

Van der Hoeven, R., McCallum, K. C., Cruz, M. R., & Garsin, D. A. (2011). Ce-Duox1/BLI-3 generated reactive oxygen species trigger protective SKN-1 activity via p38 MAPK signaling during infection in C. elegans. *PLoS pathogens*, *7*(12), e1002453.

Van Raamsdonk, J. M., & Hekimi, S. (2009). Deletion of the mitochondrial superoxide dismutase sod-2 extends lifespan in Caenorhabditis elegans. *PLoS genetics*, *5*(2), e1000361.

Van Raamsdonk, J. M., & Hekimi, S. (2012). Superoxide dismutase is dispensable for normal animal lifespan. *Proceedings of the National Academy of Sciences*, *109*(15), 5785-5790.

Vaquerizas, J. M., Kummerfeld, S. K., Teichmann, S. A., & Luscombe, N. M. (2009). A census of human transcription factors: function, expression and evolution. *Nature Reviews Genetics*, *10*(4), 252-263.

Ventura, N., Rea, S. L., Schiavi, A., Torgovnick, A., Testi, R., & Johnson, T. E. (2009). p53/CEP-1 increases or decreases lifespan, depending on level of mitochondrial bioenergetic stress. *Aging cell*, *8*(4), 380-393.

Walesky, C., & Apte, U. (2015). Role of hepatocyte nuclear factor 4α (HNF4α) in cell proliferation and cancer. *Gene expression*, *16*(3), 101.

Wolkow, C. A., Muñoz, M. J., Riddle, D. L., & Ruvkun, G. (2002). Insulin receptor substrate and p55 orthologous adaptor proteins function in the Caenorhabditis elegans daf-2/insulin-like signaling pathway. *Journal of Biological Chemistry*, *277*(51), 49591-49597.

Watts, J. L., & Browse, J. (2002). Genetic dissection of polyunsaturated fatty acid synthesis in Caenorhabditis elegans. *Proceedings of the National Academy of Sciences*, *99*(9), 5854-5859.

White, J. G., Southgate, E., Thomson, J. N., & Brenner, S. (1986). The structure of the nervous system of the nematode Caenorhabditis elegans. *Philos Trans R Soc Lond B Biol Sci*, *314*(1165), 1-340.

Wu, C., Chakrabarty, S., Jin, M., Liu, K., & Xiao, Y. (2019). Insect ATP-binding cassette (ABC) transporters: roles in xenobiotic detoxification and Bt insecticidal activity. *International journal of molecular sciences*, *20*(11), 2829.

Wu, J. Q., Kosten, T. R., & Zhang, X. Y. (2013). Free radicals, antioxidant defense systems, and schizophrenia. *Progress in Neuro-Psychopharmacology and Biological Psychiatry*, *46*, 200-206.

Wu, Y., & Han, M. (1994). Suppression of activated Let-60 ras protein defines a role of Caenorhabditis elegans Sur-1 MAP kinase in vulval differentiation. *Genes & development*, *8*(2), 147-159.

Yang, J. S., Nam, H. J., Seo, M., Han, S. K., Choi, Y., Nam, H. G., ... & Kim, S. (2011). OASIS: online application for the survival analysis of lifespan assays performed in aging research. *PloS one*, *6*(8), e23525.

Yochem, J., Sundaram, M., & Han, M. (1997). Ras is required for a limited number of cell fates and not for general proliferation in Caenorhabditis elegans. *Molecular and cellular biology*, *17*(5), 2716-2722.

Zhang, S., Li, F., Zhou, T., Wang, G., & Li, Z. (2020). *Caenorhabditis elegans* as a useful model for studying aging mutations. *Frontiers in endocrinology*, *11*, 554994.

Appendix

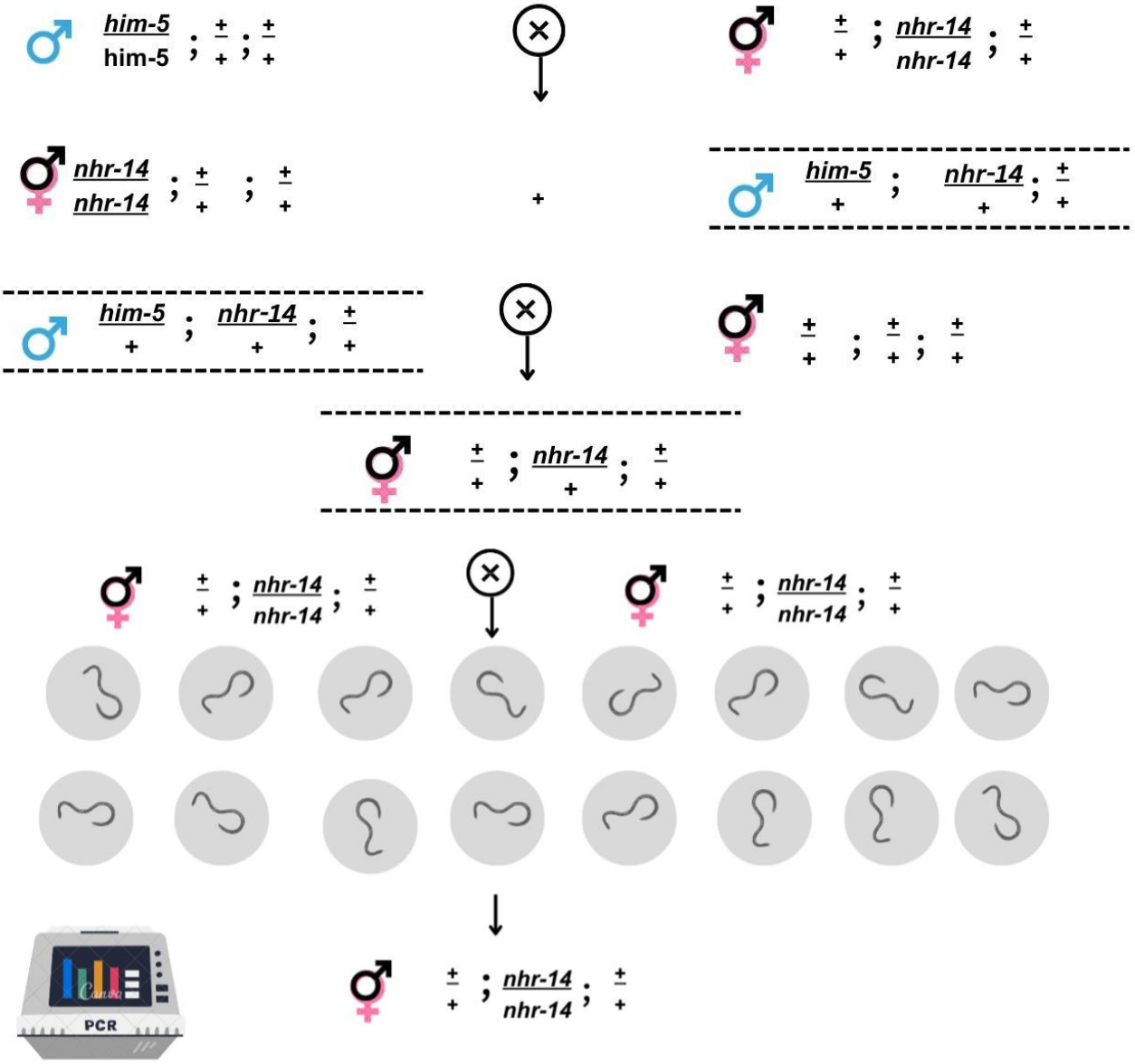

Figure S1: Schematic of the Backcross to Generate Backcrossed *nhr-14 (tm1473).*

Created using Canva.com

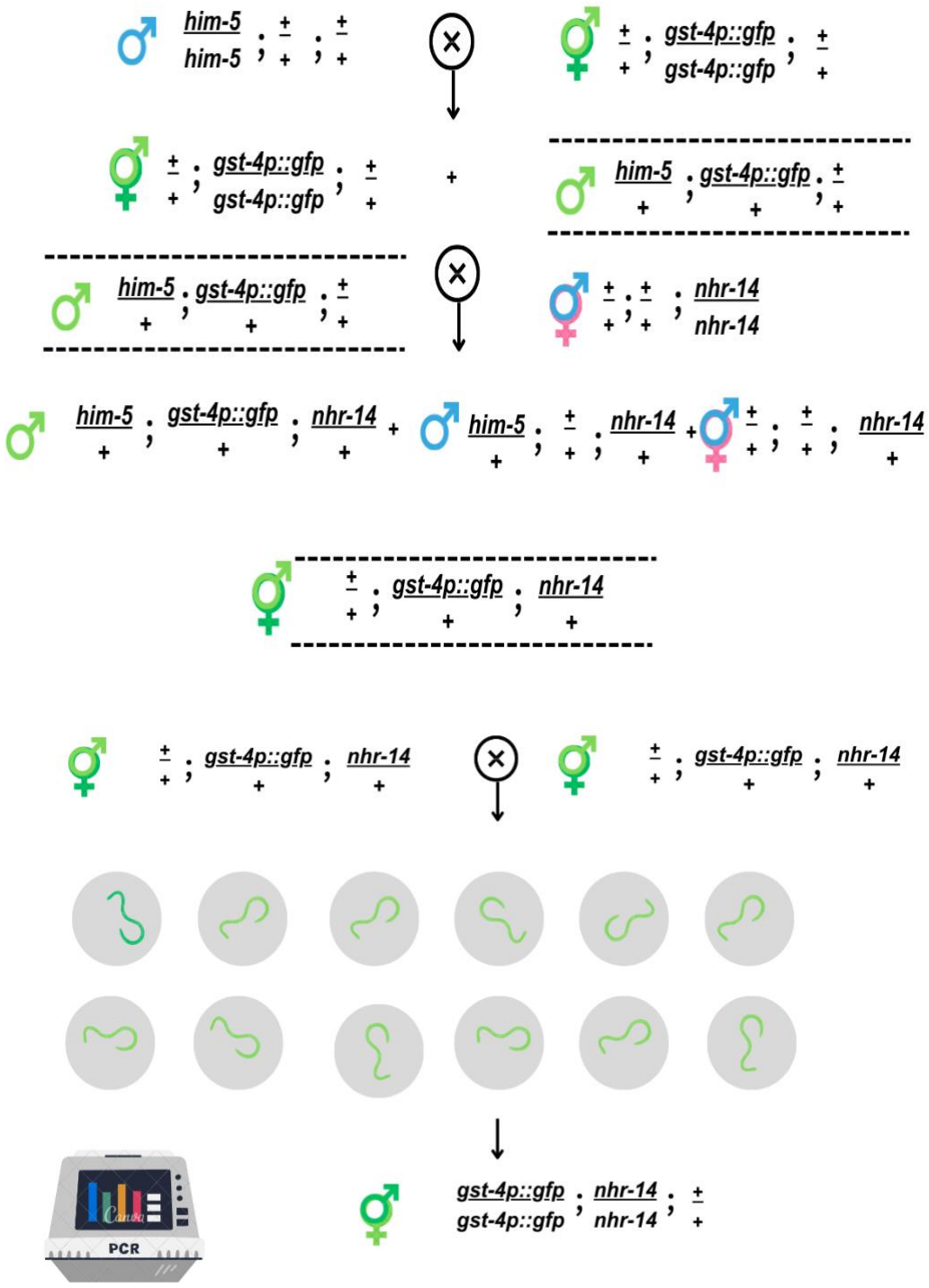

Figure S2: Schematic of the Transgenic Cross to Generate the *nhr-14(tm1473);gst-4::gfp.*

Created using Canva.com

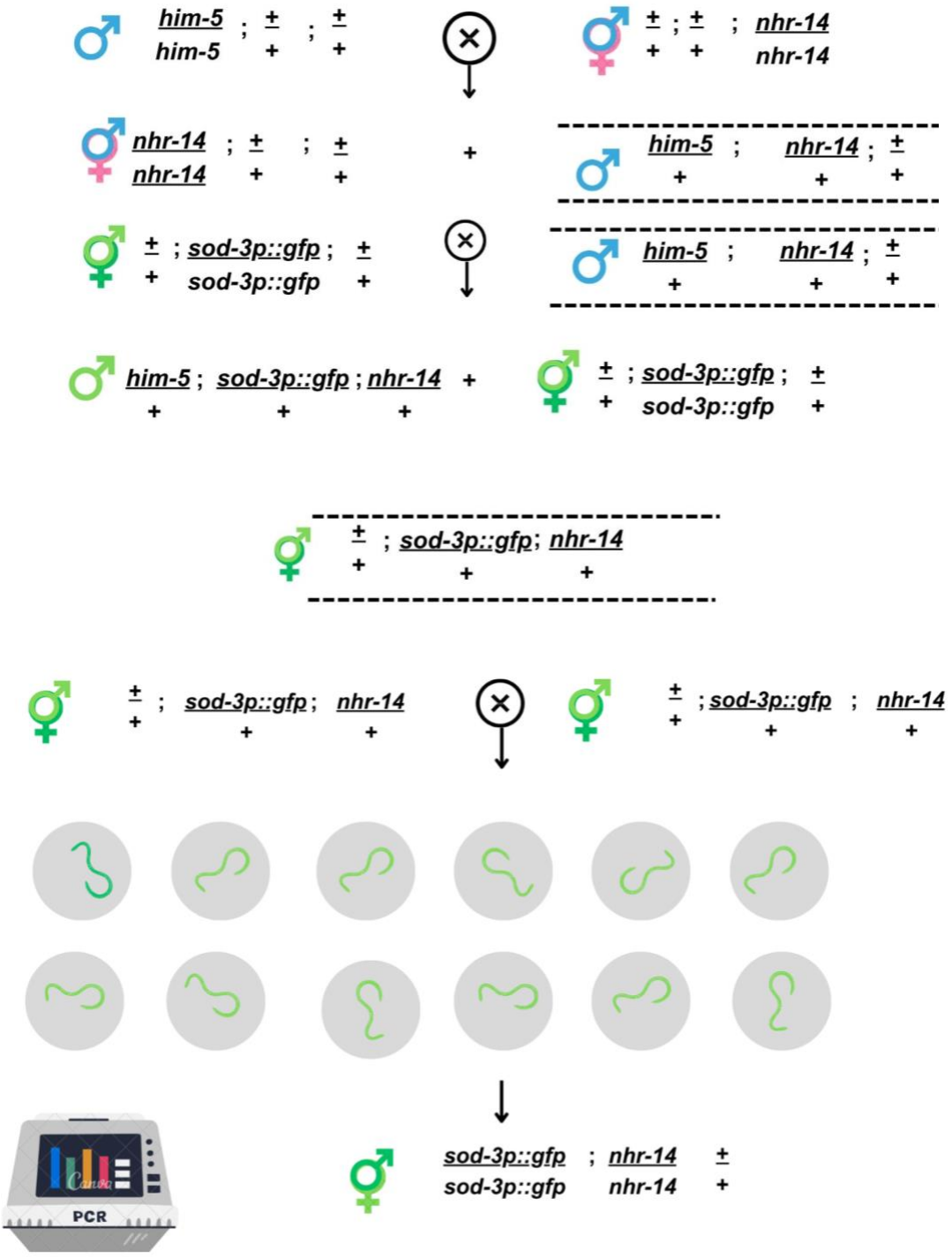

Figure S3: Schematic of the Transgenic Cross to Generate the *nhr-14(tm1473);sod-3::gfp.*

Created using Canva.com

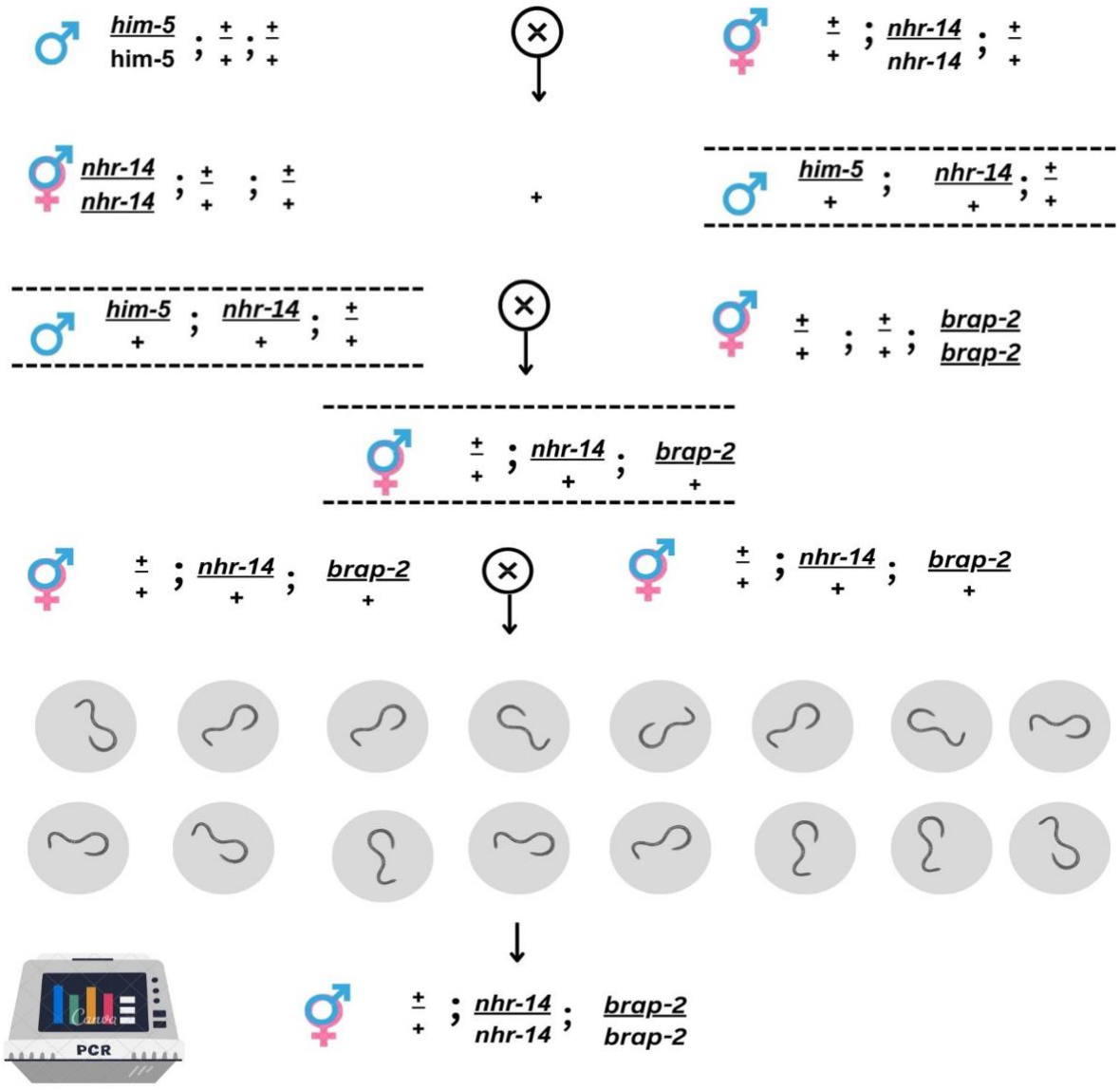

Figure S4: Schematic of the Cross to Generate Double Mutants *nhr-14(tm1473);brap-2.*

Created using Canva.com

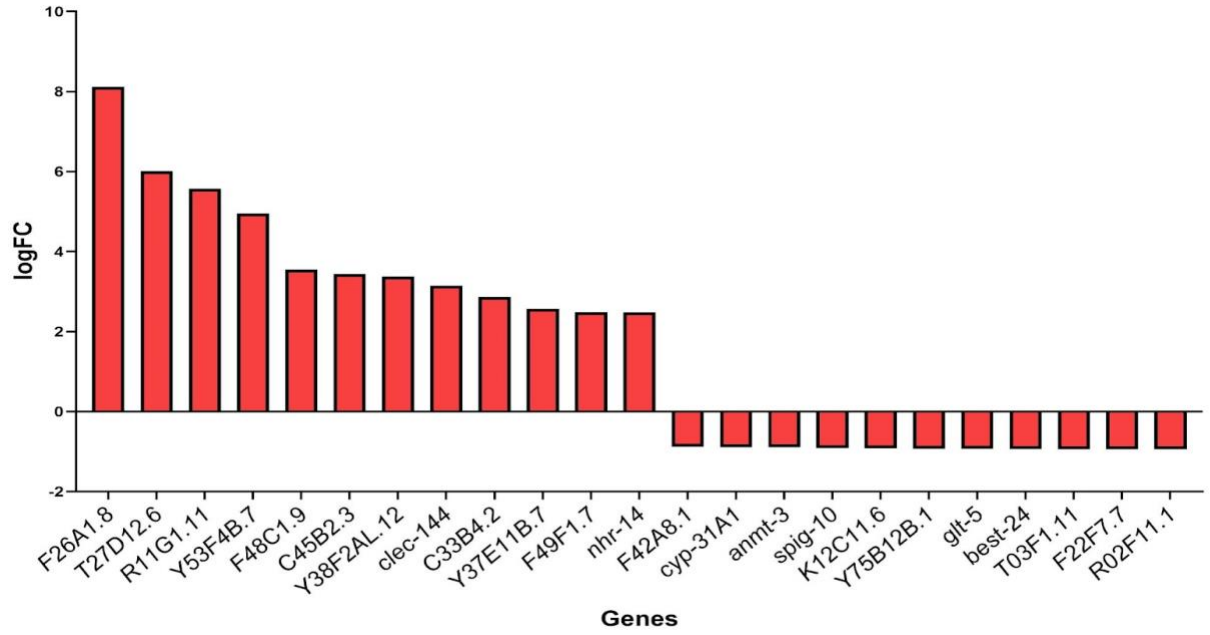

Figure S5: Top Up and Downregulated Genes in the Absence of *nhr-14(tm1473)* Under Non-Stress Conditions. Top upregulated (positive logFC) and downregulated (negative logFC) genes from RNA sequencing results from two independent trials. The most significantly upregulated genes are *F26A1.8, T27D12.6, and R11G1.11.* Interestingly, although *nhr-14* is a loss-of-function mutant, its mRNA levels are increased which suggests a balancing transcriptional response.

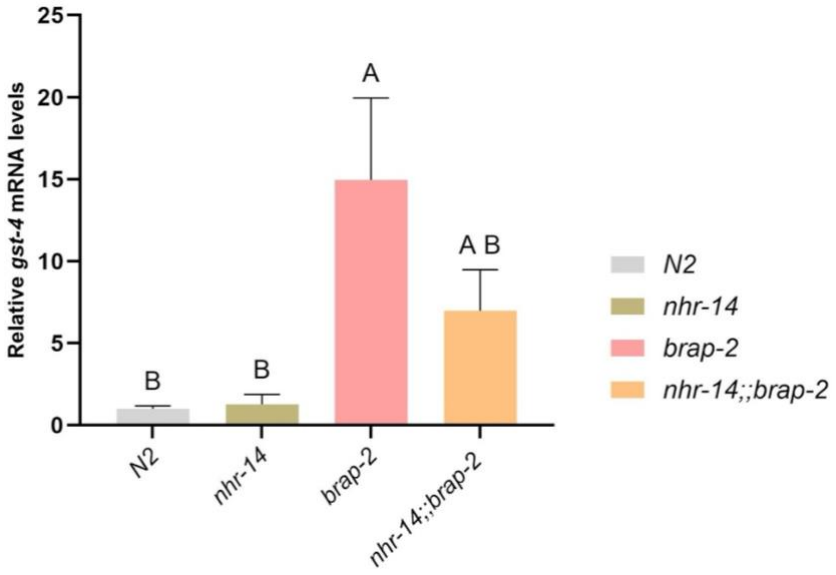

Figure S6: Relative mRNA expression Levels of *gst-4* in WT, *nhr-14(tm1473), brap-2(ok1492),* and *nhr-14(tm1473);brap-2(ok1492)* Mutants. Results were obtained from 3 independent trials, and expression was normalized to *act-1.* Different letters above bars indicate statistically significant differences between groups (Ordinary one-way ANOVA; ****p <0.0001); bars sharing the same letter are not significantly different. Error bars represent ± SEM.

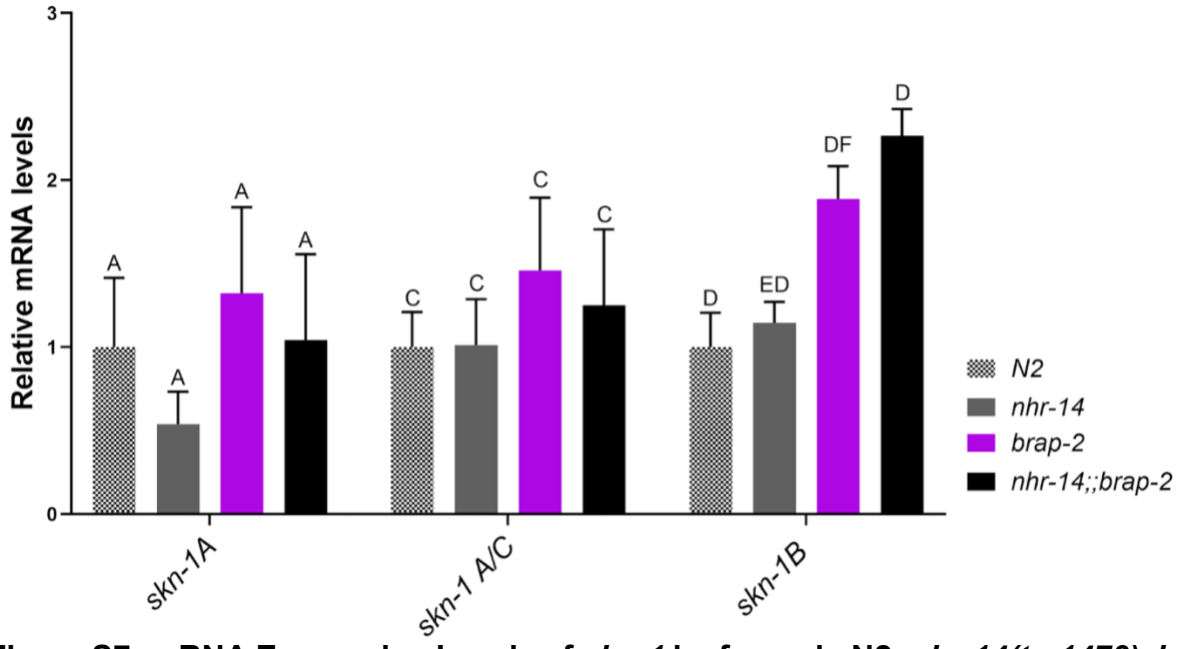

Figure S7: mRNA Expression Levels of *skn-1* isoforms in N2*, nhr-14(tm1473), brap-2(ok1492), and nhr-14(tm1473);brap-2(ok1492)* mutant worms. qRT-PCR was performed to measure the mRNA levels of the *skn-1A, skn-1A/C*, and *skn-1B* in N2, *nhr-14(tm1473)* mutant, *brap-2(ok1492)* mutant, and *nhr-14(tm1473);brap-2(ok1492)* double mutant worms. Data normalized to the housekeeping gene *act-1*. *skn-1A* and *skn-1A/C* mRNA levels did not differ significantly between strains. Results were derived from 3 independent trials. Error bars represent ± SEM; different letters indicate significant differences (Ordinary one-way ANOVA; ***p* =0.0026 for *skn-1B*).

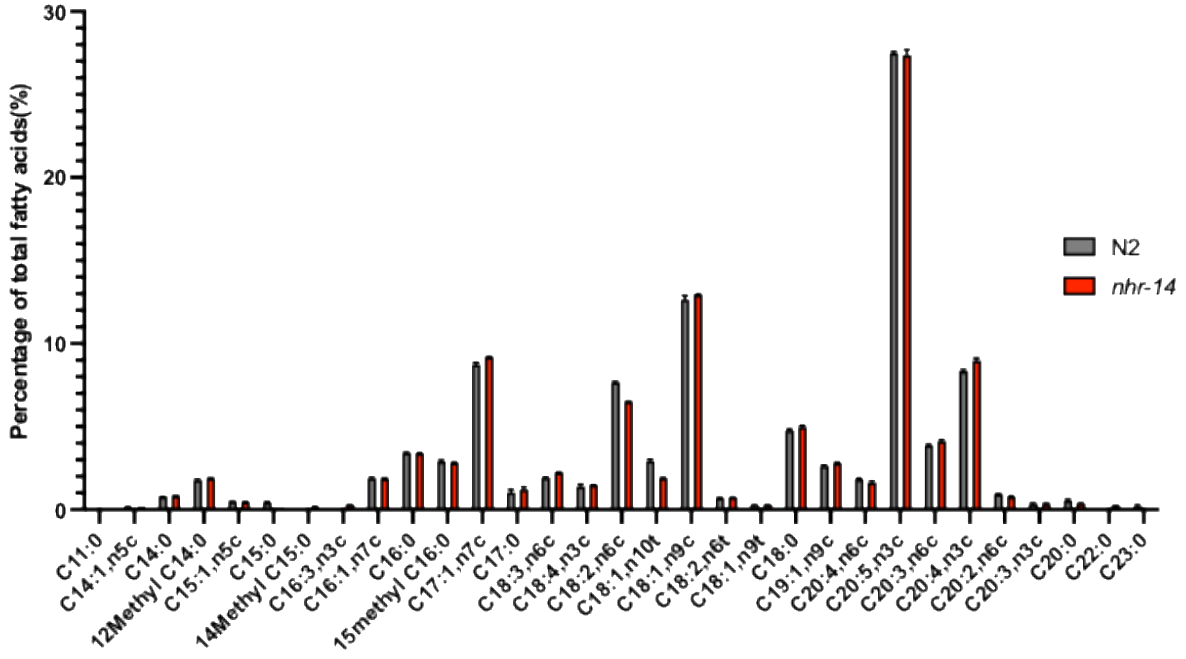

Figure S8: **Fatty Acid Composition in N2 and *nhr-14(tm1473).*** GC–MS analysis of fatty acid composition (% of total fatty acids) in N2 and *nhr-14(tm1473).* Statistical significance between N2 and *nhr-14(tm1473)* was assessed using multiple unpaired two-tailed Student's *t*-tests with false discovery rate correction (Benjamini–Krieger–Yekutieli)**.**

Table 3: Statistics for the tBHP Assay

	Strains	No. of samples	Median Survival				Hours at % mortality				
			Hours	Std. error	95% C.I.	P-value	25%	50%	75%	90%	100%
Trial 1	Wildtype (N2) on 10 mM tBHP plates	36	5.86	0.29	5.28 ~ 6.44		4	6	7	8	9
	nhr-14 on 10 mM tBHP plates	36	4.67	0.26	4.15 ~ 5.18	0.0003	3	5	6	7	8
Trial 2	Wildtype (N2) on 10 mM tBHP plates	36	3.50	0.21	3.10 ~ 3.90		3	4	5	6	7
	nhr-14 on 10 mM tBHP plates		2.86	0.18	2.52 ~ 3.21	0.0049	2	3	4	5	6
Trial 3	Wildtype (N2) on 10 mM tBHP plates	36	3.28	0.16	2.97 ~ 3.58		3	4	5	6	7
	nhr-14 on 10 mM tBHP plates	36	3.00	0.15	2.70 ~ 3.30	0.0042	2	3	4	5	6

P values are relative to wild type (N2)

Table 4: Statistics for the As Oxidative Stress Assay Using Sodium Arsenite 5mM

	Strains	No. of samples	Median Survival				Hours at % mortality				
			Hours	Std. error	95% C.I.	P-value	25%	50%	75%	90%	100%
Trial 1	Wildtype (N2) in 5mM As	36	3.08	0.33	2.44 ~ 3.73	n.s	1	3	4	5	8
	nhr-14 in 5mM As	36	1.56	0.13	1.30 ~ 1.82	0.0001	1	2	3	4	5
Trial 2	Wildtype (N2) in 5mM As	36	3.19	0.39	2.43 ~ 3.96	n.s	1	2	5	7	9
	nhr-14 in 5mM As	36	1.58	0.13	1.34 ~ 1.83	<0.0001	1	2	3	4	5
Trial 3	Wildtype (N2) in 5mM As	36	3	0.32	2.37 ~ 3.63	n.s	1	2	4	7	8
	nhr-14 in 5mM As	36	2.39	0.23	1.94 ~ 2.84	0.0037	1	2	4	5	6

P values are relative to wild type (N2)

Table 5: Statistics for the DTT ER Stress Assay

	Strains	No. of samples	Median Survival				Hours at % mortality				
			Hours	Std. error	95% C.I.	P-value	25%	50%	75%	90%	100%
Trial 1	Wildtype (N2) in 5mM As	36	4.39	0.38	3.64 ~ 5.14	n.s	2	5	6	8	9
	nhr-14 in 5mM As	36	2.08	0.27	1.55 ~ 2.61	<0.001	1	2	4	5	6
Trial 2	Wildtype (N2) in 5mM As	36	2.86	0.25	2.37 ~ 3.35	n.s	1	3	4	5	6
	nhr-14 in 5mM As	36	2.75	0.17	2.41 ~ 3.09	0.0137	2	3	4	5	6
Trial 3	Wildtype (N2) in 5mM As	36	5.39	0.32	4.75 ~ 6.03	n.s	4	6	7	8	9
	nhr-14 in 5mM As	36	3.97	0.24	3.49 ~ 4.45	0.0005	3	4	5	6	8

P values are relative to wild type (N2)

Table 6: Statistics for the Heat Assay

	Strains	No. of samples	Median Survival				Hours at % mortality				
			Hours	Std. error	95% C.I.	P-value	25%	50%	75%	90%	100%
Trial 1	Wildtype (N2) exposed to 37°C	36	5.06	0.29	4.50 ~ 5.62		4	5	6	8	9
	nhr-14 exposed to 37°C	36	4.31	0.22	3.87 ~ 4.74	0.0016	3	4	5	6	7
Trial 2	Wildtype (N2) exposed to 37°C	36	5.78	0.34	5.10 ~ 6.45		4	6	7	9	10
	nhr-14 exposed to 37°C	36	5.86	0.26	5.36 ~ 6.36	0.0169	4	6	7	8	9
Trial 3	Wildtype (N2) exposed to 37°C	36	4.89	0.21	4.48 ~ 5.29		4	5	6	7	8
	nhr-14 exposed to 37°C	36	4.53	0.21	4.12 ~ 4.94	0.0062	3	4	5	6	7

P values are relative to wild type (N2)

Table 7: Statistics for the Longevity Assay

	Strains	No. of samples	Median Survival				Days at % mortality				
			Days	Std. error	95% C.I.	P-value	25 %	50 %	75 %	90 %	100 %
Trial 1	Wildtype (N2)	36	19.5	0.70	18.13 ~ 20.87	n.s	16	20	22	26	27
	nhr-14	36	16.28	0.50	15.30 ~ 17.26	0.0001	13	16	19	20	22
Trial 2	Wildtype (N2)	36	19.92	0.65	18.64 ~ 21.19	n.s	18	19	22	25	30
	nhr-14	36	14.17	0.43	13.31 ~ 15.02	<0.001	12	14	15	18	19
Trial 3	Wildtype (N2)	36	21.94	0.65	20.67 ~ 23.21	n.s	19	21	25	26	28
	nhr-14	36	10.44	0.41	9.65 ~ 11.24	<0.0001	9	10	12	14	15

P values are relative to wild type (N2)

Table 8: List of Forward and Reverse Primers used for qRT-PCR

Genes	TM (°C)	Sequence
acdh-4	58.99 59.96	F: GCAAGTATTGTCGGAGCAGG R: AGGGCCACCGTACTTTTCAG
acdh-8	60.04 59.89	F: TGGAATCGGATTGCCGTTCA R: TCCTGGTCCACCGTACTTCT
acs-18	60.25 60.04	F: CTGGACGTCCGAAAGGTGTT R: AAGCTTGGGATCACCACGAG
acs-2	60.04 59.97	F: ACCAACAGCTACATCCACGG R CGACACGATCTCCCTTCTCG
act-1	63.9 64.1	F: GTCGGTATGGGACAGAAGGA R: GCTTCAGTGAGGAGGACTGG
cdc-42	67.6 67.7	F: TCGACAATTACGCCGTCACA R: AGGCACCCATTTTTCTCGGA
ctl-1	68.4 65.0	F: GTGTCGTTCATGCCAAGGGA R: CCCAGTTACCCTCCTCGGTA
daf-16	69.3 63.9	F: TGGAATTCAATCGTGTGGAA R: ATGAATATGCTGCCCTCCAG
dhs-8	64.2 65.4	F: AAAAGGATCGGGTGGGTACA R: AAACGACATGTGCTCCTGCT
fmo-1	57.3 56.8	F: GGAGCCGACTTGGACATGAA R: CACTTGTGCGTGATCGTTCG
fmo-1	57.3 56.8	F: GGAGCCGACTTGGACATGAA R: CACTTGTGCGTGATCGTTCG
gcs-1	63.8 63.8	F: CCAATCGATTCCTTTGGAGA R: GCTACTTCCGGGAATGTGAA
gst-4	64.0 63.6	F: TGCTCAATGTGCCTTACGAG R: AGTTTTTCCAGCGAGTCCAA
hacd-1	59.9 60.11	F: CCCCTGGTGGCAATTTTTGG R: GCAATTTCCTCCAAGGCTGC
hsp-16.2	54.9 54.2	F: CTCAACGTTCCGTTTTTGGTG R: TGGATTGATAGCGTACGACC
mtl-1	56.2 57.5	F: TGCAAGTGCGGAGACAAATG R: GTTCCCTGGTGTTGATGGGT
sdz-8	64.7 60.4	F: CTGCTGAGGTACGGAACGAA R: TCTGTAFFCGACAACTGGGA
skn-1 A	56.5 55.4	F: GCGACGAGACGAGACGATAA R: CCGATCGTATGACGATGATT
skn-1 A/C	57.4 58.1	F: TACTCACCGAGCATCCACCA R: TGATCAGCAGGAGCCACTTG
skn-1B	57.1 54.7	F: CTCCAGCAGCTGTCAACTCT R: TGCATTCCAATGTAGGCGTA

sod-1	65.7 68.1	F: ATTTCTGCCGGTCCACACTT R: CCATAGATCGGCCAACGACA
sod-2	67.5 65.9	F: GAGGCGGTCTCCAAAGGAAA R: GAACAGCCGACAGTTGATGC
sod-3	63.9 64.0	F: GGATGGTGGAGAACCTTCAA R: AAGGATCCTGGTTTGCACAG
tba-1	66.4 67.4	F: AGACCAACAAGCCGATGGAG R: TCAGTTCCTTTCCGACGGTG
ugt-13	65.0 65.0	F: CCGGATTCCTGGATCGACTG R: TTGTCGCAGTAGTTGGGACC

Table 9: List of *C. elegans* Strains

Strains	Description
N2	Bristol Wildtype
CF1553	*muls84(sod-3p::gfp), backcrossed*
CL2166	*dvls19(gst-4p::gfp), backcrossed*
DR466	*him-5(e1490)*
	nhr-14(tm1473);sod-3::gfp
YF15	*brap-2(ok1492)*
YF229	*nhr-14(tm1473), backcrossed*
YF230	*nhr-14(tm1473);gst-4::gfp*
YF231	*nhr-14(tm1473);brap-2(ok1492)*

Table 10: List of Primers used for Genotyping *nhr-14* with SW-PCR

Name	TM (°C)	Sequence
TK352	57.7	GGCACACCAAGTCCCAAGA
TK353	57.4	GGGCTCTTACCGACTGTCC
TK354	65.8	ACAGTATCGATTCCCTTCCG

Table 11: TF2DNA 2018 in Upregulated Genes

Index	Name	P-value	Adjusted p-value	Z-score	Combined score
1	*elt-3_PMID-24194598*	0.00006805	0.003947	-1.78	17.12
2	*nhr-86_PMID-25215497*	0.04031	0.9999	-1.80	5.77
3	*skn-1_PMID-24194598*	0.05199	0.9999	-1.40	4.15
4	*nhr-49_PMID-25215497*	0.09566	0.9999	-1.47	3.45
5	*ceh-24_PMID-25215497*	0.1284	0.9999	-1.53	3.14
6	*hlh-1_PMID-19632181*	0.2330	0.9999	-1.98	2.88
7	*pha-2_PMID-25215497*	0.1557	0.9999	-1.24	2.30
8	*hlh-11_PMID-19632181*	0.3132	0.9999	-1.33	1.54
9	*eor-1_PMID-25215497*	0.3443	0.9999	-1.28	1.37
10	*unc-86_PMID-25215497*	0.3625	0.9999	-1.23	1.25

Table 12: TF2DNA 2018 in Downregulation Genes

Index	Name	P-value	Adjusted p-value	Z-score	Combined score
1	*hlh-30_PMID-19632181*	1.679e-9	9.908e-8	-1.80	36.35
2	*hlh-26_PMID-19632181*	0.002037	0.06009	-1.73	10.73
3	*mxl-3_PMID-19632181*	0.01831	0.3602	-1.66	6.64
4	*athp-1_PMID-25215497*	0.1550	1.000	-1.53	2.85
5	*sex-1_PMID-25215497*	0.1806	1.000	-1.63	2.79
6	*cfi-1_PMID-25215497*	0.4241	1.000	-1.30	1.11
7	*mab-3_PMID-24194598*	0.4586	1.000	-1.43	1.11
8	*egl-38_PMID-25215497*	0.4685	1.000	-1.25	0.95
9	*daf-16_PMID-25215497*	0.4662	1.000	-1.13	0.86
10	*ref-1_PMID-19632181*	0.5481	1.000	-1.32	0.79

Table 13: KEGG Enrichment of Upregulated genes in *nhr-14 (tm1473)* Mutants Compared to N2 Wild-Type Under Normal Conditions Using Wormenricher.

Index	Name	P-value	Adjusted p-value	Z-score	Combined score
1	Homologous recombination	0.02255	0.3256	-2.28	8.66
2	Non-homologous end-joining	0.06819	0.4124	-3.11	8.36
3	mRNA surveillance pathway	0.008720	0.3256	-1.28	6.06
4	ABC transporters	0.03427	0.3256	-1.74	5.86
5	Nitrogen metabolism	0.1317	0.4124	-2.42	4.91
6	TGF-beta signaling pathway	0.08303	0.4124	-1.93	4.81
7	Lysosome	0.02902	0.3256	-1.20	4.23
8	Ether lipid metabolism	0.1520	0.4124	-2.13	4.00
9	Peroxisome	0.05968	0.4124	-1.19	3.35
10	Glutathione metabolism	0.1160	0.4124	-1.43	3.07
11	Butanoate metabolism	0.1910	0.4313	-1.84	3.05
12	Arginine biosynthesis	0.1814	0.4313	-1.70	2.90
13	Phosphatidylinositol signaling system	0.1047	0.4124	-1.27	2.86
14	Glycerophospholipid metabolism	0.1395	0.4124	-1.38	2.71
15	Longevity regulating pathway	0.09569	0.4124	-1.05	2.47
16	Tyrosine metabolism	0.2462	0.4313	-1.28	1.79
17	Spliceosome	0.1412	0.4124	-0.89	1.73
18	Glycine, serine and threonine metabolism	0.2724	0.4313	-1.31	1.71
19	Arginine and proline metabolism	0.2638	0.4313	-1.24	1.65
20	RNA polymerase	0.2550	0.4313	-1.14	1.56
21	Basal transcription factors	0.3456	0.4631	-1.30	1.38
22	Inositol phosphate metabolism	0.3300	0.4631	-1.20	1.33
23	Drug metabolism	0.2061	0.4313	-0.84	1.32
24	Ribosome biogenesis in eukaryotes	0.2448	0.4313	-0.88	1.24
25	ErbB signaling pathway	0.3609	0.4631	-1.08	1.10
26	mTOR signaling pathway	0.2319	0.4313	-0.75	1.10
27	Sphingolipid metabolism	0.3379	0.4631	-0.90	0.98
28	Metabolism of xenobiotics by cytochrome P450	0.3758	0.4631	-0.96	0.94
29	Tryptophan metabolism	0.3533	0.4631	-0.90	0.94
30	Autophagy	0.2622	0.4313	-0.66	0.88
31	FoxO signaling pathway	0.5011	0.5666	-0.78	0.54
32	Calcium signaling pathway	0.5070	0.5666	-0.57	0.39

33	Valine, leucine and isoleucine degradation	0.4452	0.5287	-0.35	0.29
34	RNA transport	0.3778	0.4631	-0.05	0.05
35	Purine metabolism	0.5721	0.6211	0.06	-0.04
36	Wnt signaling pathway	0.5919	0.6247	0.19	-0.10
37	Ubiquitin mediated proteolysis	0.6416	0.6589	0.31	-0.14
38	Protein processing in endoplasmic reticulum	0.7993	0.7993	0.74	-0.17

Table 14: KEGG Enrichment of Downregulated Genes in *nhr-14 (tm1473)* Mutants Compared to N2 Wild-Type Under Normal Conditions Using Wormenricher.

Index	Name	P-value	Adjusted p-value	Z-score	Combined score
1	Fatty acid degradation	0.01796	0.6108	-1.79	7.21
2	Valine, leucine and isoleucine degradation	0.05832	0.7006	-2.33	6.62
3	Fatty acid biosynthesis	0.1016	0.7006	-2.23	5.10
4	Cysteine and methionine metabolism	0.09270	0.7006	-1.93	4.60
5	Glycine, serine and threonine metabolism	0.1030	0.7006	-1.82	4.15
6	Butanoate metabolism	0.1741	0.7895	-2.21	3.87
7	Tryptophan metabolism	0.2031	0.7895	-2.11	3.36
8	Fatty acid elongation	0.2364	0.7895	-1.87	2.69
9	Lysine degradation	0.2253	0.7895	-1.69	2.52
10	Sulfur relay system	0.3496	0.7895	-2.19	2.30
11	Nitrogen metabolism	0.4033	0.7895	-2.36	2.14
12	Apoptosis	0.4284	0.7895	-2.17	1.84
13	Alanine, aspartate and glutamate metabolism	0.3774	0.7895	-1.69	1.65
14	Sulfur metabolism	0.4525	0.7895	-1.68	1.33
15	Phenylalanine metabolism	0.3770	0.7895	-1.30	1.27
16	Terpenoid backbone biosynthesis	0.5188	0.7895	-1.81	1.19
17	Glyoxylate and dicarboxylate metabolism	0.4512	0.7895	-1.46	1.16
18	Pantothenate and CoA biosynthesis	0.4284	0.7895	-1.28	1.08
19	Arginine biosynthesis	0.5188	0.7895	-1.59	1.04
20	Fructose and mannose metabolism	0.5771	0.7895	-1.47	0.81
21	Biosynthesis of unsaturated fatty acids	0.6120	0.7895	-1.45	0.71
22	Proteasome	0.5198	0.7895	-0.94	0.62
23	Glutathione metabolism	0.6281	0.7895	-1.00	0.46
24	beta-Alanine metabolism	0.6440	0.7895	-0.95	0.42
25	ABC transporters	0.6590	0.7895	-0.98	0.41
26	Arginine and proline metabolism	0.6734	0.7895	-1.02	0.40
27	Tyrosine metabolism	0.6440	0.7895	-0.92	0.40
28	Longevity regulating pathway	0.5542	0.7895	-0.66	0.39

29	Amino sugar and nucleotide sugar metabolism	0.7784	0.8270	-0.90	0.23
30	Calcium signaling pathway	0.7251	0.7952	-0.69	0.22
31	Peroxisome	0.6259	0.7895	-0.42	0.20
32	Propanoate metabolism	0.7130	0.7952	-0.45	0.15
33	Autophagy	0.9744	0.9860	-0.21	0.01
34	Lysosome	0.9860	0.9860	-0.38	0.01

Table 15: Top 10 Upregulated Genes in *nhr-14(tm1473)* Mutation.

GeneID	Gene Name	Log2 Fold Change	FDR
WBGene00017806	*f26a1.8*	8.11632762891898	1.07363505965535E-42
WBGene00194848	*t27d12.6*	6.01186731693776	4.228393150367E-37
WBGene00304816	*r11g1.11*	5.57206134986142	2.33805026566827E-11
WBGene00013154	*y53f4b.7*	4.95409420804694	1.81892659537752E-07
WBGene00018601	*f48c1.9*	3.5517269795354	1.13413479275132E-14
WBGene00016660	*c45b2.3*	3.43817692344831	1.61822353328737E-05
WBGene00219413	*y38f2al.12*	3.37591753370023	0.00026547232562584
WBGene00012086	*clec-144*	3.14551506706437	0.000731523118613693
WBGene00007891	*c33b4.2*	2.86714252511095	6.823751850442E-07
WBGene00021379	*y37e11b.7*	2.57263506701355	6.14086775625662E-10

Table 16: Top 10 Downregulated Genes in *nhr-14(tm1473)*

GeneID	Gene Name	Log2 Fold Change	FDR
WBGene00000676	*col-102*	-10.038731962772	6.79683826006402E-09
WBGene00017325	*f10c1.3*	-7.734514266262	3.28727213288018E-13
WBGene00000617	*col-40*	-6.50031221935868	6.51400715788549E-11
WBGene00009680	*msd-1*	-6.04854980016098	2.45485450551122E-12
WBGene00009708	*f44g3.7*	-5.94412970789344	3.01649392436012E-08
WBGene00018081	*f36a4.2*	-5.59969948175233	1.77429129734825E-10
WBGene00000593	*col-2*	-5.32076971221347	4.06762827205051E-11
WBGene00010168	*f56h6.7*	-5.31806847061074	2.15294871555019E-08
WBGene00000613	*col-36*	-5.28537727011007	1.81116400864834E-11
WBGene00001944	*his-70*	-5.24434373449957	1.86116512551E-10

Table 17: GO Cellular Component 2018 Upregulated

Index	Name	P-value	Adjusted p-value	Z-score	Combined score
1	membrane raft (GO:0045121)	5.919e-7	0.00004203	-1.86	26.63
2	condensed chromosome (GO:0000793)	0.00001554	0.0005518	-2.12	23.50
3	chromatin (GO:0000785)	0.001829	0.03070	-2.00	12.59
4	condensed nuclear chromosome (GO:0000794)	0.0008767	0.02075	-1.71	12.04
5	90S preribosome (GO:0030686)	0.006935	0.07034	-2.25	11.19
6	DNA-directed RNA polymerase I complex (GO:0005736)	0.009686	0.07641	-2.04	9.48
7	nuclear chromosome (GO:0000228)	0.002162	0.03070	-1.43	8.76
8	preribosome (GO:0030684)	0.003846	0.04551	-1.52	8.46
9	sex chromosome (GO:0000803)	0.07877	0.2431	-3.16	8.02
10	X chromosome (GO:0000805)	0.07877	0.2431	-2.99	7.60

Table 18: GO Molecular Function 2018 Upregulated Genes

Index	Name	P-value	Adjusted p-value	Z-score	Combined score
1	metalloaminopeptidase activity (GO:0070006)	0.0005167	0.02549	-2.34	17.72
2	aminopeptidase activity (GO:0004177)	0.0002552	0.01889	-1.88	15.54
3	phosphatidylinositol kinase activity (GO:0052742)	0.004610	0.1347	-2.79	15.00
4	kinase activity (GO:0016301)	0.0001316	0.01889	-1.33	11.92
5	transition metal ion binding (GO:0046914)	0.005905	0.1347	-2.18	11.20
6	phosphoric diester hydrolase activity (GO:0008081)	0.009686	0.1347	-2.36	10.96
7	RNA polymerase I activity (GO:0001054)	0.009686	0.1347	-2.25	10.45
8	metal ion transmembrane transporter activity (GO:0046873)	0.06790	0.2555	-3.86	10.37
9	cyclin-dependent protein kinase activity (GO:0097472)	0.01456	0.1347	-2.39	10.12
10	transcriptional repressor activity, RNA polymerase II core promoter proximal region sequence-specific binding (GO:0001078)	0.01284	0.1347	-2.16	9.41

Table 19: GO Biological Process 2018 in Upregulated Genes

Index	Name	P-value	Adjusted p-value	Z-score	Combined score
1	positive regulation of striated muscle contraction (GO:0045989)	0.001966	0.06415	-3.77	23.51
2	regulation of striated muscle contraction (GO:0006942)	0.003613	0.06485	-3.25	18.27
3	regulation of sarcomere organization (GO:0060297)	0.003613	0.06485	-2.99	16.82
4	positive regulation of sarcomere organization (GO:0060298)	0.003613	0.06485	-2.93	16.45
5	positive regulation of striated muscle cell differentiation (GO:0051155)	0.003613	0.06485	-2.92	16.40
6	nitrogen compound transport (GO:0071705)	0.003613	0.06485	-2.64	14.83
7	defense response to fungus (GO:0050832)	0.0002194	0.03938	-1.72	14.52
8	peptide catabolic process (GO:0043171)	0.001119	0.04464	-2.11	14.34
9	positive regulation of cell development (GO:0010720)	0.003613	0.06485	-2.52	14.19
10	myosin filament assembly (GO:0031034)	0.005718	0.08925	-2.68	13.86

Table 20: GO Cellular Component 2018 Downregulation Genes

Index	Name	P-value	Adjusted p-value	Z-score	Combined score
1	pseudopodium (GO:0031143)	0.00001228	0.0005159	-2.14	24.24
2	integral component of mitochondrial membrane (GO:0032592)	0.001892	0.03974	-2.34	14.64
3	integral component of mitochondrial outer membrane (GO:0031307)	0.03229	0.2198	-3.53	12.11
4	intrinsic component of mitochondrial outer membrane (GO:0031306)	0.04187	0.2198	-3.13	9.93
5	intrinsic component of mitochondrial inner membrane (GO:0031304)	0.02763	0.2198	-2.46	8.84
6	chromatin (GO:0000785)	0.01339	0.1406	-2.00	8.61
7	nuclear chromatin (GO:0000790)	0.004316	0.06043	-1.19	6.48
8	integral component of mitochondrial inner membrane (GO:0031305)	0.03785	0.2198	-1.53	5.00
9	nuclear chromosome part (GO:0044454)	0.08198	0.3826	-1.75	4.38
10	mitochondrial intermembrane space (GO:0005758)	0.2600	0.9790	-2.41	3.24

Table 21: GO Molecular Function 2018 in Downregulation

Index	Name	P-value	Adjusted p-value	Z-score	Combined score
1	protein kinase activity (GO:0004672)	6.968e-7	0.00004111	-1.14	16.21
2	protein serine/threonine kinase activity (GO:0004674)	7.603e-8	0.000008971	-0.93	15.27
3	inorganic phosphate transmembrane transporter activity (GO:0005315)	0.009519	0.2247	-2.89	13.46
4	stearoyl-CoA 9-desaturase activity (GO:0004768)	0.03229	0.3861	-3.61	12.41
5	non-membrane spanning protein tyrosine kinase activity (GO:0004715)	0.00007483	0.002943	-1.24	11.78
6	neuropeptide receptor binding (GO:0071855)	0.01230	0.2419	-2.64	11.62
7	acyl-CoA desaturase activity (GO:0016215)	0.03229	0.3861	-3.31	11.37
8	sugar transmembrane transporter activity (GO:0051119)	0.04187	0.3861	-3.16	10.04
9	sodium:potassium-exchanging ATPase activity (GO:0005391)	0.05236	0.3861	-3.33	9.81
10	potassium-transporting ATPase activity (GO:0008556)	0.05236	0.3861	-3.29	9.72

Table 22: GO Biological Process 2018 in Downregulation Genes

Index	Name	P-value	Adjusted p-value	Z-score	Combined score
1	peptidyl-serine modification (GO:0018209)	3.215e-11	4.132e-9	-1.46	35.33
2	peptidyl-serine phosphorylation (GO:0018105)	2.655e-11	4.132e-9	-1.23	29.98
3	protein phosphorylation (GO:0006468)	5.878e-9	5.035e-7	-1.42	27.00
4	peptidyl-tyrosine autophosphorylation (GO:0038083)	0.00007483	0.004808	-1.45	13.81
5	enzyme linked receptor protein signaling pathway (GO:0007167)	0.0001796	0.007694	-1.58	13.65
6	phosphate ion transport (GO:0006817)	0.01230	0.2874	-2.89	12.72
7	phosphate ion transmembrane transport (GO:0035435)	0.01230	0.2874	-2.86	12.59
8	transmembrane receptor protein tyrosine kinase signaling pathway (GO:0007169)	0.002116	0.06797	-2.00	12.30
9	peptidyl-tyrosine phosphorylation (GO:0018108)	0.0001285	0.006603	-1.29	11.60

Table 23: GC–MS Fatty Acid Composition Comparing N2 and *nhr-14.*

Percentage of total fatty acids(%)						
Fatty acid	**N2**			***nhr-14***		
C11:0	0.0000	0.0000	0.0000	0.0000	0.0000	0.0000
C14:1，n5c	0.1767	0.1598	0.1627	0.1653	0.1826	0.1827
C14:0	0.8023	0.7452	0.754	0.8045	0.8415	0.8475
12Methyl C14:0	1.8678	1.7804	1.6803	1.9152	1.8741	1.8803
C15:1，n5c	0.5004	0.5095	0.4494	0.4747	0.4693	0.4418
C15:0	0.3248	0.3572	0.55	0.125	0.1151	0.112
14Methyl C15:0	0.0000	0.0000	0.0000	0.1199	0.1492	0.2136
C16:3，n3c	0.0000	0.0000	0.0000	0.2545	0.2937	0.2779
C16:1，n7c	1.9733	1.8101	1.8988	1.8137	1.886	1.9067
C16:0	3.398	3.3751	3.5004	3.3495	3.3999	3.4202
15methyl C16:0	3.0771	2.7498	2.8758	2.7714	2.8806	2.8047
C17:1，n7c	8.9438	8.5248	8.7095	9.2341	9.1343	9.1702
C17:0	0.9151	1.4133	0.766	1.4752	1.1984	0.9495
C18:3，n6c	1.9153	2.0025	1.8495	2.2235	2.2501	2.2334
C18:4，n3c	1.3125	1.6263	1.2222	1.4568	1.4733	1.5087
C18:2，n6c	7.7734	7.5947	7.6193	6.5413	6.494	6.4902
C18:1，n10t	2.7596	2.875	3.1462	1.9579	1.8715	1.8757
C18:1，n9c	13.0259	12.2298	12.715	12.969	12.9525	12.8772
C18:2，n6t	0.7668	0.6364	0.6833	0.759	0.7337	0.7226
C18:1，n9t	0.2582	0.3063	0.222	0.3017	0.2554	0.2548
C18:0	4.696	4.6746	4.9259	5.1023	4.9456	4.8673
C19:1，n9c	2.6666	2.5071	2.6996	2.7313	2.8602	2.8039
C20:4，n6c	1.9128	1.8181	1.7445	1.6193	1.4652	1.7858
C20:5，n3c	27.2991	27.5022	27.6494	26.8774	27.1556	28.0294
C20:3，n6c	3.7418	3.8675	3.9906	4.1186	4.2694	4.0013
C20:4，n3c	8.1268	8.3946	8.4713	8.9823	9.2221	8.684
C20:2，n6c	0.8857	0.9804	0.904	0.8192	0.7899	0.6859
C20:3，n3c	0.3067	0.4618	0.2714	0.3707	0.3051	0.3958
C20:0	0.4532	0.7295	0.4145	0.4275	0.336	0.3492
C22:0	0.0000	0.0000	0.0000	0.2391	0.1958	0.2277
C23:0	0.1203	0.3682	0.1244	0.0000	0.0000	0.0000